



**Michigan
Technological
University**

Michigan Technological University
Digital Commons @ Michigan Tech

Dissertations, Master's Theses and Master's Reports

2016

DESIGN OF REAL-TIME COMBUSTION FEEDBACK SYSTEM AND EXPERIMENTAL STUDY OF AN RCCI ENGINE FOR CONTROL

Jayant Kumar Arora

Michigan Technological University, jkarora@mtu.edu

Copyright 2016 Jayant Kumar Arora

Recommended Citation

Arora, Jayant Kumar, "DESIGN OF REAL-TIME COMBUSTION FEEDBACK SYSTEM AND EXPERIMENTAL STUDY OF AN RCCI ENGINE FOR CONTROL", Open Access Master's Thesis, Michigan Technological University, 2016.

<https://digitalcommons.mtu.edu/etdr/148>

Follow this and additional works at: <https://digitalcommons.mtu.edu/etdr>



Part of the [Automotive Engineering Commons](#), and the [Heat Transfer, Combustion Commons](#)

DESIGN OF REAL-TIME COMBUSTION FEEDBACK SYSTEM AND
EXPERIMENTAL STUDY OF AN RCCI ENGINE FOR CONTROL

By

Jayant Kumar Arora

A THESIS

Submitted in partial fulfillment of the requirements for the degree of

MASTER OF SCIENCE

In Mechanical Engineering

MICHIGAN TECHNOLOGICAL UNIVERSITY

2016

© 2016 Jayant Kumar Arora

This thesis has been approved in partial fulfillment of the requirements for the Degree of MASTER OF SCIENCE in Mechanical Engineering.

Department of Mechanical Engineering - Engineering Mechanics

Thesis Advisor: *Dr. Mahdi Shahbakhti*

Committee Member: *Jeremy Worm*

Committee Member: *Dr. Mohsen Azizi*

Department Chair: *Dr. William W. Predebon*

Dedication

To my parents and brother.

Contents

List of Figures	xi
List of Tables	xv
Acknowledgments	xix
List of Abbreviations	xxi
Abstract	xxvii
1 Introduction	1
1.1 Literature review	4
1.1.1 CI combustion	4
1.1.2 HCCI, PCCI and PPCI combustion	6
1.1.3 RCCI combustion	9
1.2 Scope and organization of thesis	11
2 Experimental setup and procedure	15
2.1 Engine setup	15
2.1.1 Fuel injection	18

2.1.2	Exhaust gas recirculation	19
2.2	Data acquisition and control setup	21
2.3	Test fuels	21
2.4	Test procedure and data analysis	23
2.4.1	Test procedure and matrix	23
2.4.2	Data analysis	25
2.4.2.1	Volume calculation	26
2.4.2.2	Pressure filtering	27
2.4.2.3	IMEP calculation	28
2.4.2.4	Heat release calculation	29
2.4.2.5	Mass fraction burn	30
2.4.2.6	Polytropic index	31
2.5	Uncertainty analysis	31
3	Engine mapping and parametric studies	35
3.1	Engine maps	36
3.1.1	Mapping without EGR	36
3.1.2	Mapping with EGR	41
3.2	Parametric studies	45
3.2.1	Intake temperature	45
3.2.2	Premixed Ratio	48
3.2.3	Start of injection	52

3.2.4	EGR fraction	55
4	Transient study and combustion mode switching	61
4.1	Actuator dynamics	62
4.1.1	Throttle	64
4.1.2	Cam phasor	66
4.1.3	Supercharger	68
4.2	Transient response - RCCI domain	74
4.3	Combustion mode switching	80
5	Combustion feedback for real-time engine control	89
5.1	Hardware and setup	90
5.2	Algorithms and calculations	94
5.2.1	Pressure measurement and conditioning	94
5.2.2	IMEP, PP, LPP calculation	96
5.2.3	Heat release calculation	97
5.2.4	CA50 calculation	100
5.3	Validation and results	105
5.4	Resource allocation	110
5.5	Closed-loop combustion control - IMEP and CA50	111
6	Conclusion and future work	115
6.1	Summary and conclusion	115

6.2 Future work	118
References	123
A Experimental Data Summary	133
B FPGA Model	153
B.1 Angle Counter	153
B.2 Pressure Calculation	154
B.3 Volume Calculation	155
B.4 IMEP, Peak Pressure and Location of peak pressure	156
B.5 Heat Release Calculation	158
B.6 CA50 Calculation	158
C Thesis Files	171
D Permissions	175

List of Figures

1.1	Soot, CO/HC and NO _x formation with respect to local equivalence ratio (ϕ) and flame temperature [1](letter of permissionD.1)	4
1.2	Thesis organization	12
2.1	Engine Setup	16
2.2	EGR setup (a) Control (b) Measurement	19
2.3	Data Acquisition and Control Setup	22
3.1	Operating region for different intake temperatures at intake pressure 95 kPa	39
3.2	Engine map - intake temperature 40, 60, 80, 100 (°C), MAP 95 kPa, PR 20, 40, 60 (-). Reference test conditions A.4 in appendix	40
3.3	Engine Map - intake temperature 40, 60, 80, 100 (deg-C), MAP 95 kPa, PR 20, 40, 60 (-), n-heptane and iso-octane fuels (*Referred from work by Kaushik Kannan)	41
3.4	Engine maps - Intake temperature 60, 80 (°C),MAP 95 kPa, PR 20, 40 (-)	44
3.5	Effect of intake air temperature	46

3.6	Effect of premixed ratio	50
3.7	Effect of start of injection	53
3.8	Maps for effect of start of injection	54
3.9	Effect of EGR - SOI same	57
3.10	Effect of EGR - CA50 same	58
4.1	Throttle step response	66
4.2	Intake cam phasor step response	67
4.3	Supercharging dynamics: engine boost step-up and step-down response at constant engine speeds	70
4.4	Supercharger map: engine speed vs motor frequency	71
4.5	Supercharger Response: Engine Speed Switch N(RPM)=1000, 1600, 1000, MAP(kPa)=120	73
4.6	Combustion metrics of RCCI engine for premixed ratio step-change	78
4.7	Combustion metrics of RCCI engine for mass of fuel step-change . .	80
4.8	Fuel quantity calculation for switching to SI mode	83
4.9	Combustion metrics for RCCI→SI→RCCI mode switching (*COV _{IMEP} calculation for SI mode does not include the misfire cycle)	85
4.10	Combustion metrics for HCCI→SI→HCCI mode switching (*COV _{IMEP} are calculated for the steady-state engine cycles)	87
5.1	FPGA - setup and the software model designed and implemented in this thesis	93

5.2	Comparison of raw and filtered pressure trace	95
5.3	Comparison of conventional model and reduced model for calculating the net cumulative heat release	99
5.4	Effect of γ on reduced HRR model	100
5.5	Comparison of reduced heat release model and Rassweiler–Withrow Model	101
5.6	Two-stage RCCI heat release for test condition EXP31 201 Appendix A.2	103
5.7	SOC identification for two-stage heat release	104
5.8	Comparison of on-line FPGA and post-processed combustion parame- ters	107
5.9	Real-time calculated combustion metrics during the PR switch . . .	108
5.10	Real-time calculated combustion metrics during the SOI switch . .	109
5.11	RCCI combustion control strategy to obtain desired engine load and combustion phasing	112
5.12	IMEP-CA50 closed-loop combustion control for the RCCI engine . .	114
B.1	Angle Counter	162
B.2	Pressure Calculation	163
B.3	Volume Calculation	164
B.4	IMEP, PP and LPP Calculations	165
B.5	Heat Release Calculation	166

B.6	Start of Combustion	167
B.7	End of Combustion	168
B.8	CA50	169
D.1	Letter of permission for figure 1.1	175

List of Tables

2.1	Engine specifications	17
2.2	Test fuel properties	22
2.3	Test matrix for engine mapping	24
2.4	Test matrix for engine mapping with EGR	25
2.5	List of measured parameters and their associated uncertainties *	32
2.6	Uncertainty values for dependent parameters.*	33
2.7	Test condition for the repeatability analysis	34
2.8	Test setup repeatability	34
3.1	Engine test conditions to study the effect of intake temperature	45
3.2	Engine test conditions to study the effect of premixed ratio	49
3.3	Engine test conditions to study the effect of start of injection	52
3.4	Engine test conditions to study the effect of EGR fraction with a fixed SOI	56
3.5	Engine test conditions to study the effect of EGR fraction with fixed CA50	56

4.1	List of available actuators for controlling the engine operating conditions	64
4.2	Supercharger setup [2]	69
4.3	Engine test conditions to study transient dynamics during premixed ratio switch	77
4.4	Engine test conditions to study transient dynamics during mass of fuel switch	79
4.5	Engine test conditions for combustion mode switch from RCCI→SI→RCCI	81
4.6	Engine test conditions for combustion mode switch from SI→HCCI→SI	86
5.1	FPGA board and I/O Specification	92
5.2	Engine test conditions for premixed ratio switch	108
5.3	Engine test conditions for SOI switch	109
5.4	FPGA resource allocation*	110
5.5	PI controller gains for the designed RCCI combustion controller	113
5.6	Engine test conditions for IMEP-CA50 control	113
A.1	Operating Conditions for RCCI Mapping Data - Naturally Aspirated	134
A.2	Optimized map Test points without EGR	143
A.3	Operating Conditions for RCCI Mapping Data - NA with EGR	144
A.4	Optimized map Test points with EGR 0-15%	150

A.5	Optimized map Test points EGR 0%	151
C.1	Test Data Files - Raw and Processed Folder location: \Thesis_Files	171
C.2	Figure Files Folder location: \Thesis_Files\Figures	172
C.3	Data Analysis Scripts Folder location: \Thesis_Files\Data_Analysis_Code	173
C.4	Test Setup Files Folder location: \Thesis_Files\APRC Test Setup Files	174

Acknowledgments

Firstly, I would like to thank my family who always encouraged and supported my decision of pursuing masters in US.

Next, I am thankful to my advisor, Dr. Mahdi Shahbakhti , for giving me this great opportunity of working as part of his team. I am also thankful to Jeremy Worm and Dr. Mohsen Azizi for accepting to be my committee members.

I would also like to acknowledge my colleagues Kaushik Kannan, Dr. Hamit Solmaz, Nithin Teja Kondipati and Akshat Raut for their help with my work. I also want to thank Paul Dice for his support and input towards the experimental part of my research.

List of Abbreviations

Acronyms

aBDC	After Bottom Dead Center
aTDC	After Top Dead Center
TDC	Top Dead Center
BDC	Bottom Dead Center
CAD	Crank Angle Degree
CA50	Crank Angle for 50% Burnt Fuel
CO	Carbon Monoxide
EGR	Exhaust Gas Recirculation
EOC	End of Combustion
EVC	Exhaust Valve Closing
EVO	Exhaust Valve Opening
HCCI	Homogeneous Charge Compression Ignition
HEV	Hybrid Electric Vehicle
ICE	Internal Combustion Engine
IMEP	Indicated Mean Effective Pressure
IVC	Intake Valve Closing
IVO	Intake Valve Opening

LTC	Low Temperature Combustion
NHTSA	National Highway Traffic Safety Administration
NO _x	Nitrogen Oxides
ON	Octane Number
PCCI	Premixed Charge Compression Ignition
PI	Proportional Integral
PID	Proportional Integral Derivative
PM	Particulate Matter
PRF	Primary Reference Fuel
RCCI	Reactivity Controlled Charge Compression Ignition
RPM	Revolution per Minute
SI	Spark Ignition
SOC	Start of Combustion
TWC	Three Way Catalyst
HC	Hydrocarbon
FPGA	Field Programmable Gate Array
FY	Financial Year
PHEV	Plug-In Hybrid Electric Vehicle
CI	Compression Ignition
PPCI	Partially Premixed Combustion Ignition
DPF	Diesel Particulate Filter

SCR	Selective Catalytic Reduction
LNT	Lean NO _x Traps
PRR	Pressure Rise Rate
LHV	Lower heating Value
PFI	Port Fuel Injection
DI	Direct Injection
UEGO	Universal Exhaust Gas Oxygen
NI	National Instruments
COV	Coefficient of Variance
PR	Premixed Ratio
ISFC	Indicated Specific Fuel Consumption
BSFC	Break Specific Fuel Consumption
BMEP	Break Mean Effective Pressure
CA10	Crank Angle for 10% Burnt Fuel
CA90	Crank Angle for 90% Burnt Fuel
MFB	Mass Fraction Burn
HRR	Heat Release Rate
CHRR	Cumulative Heat Release Rate
MAP	Manifold Absolute Pressure
GDI	Gasoline Direct Injection
LTHR	Low Temperature Heat Release

HTHR	High Temperature Heat Release
SOI	Start of Injection
CR	Compression Ratio
WOT	Wide Open Throttle
MPRR	Maximum Pressure Rise Rates
ITE	Indicated Thermal Efficiency
A/D	Analog To Digital Converter
I/O	Input Output
RAM	Random Access Memory
LUT	Lookup Table
MSPS	Million Samples Per Second
AHRR	Apparent Heat Release Rate
kB	Kilo Bytes
rev	Revolution
Qty	Quantity
KSPS	Kilo Samples per Second

Symbols

AFR	Air Fuel Ratio (-)
BSFC	Brake Specific Fuel Consumption ($\frac{g}{kW.h}$)
C_v	Average Constant-volume Specific Heat Capacity ($\frac{kJ}{kg.K}$)

C_p	Constant Pressure Specific Heat Capacity ($\frac{kJ}{kg.K}$)
CA50	Crank Angle for 50% Burnt Fuel (CADaTDC)
ΔP	Pressure Difference (kPa)
EGR	Exhaust Gas Recirculation Fraction (-)
η	Efficiency (-)
h	Convective Heat Transfer Coefficient ($\frac{W}{m^2.K}$)
IMEP	Indicated Mean Effective Pressure (kPa)
λ	AFR over Stoichiometric AFR (-)
LHV	Low Heating Value (kJ/kg)
N	Engine Speed (RPM)
n	Ratio of Specific Heat Capacities (-)
ON	Octane Number (-)
P	Pressure (kPa)
ϕ	Fuel Equivalence Ratio (-)
SOC	Start Of Combustion Moment (CADaTDC)
t	Time (sec)
K_p	Proportional gain (-)
K_i	Integral gain (-)
τ	Time Constant (sec)
V	Volume (m^3), but Voltage (V) in Chapters 5.1
x_b	Burn fraction (-)

Subscripts

<i>eoc</i>	End of Combustion
<i>max</i>	Maximum
<i>soc</i>	Start of Combustion

Abstract

Premixed compression ignition (PCI) technologies offer high efficiency and low emissions but are usually confined by limited operation range as well as high pressure rise and heat release rate. In this work, a more recently developed PCI mode is explored where in-cylinder blending of two fuels with different auto-ignition characteristics (diesel and gasoline) is utilized to create reactivity stratification such that heat release rate and combustion timing can be controlled. This mode has been defined as Reactivity Controlled Compression Ignition (RCCI).

As part of this thesis, the main aim is to study various parameters that can be used to control combustion phasing. Also, steady state mapping of the engine is done so as to explore the operating range for the current engine setup. Best efficiencies as well as highest loads are obtained for higher Premixed Ratio (PR) values and advanced Start of Injection (SOI) timings, where as lower PR fuel blends are needed to achieve low load limit. The analysis is also extended to transient RCCI operation for observing various dynamics involved and their effects on combustion phasing. As part of realizing full-load range operation, switching to conventional Spark-Ignition (SI) combustion mode is also carried out. Various dynamics involved in the switching process are captured.

A cycle-by-cycle closed loop combustion controller is designed and implemented on the engine to achieve optimum combustion phasing during transient engine operation.

To provide feedback of combustion parameters like engine load and combustion phasing to the closed loop controller, a real-time combustion feedback system is designed and implemented utilizing Field Programmable Gate Array (FPGA).

Chapter 1

Introduction

Increase in greenhouse gases (GHG) emission has been one of the major cause of global climatic change. The main source for GHG is attributed to fossil fuel combustion. Even though there is an expected increase in dependency on non-fossil fuels or renewables, still three-quarters of the energy is projected from fossil fuels by the year 2040 [3]. One of the main industry, that depends on liquid fossil fuels, primarily petroleum, is the transportation sector. Governments around the world have started implementing regulations and norms so that vehicle manufactures push towards technologies lowering the dependency on petroleum as well reducing GHG emissions.

National Highway Traffic Safety Administration (NHTSA) has implemented standards where manufacturers need to improve the fuel economy by around 35% from

FY2017 to FY2025 [4]. For achieving these targets, there are various areas for improvements. These areas include SI and Diesel engine technology, body and accessories, fuel cell technology and hybridization [5]. In past few years hybridization has been one of the main drives to reduce this dependency on fossil fuels, but a study by Kromer [6] highlights the challenges involved in realizing vehicles entirely dependent on electricity from infrastructure, technical development of battery technology and well-to-wheel economy point of view, and this study suggested that for the next decade, requirements to meet government standards will come from improvement of conventional technologies. The increased popularity and fuel economy improvements of electric power-trains will even drive improvement in conventional technologies mainly that relate to engines.

The internal combustion engine is the primary source of mobile power in transportation sector. The technologies encompassing engines are mainly Spark-Ignition (SI-Gasoline based) and Compression Ignition (CI-Diesel based). Diesel or CI engines are more efficient compared to SI engines mainly as diesel fuel allows the engine to run with higher compression ratio [7]. At the same time, CI mode also runs unthrottled which reduces pumping losses. But in countries like the USA, CI engine has not been a sought after technology in light-duty sector due to issues on emissions front. There are technologies available to address these issues but due to additional setup requirements, operational costs and durability concerns they are not very popular [5]. Thus more concentration has been given to SI engine technologies. There is

another technology that has been there for many years but due to issue of limited operational load and controllability, has not yet been realized in production vehicles. These are categorized as Low Temperature Combustion (LTC) technologies namely Homogeneous Charge Compression Ignition (HCCI), Premixed Charge Compression Ignition (PCCI), Partially Premixed charge Compression Ignition (PPCI) and recently developed RCCI mode. These technologies offer CI-like efficiencies and SI-like low emissions, thus solving issues on both fronts; that is, fuel economy and emissions. CI engines involve issue of emissions mainly due to non-homogeneous fuel-air mixtures which cause localized hot regions owing to local fuel rich zones, causing reactions which converts free nitrogen to NO_x. This issue is addressed by these LTC modes as they are usually homogeneous (HCCI) or highly premixed (PCCI, PPCI and RCCI), thereby reducing the number of fuel rich zones which increases in-cylinder temperatures, thus reducing fronts for Nitrous Oxides (NO_x) formation. Even though these LTC modes offer possibilities of zero NO_x emissions, but due to low in-cylinder temperatures soot formation increases. Figure 1.1 depicts formation of soot and NO_x based on flame temperature and in-cylinder local equivalence ratio.

These LTC technologies despite offering very good improvements in fuel economy and emissions, lack capability to achieve full load range operation. To realize this, these combustion modes can be coupled with conventional modes like CI or SI [8]. In further sections more elaborate review has been done in context to all the LTC combustion technologies. As part of this thesis , a study has been carried out on

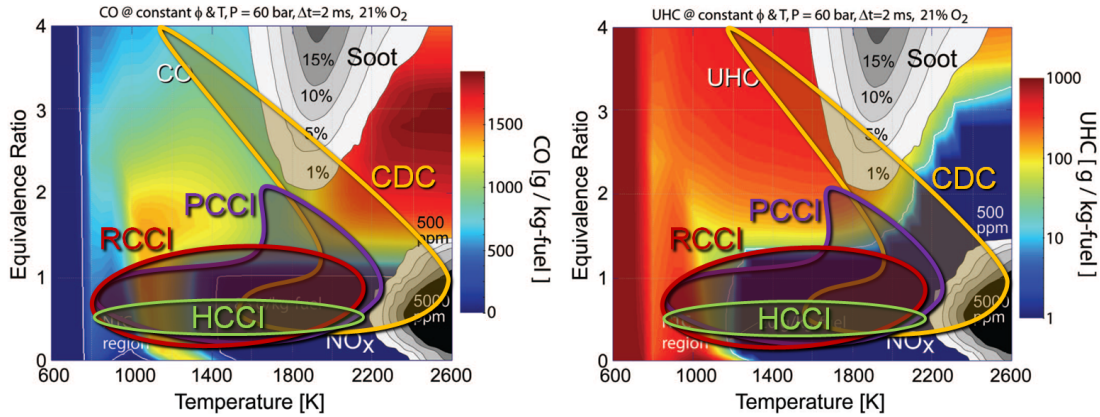


Figure 1.1: Soot, CO/HC and NO_x formation with respect to local equivalence ratio (ϕ) and flame temperature [1](letter of permissionD.1)

RCCI operation mode as it has shown to offer better controllability and expanded load range compared to other premixed combustion modes [9][10][11].

1.1 Literature review

1.1.1 CI combustion

As highlighted in the previous section, CI engines can offer better efficiency compared to SI engines mainly due to un-throttled operation as well as ability to use higher CR. Despite this advantage there are issues involved on cost as well as emissions front, that stops this technology to be a popular option for passenger cars.

CI engines or Conventional Diesel Engines have two main issues on emissions front, NO_x and Soot. In regard to this, study for diesel emissions review was carried out

by Johnson [12]. The problem of soot can be addressed by use of Diesel Particulate Filters (DPF). The two main processes by which soot deposited on DPF can be removed are active and passive regeneration. In active regeneration the temperature of exhaust stream is increased by dosing extra fuel, oxidizes soot on the filters. Second process, that is passive regeneration utilizes NO_2 in the exhaust stream to oxidize soot. This technique does not require any extra fuel injection. At temperatures $>485^\circ\text{C}$, NO_2 reduction to NO becomes more prevalent. This reduces regeneration at higher engine loads where exhaust temperature becomes high. In those cases engine will have to switch to passive regeneration modes, which again will incur fuel penalties. In SI engines the issue of NO_x and soot is addressed using three way catalyst (TWC) systems. These systems operate for stoichiometric engine operation thus can't be used for CI engines. To cope with issue of NO_x in CI engines there are technologies available such as Selective Catalytic Reduction (SCR) systems and Lean NO_x Traps (LNT). SCR is the leading technology for NO_x control in heavy as well as light duty applications. SCR involves usage of urea. This gets converted to ammonia which in turn reduces NO_x to nitrogen. These systems have very high NO_x conversion efficiency. Still SCR systems offer major issues on two fronts. Firstly NO_x conversion efficiencies at low temperature or low loads. The conversion efficiency of SCR system is dependent on available ammonia, which in turn depends on proper injection of urea. At temperatures below 200°C there are issues on part of urea injection mainly attributed to its evaporation. New type of mixers have shown to expand the lower

limits on these temperatures. Second issue that faces SCR systems is additional cost requirement for urea as well as installation for its delivery system. The latter case limits the usage of these systems on passenger vehicles as more space will be needed for installation.

Another technology that is feasible to use on passenger vehicles is LNT. The NO_x reduction chemistry in these systems are independent of urea. Therefore they can find a good application area in passenger cars. LNT's offer lower conversion efficiencies as compared to SCR system. This reduces even more with increased exhaust temperatures thus not suitable for heavy duty applications. For light duty applications LNT is a sought after technology where as SCR systems seem to be suitable for heavy duty applications. But to reduce dependency on these systems we can use alternative combustion modes such as LTC that have ultra-low NO_x emissions. They are discussed in upcoming sections.

1.1.2 HCCI, PCCI and PPCI combustion

Low temperature combustion modes have been a major area of research in recent time due to their high thermal efficiencies and low emissions benefits. These technologies have existed for a while but due to innate issues like limited operation load range, control of combustion phasing and high pressure rise rates, they have not been realized in real-world applications. A brief review of these technologies is done in this section.

In HCCI mode fuel is injected in the port using low pressure injectors very early during the intake cycle, which allows homogeneous mixing of air and fuel. This results in volumetric combustion of the charge, having very high heat release rate and small combustion duration which ideally allows less heat loss to walls and thus improve thermal efficiency. At the same time, this volumetric combustion poses issue of high Pressure Rise Rates (PRR). It is important to explore how this rise can be limited and controlled. Study by Najt and Foster [13] shows application of HCCI mode on a 4-stroke engine. They concluded that autoignition of the charge is highly controlled by chemical kinetics but pointed the possibility of controlling it by varying certain operating parameters such as equivalence ratio, Exhaust Gas Recirculation (EGR) and fuel type. This was further explored by Thring [8] and showed the operation at low loads using high EGR quantities and high intake temperatures. The study highlighted that lower CR was more suitable for HCCI and thus suggested that a conventional gasoline engine can be used to operate in HCCI mode at low loads and then switch to SI mode for full load range operation. Olsson et al. [14] used fuel blends with different reactivities to control combustion phasing over various speeds at lower loads. The study highlighted that despite having no direct control on the combustion timing, secondary parameters like fuel reactivity, ϕ , EGR fraction, etc can be varied to control it. Even with this control of timing was very difficult and complex as all the parameters were needed to be varied in conjunction with each other to achieve optimum combustion timing. This highlighted the lack of a direct

combustion timing control knob in HCCI mode as compared to spark timing in SI mode and injection timing in CI mode.

Another premixed combustion type, where fuel is injected directly inside cylinder, known as PCCI (if an early direct injection is done) or PPCI (if late injection is done) promises high thermal efficiencies and lower emissions. The concept was explored by Okude et al. [15]. Increased EGR fraction was utilized to advance the start of direct fuel injection, allowing enough time for proper mixing of fuel and air. This resulted in combustion accompanied with very less smoke. EGR fraction was increased with increasing engine speed and load to reduce knock as well to advance start of injection. This resulted in reduction of combustion efficiency. To counter this, split injection of fuel was carried out. The amount of fuel injected during first injection was reduced so as to delay autoignition of the charge. The second injection was done near TDC. This resulted in a volumetric + diffusion type combustion mode. They were able to achieve higher loads. Engine out NO_x and Soot was reduced by around 80-90% but fuel efficiency decreased compared to that of conventional diesel combustion. The study mainly relied on EGR for control of combustion phasing, whose constituents in turn are dependent on combustion characteristics. Due to this, during transient events, use of EGR is not a very good parameter to closely control combustion timing events. Kokjohn et al. [11] and Hanson et al. [16] carried out dual fuel study for control over combustion phasing. In-cylinder fuel blending strategy was carried out by port fuel injection of gasoline and direct injection of diesel. By varying the reactivity

of fuel (ratio of diesel to gasoline) combustion phasing was controlled. Diesel being the more reactive fuel, acted as initiator of the ignition process. Its quantity in the mixture as well its injection timing allowed control over combustion phasing even at higher loads. Resulting combustion had very low NO_x and soot emissions and high thermal efficiencies. This concept was further explored and was then defined as RCCI, which is explained in next section.

1.1.3 RCCI combustion

As highlighted in the previous section, blends with different reactivities can be used to limit the heat release rates for PCI modes. Bessonette et al. [17] carried out a study using different fuels derived from gasoline and diesel for expanding HCCI operation range. Highest loads were achieved using low reactivity fuel blends (gasoline type) where as lowest load limits were met using higher reactivity fuel blends (diesel type). Inagaki et al. [9] highlighted that varying fuel reactivity can control ignition timing events by effecting Low Temperature Oxidation (LTO) and High Temperature Oxidation (HTO) reactions but does not have much role in controlling heat release rate. Thus a dual fuel spatially stratified approach was carried out where low reactivity fuel (iso-octane) was injected through port where as high reactivity fuel(diesel) was introduced directly in-cylinder causing ϕ inhomogeneity. This basically caused certain

areas of the charge to burn faster compared to other, thus avoiding volumetric combustion as in case of HCCI. Operation was achieved even without EGR. This concept was further explored [11][16][18] for effect of various parameters - Fuel Reactivity, Injection Timing (SOI), Split Injection, Intake cam phasing (effective compression ratio) and charge stratification. This combustion mode has been defined as RCCI [19] where global fuel reactivity or ϕ is used to control combustion timing where as local ϕ is responsible for control of combustion duration. Kokjohn et al. [19] carried out sweeps showing engine operation from low to high load with high gross indicated efficiencies. Also comparison between RCCI and Conventional Diesel Combustion(CDC) at mid loads (9 bar) was shown. RCCI resulted in 6% higher gross indicated efficiencies compared to CDC while producing less NOx and Soot by an order of 3. Simulation study of both the processes showed that RCCI mode was able to recover around 8% heat loss energy thus resulting in higher efficiency. On control front, this mode provides various control parameters like SOI, PR, fuel split ,etc. to regulate combustion phasing as well as burn rates. Compared to other LTC modes, RCCI gives wider operation range. Still RCCI is also limited by full load range operation as compared to SI and CI modes. For creating reactivity gradient RCCI incorporates direct injection of high reactive fuel. As the load increases amount of high reactivity fuel reduces to zero, resulting into HCCI type combustion, which limits its operation. In context to this, a recent study [20] combined benefits of RCCI and PPCI to expand load range of the engine. For this, two Direct rails and one port fuel rail were installed on the

engine. In this mode, the fuel energy percentage coming from RCCI mode (DI diesel + PFI gasoline) was reduced and instead provided by a late gasoline direct injection. The third injection was done near TDC. This resulted in a diffusion type combustion, which gave a long tail of heat release. By adjusting the timing and quantity of this injection combustion duration and load can be controlled. The mode has been defined as Direct Dual Fuel Stratification (DDFS). DDFS ran with efficiencies and emissions comparable to RCCI, but without EGR and low PRR. The study forwarded another way of load range expansion.

1.2 Scope and organization of thesis

Various advantages of RCCI, like high efficiency, low NO_x, PM emissions and added controllability compared to other LTC modes was highlighted in the previous section. The current study is carried out to look at the scope of RCCI combustion for real-time application. This thesis aims to:

- † Explore RCCI combustion control knobs comprising fuel reactivity, SOI, intake temperature, EGR fraction and its effects on the combustion phasing and the engine performance. Chapter 3
- † Study RCCI combustion during transient engine operation to characterize and observe various dynamics and parameters affecting the combustion phasing and

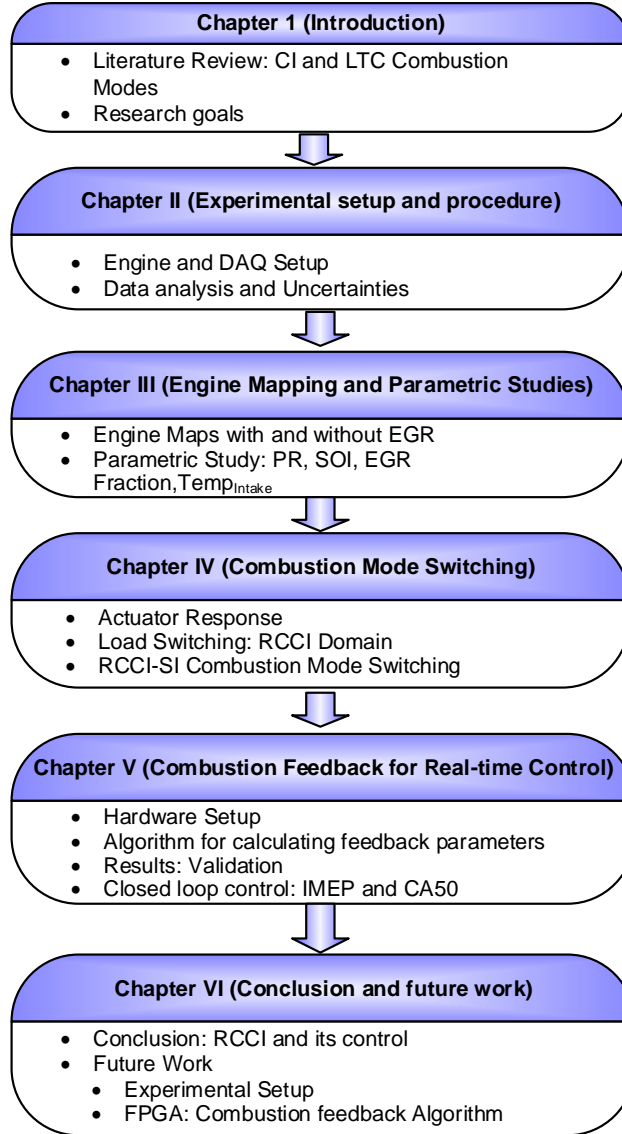


Figure 1.2: Thesis organization

the engine performance. Chapter 4

† Extend the operating range of an RCCI engine by switching over to a conventional SI combustion mode and study various dynamics and factors involved during the process. Chapter 4

† Develop an economical and computationally fast real-time combustion feedback

system that can be utilized for closed-loop cycle-by-cycle RCCI combustion control. Chapter 5

- † Design and implement a closed loop combustion controller to control the combustion phasing and the engine loads during transient engine operation. Chapter 5

The details about thesis organization are highlighted in Figure 1.2.

Chapter 2

Experimental setup and procedure

The chapter is divided mainly into two parts. The first part introduces the engine test setup, its control and data acquisition systems. The second part of the chapter concentrates on the testing procedures and the data analysis.

2.1 Engine setup

A stock GDI engine was modified and instrumented for operation in RCCI combustion mode. Figure 2.1 shows the test setup.

The engine specifications are shown in Table 2.1. The turbocharger on the engine was disabled and all the experiments in this thesis were performed at naturally aspirated

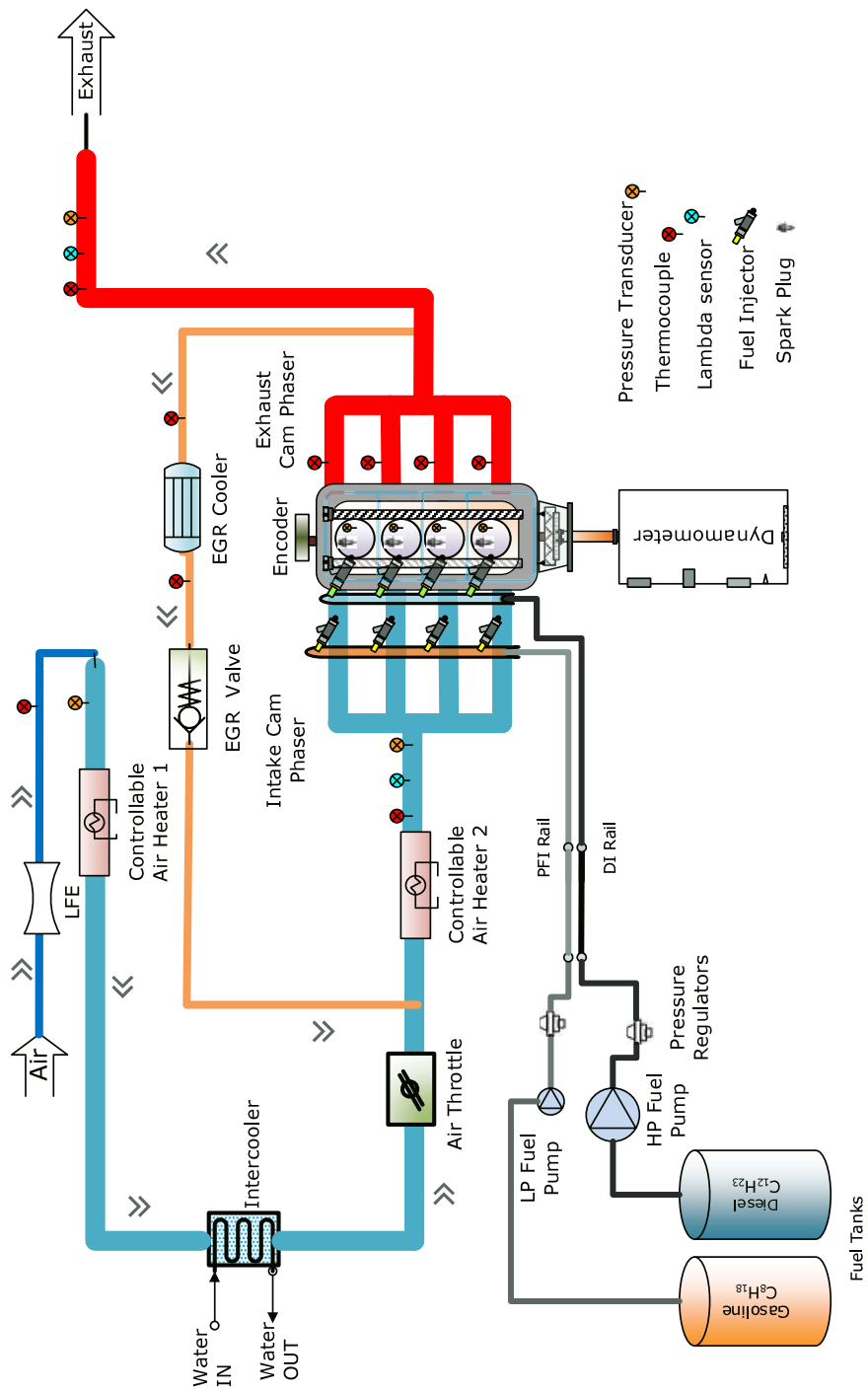


Figure 2.1: Engine Setup

Table 2.1
Engine specifications

Make	General Motors
Model	Ecotec 2.0 L Turbocharged
Engine Type	4 Stroke, Gasoline
Fuel System	Direct Injection
No of Cylinders	4
Displaced Volume	1998 [cc]
Bore	86 [mm]
Stroke	86 [mm]
Compression ratio	9.2:1
Max engine power	164 @ 5300 [kW@rpm]
Max engine torque	353 @ 2400 [Nm@rpm]
Firing order	1-3-4-2
IVO	25.5/-24.5 [°CAD bTDC]
IVC	2/-48 [°CAD bBDC]
EVO	36/-14 [°CAD bBDC]
EVC	22/-28 [°CAD bTDC]
Valve Lift	10.3 [mm]

conditions. Two in-line air heaters were also installed on the setup, to preheat the inducted air charge. The main modification and instrumentation carried out as part of this thesis, was on the port fuel injection and the Exhaust Gas Recirculation (EGR) system. Other details about the instrumentation and installation on the setup can be referred from previous works [2][21][22].

2.1.1 Fuel injection

RCCI mode is a dual fuel combustion mode where high reactivity fuel (Diesel) is injected directly in the cylinder whereas low reactivity fuel (Gasoline) is injected in the port. As shown in the engine specifications, Table 2.1, the stock engine has a direct injection fuel rail system. This stock high-pressure rail and injectors were utilized for the experiments. An external high pressure pump was used for the fuel delivery. Other than this, the intake manifold was modified for the port fuel injection [23]. The manifold was designed for injection of two different fuels, thus had two low-pressure rails. This was mainly done so that in-cylinder fuel blending can be carried out for HCCI combustion mode. For RCCI combustion only one low-pressure rail was utilized. The port fuel rail pressure was not regulated and kept constant at 3 bar. The calibration of the low-pressure injectors was done at this pressure. Details about the setup, calibrations and injector control can be referred from Kannan [24]. The amount of fuel injected from each rail depended on the total fuel quantity and the premixed ratio commanded. Premixed Ratio (PR) is defined as the ratio of energy contributed by the premixed port injected fuel (gasoline) to the total energy of the fuel [25]. It is represented by the Equation (2.1), where m_g and m_d are the mass of gasoline and diesel respectively, whereas LHV_g and LHV_d are the lower heating values for gasoline and diesel respectively. Based on this equation, a simulink model was built, which calculated the required fuel quantity to be commanded for both the

rails, DI and PFI. The details regarding the model can be referred from Kannan [24].

$$PR = \frac{m_g LHV_g}{m_g LHV_g + m_d LHV_d} \quad (2.1)$$

2.1.2 Exhaust gas recirculation

For the EGR, exhaust tail-pipe was tapped after the turbocharger, then carried via an EGR cooler and a valve to the intake line. The EGR line was connected after the throttle body and before the second intake air-heater. EGR was not cooled and was therefore used to heat the incoming air charge, to reduce the load on air-heater. Details about the setup are mentioned in the previous work by Kothari [21].

As part of this thesis, the control and measurement of EGR was designed and im-

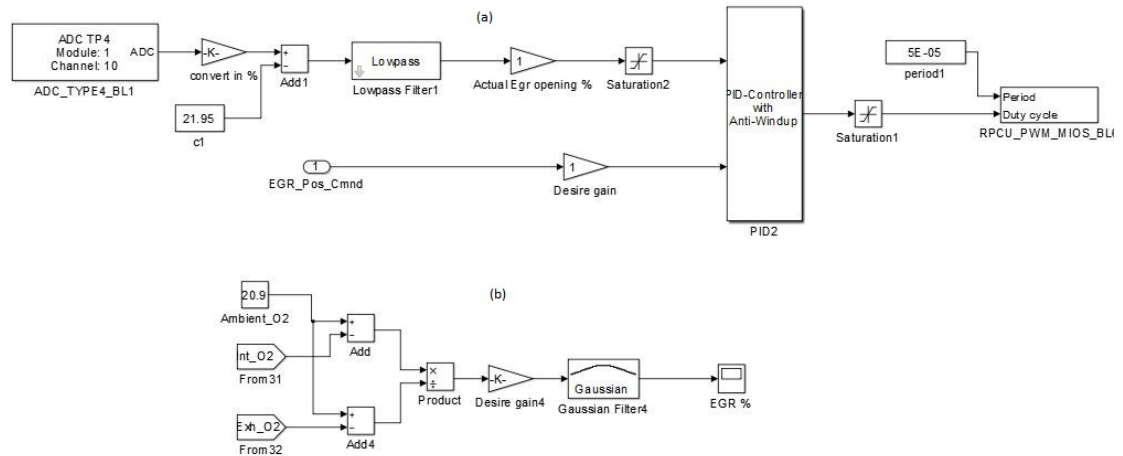


Figure 2.2: EGR setup (a) Control (b) Measurement

plemented. A Proportional-Integral (PI) controller was designed to control the valve opening. The details are shown in the Figure 2.2(a).

For measurement of the EGR fraction, Equation (2.2) was used, where X_{O_2amb} , X_{O_2man} and X_{O_2exh} are concentrations of oxygen in the ambient air, the intake manifold and the exhaust manifold, respectively [26]. For ambient air concentration, a value of 0.209 (-) was taken, whereas the concentrations of intake and exhaust were reported by λ (UEGO) sensors installed at the intake line and the exhaust tail-pipe. The simulink model for measurement is shown in the Figure 2.2(b). The details about the λ model can be referred from the previous work by Kothari [21].

$$EGR = \frac{X_{O_2amb} - X_{O_2man}}{X_{O_2amb} - X_{O_2exh}} \quad (2.2)$$

While carrying out the EGR study, the amount of exhaust gas recirculation possible was very low. There was no restriction offered post-exhaust, therefore the ΔP between exhaust and intake was very small. To increase the value of ΔP an external restriction was introduced by inserting a fixed orifice. With this, the amount of EGR fraction available throughout the operating range was around 15-20 %.

2.2 Data acquisition and control setup

Figure 2.3 shows the data acquisition and the control setup. dSPACE Microautobox was used to control the engine where as National Instruments system was used to control the dynamometer. As for the data acquisition, ACAP combustion analyzer captured the engine in-cylinder pressure signal and the crank angle encoder signal. The in-cylinder pressure was measured using PCB Piezotronics 115A04 transducer. Encoder products company's crank shaft encoder, model no. 260, was used to measure the engine angle, with resolution of 1 Crank Angle Degree (CAD). NI chassis was used to record the temperature data where as other operating conditions were recorded by dSPACE. The details about the command and feedback, to and from the devices, is shown in the Figure 2.3.

2.3 Test fuels

For all the steady state, parametric study and RCCI domain transient experiments, diesel was used as the high reactivity fuel and gasoline as the low reactivity fuel. For the RCCI-SI combustion mode switching, n-heptane was used as the high reactivity fuel where as iso-octane as the low reactivity fuel. Fuel specifications for n-heptane, iso-octane, diesel and gasoline are mentioned in the Table 2.2.

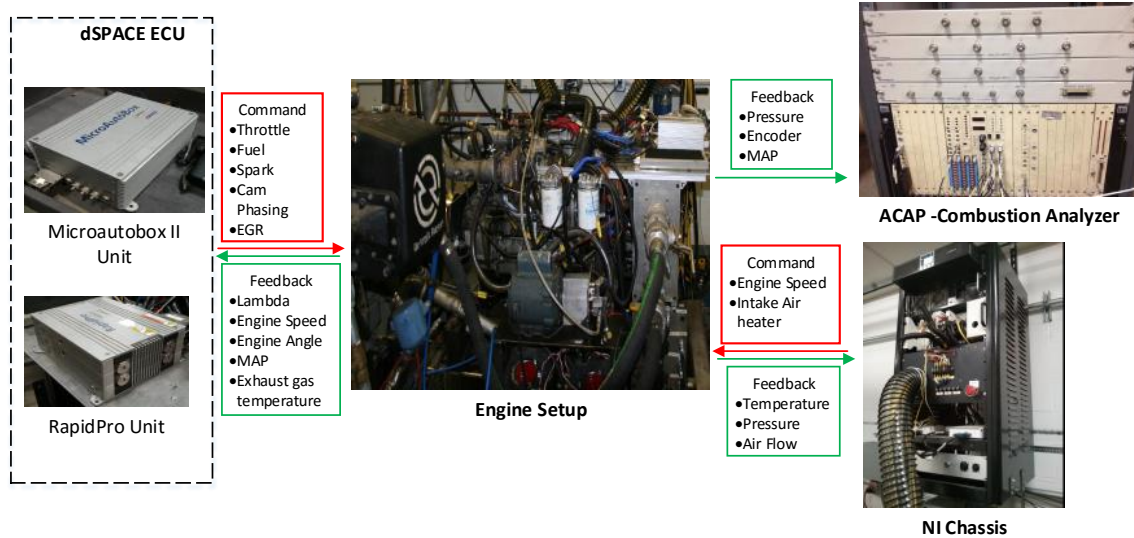


Figure 2.3: Data Acquisition and Control Setup

Table 2.2
Test fuel properties

Property	n-heptane [27]	iso-octane [27]	USLD-2 [28]	Gasoline [27]
Higher Heating Value[MJ/kg]	48.07	47.77	45.68	46.53
Lower Heating Value [MJ/kg]	44.56	44.30	42.89	43.45
Density [kg/m ³]	686.6	693.8	848	744
Octane Number [-]	0	100	48.7*	87**
H/C ratio [-]	2.29	2.25	1.833	1.93

*Cetane Index

** $(RON+MON)/2$

2.4 Test procedure and data analysis

This section explains the experimental test procedure and engine data analysis. The section concentrates on the steady state testing. For the transient tests, the explanation is included in their respective sections, along with its results.

2.4.1 Test procedure and matrix

For the steady state testing of the engine, fuel quantity sweeps were carried out from lean to rich limits, for a set of engine operating conditions. The lean limit was restricted as the operating condition where the COV_{IMEP} was less than 10% [29]. Similarly, the rich limit was restricted based on the Maximum Pressure Rise Rates (MPRR). An upper limit of 8 bar/CAD was set for MPRR, as beyond this audible engine knock started to occur for all the operating speeds [10].

For deciding the test matrix for engine mapping, there were 4 main operating conditions taken into account - fuel quantity, T_{intake} , engine speed and PR. Based on this a test matrix was designed for naturally aspirated engine operation and is shown in the Table 2.3.

For RCCI operation, other than T_{intake} , PR and engine speed there are two more factors that regulate the performance of the engine. Firstly, the fuel quantity and

Table 2.3
Test matrix for engine mapping

PR [-]	T_{intake} [° C]	Engine Speed [RPM]
20	40	800
	60	1000
	80	1200
	100	1400
		1600
		1800
40	40	800
	60	1000
	80	1200
	100	1400
		1600
		1800
60	40	800
	60	1000
	80	1200
	100	1400
		1600
		1800

secondly the Start of Injection (SOI) of high reactivity fuel. As already discussed, the fuel quantity was varied from lean to rich range. SOI timing was adjusted to attain a CA50 value of 5 - 10 CAD aTDC. This was done to achieve an optimum combustion performance [30]. After deciding on the SOI timing, a fuel quantity sweep was carried out at a baseline operating condition.

On a similar front, a steady state test matrix for EGR incorporated engine mapping was also designed. For the EGR experiments there was one more parameter involved, that was the EGR fraction. The test matrix is shown in the Table 2.4. Experiments with only PR 20 and 40 fuel blends were carried out, as the main aim of the study

Table 2.4
Test matrix for engine mapping with EGR

PR [-]	EGR Fraction [%]	T_{intake} [° C]	Engine Speed [RPM]
20	0	60	800
	5	80	1000
	15		1200
			1400
			1600
			1800
40	0	60	800
	5	80	1000
	15		1200
			1400
			1600
			1800

was to investigate the effects of EGR.

2.4.2 Data analysis

For combustion analysis the main parameter needed is the in-cylinder pressure signal synced with the engine crank angle. Other than this, operating condition values are needed. In the setup, as mentioned earlier in the Section 2.2, the pressure data was collected by ACAP combustion analyzer where as the operating condition data was collected by dSPACE and LabView.

A MATLAB script was written, which extracted and processed the raw data from the files recorded using the three data acquisition systems. The code processed the data and created a mat file that had all the needed calculated combustion parameters as

well the operating conditions. The script calculated various parameters like averaged in-cylinder pressure trace, IMEP, COV_{IMEP} , $\eta_{Th,Ind}$, η_{Comb} , ISFC, BMEP, BSFC, $\eta_{Th,Brk}$, CA10, CA50, CA90, MFB, MPRR, RI, PP, LPP, HRR and CHRR, η_{Vol} , etc. The details about the main calculations carried out by the code are shown in the upcoming sections.

2.4.2.1 Volume calculation

Combustion analysis requires value of volume (V) and change in volume (dV) at every crank angle, for calculating cyclic work, heat release and other combustion metrics. This was calculated using the Equation (2.3). This equation is derived from the engine geometry [31].

$$V = V_c + V_c \times \frac{1}{2} \times (r_c - 1) [R + 1 - \cos\theta - \sqrt{R^2 - \sin^2\theta}] \quad (2.3)$$

where, V_c is the clearance volume, r_c is the compression ratio, θ is instantaneous crank angle and $R = \frac{\text{Connecting rod length}}{\text{Crank radius}}$.

2.4.2.2 Pressure filtering

The pressure data synced with engine crank angle is the most important measurement for combustion analysis. For measuring the pressure, piezoelectric sensors were used. The piezoelectric sensor has a coherent issue of drift, as a result of which an absolute pressure reference needs to be provided to the signal. This was taken care by the combustion analyzer, by taking a reference from the MAP sensor, installed on the engine. Other than the aforementioned issue, pressure signal is also marred by the problem of noise. So before any data analysis is done, it is important that the filtering of the signal is carried out.

While carrying out the filtering of the pressure data, it is important that we do not remove the frequencies of interest. A spectral analysis was carried out, to find the cutoff frequencies for the filter, on the pressure data collected at different engine speeds. Based on that, a first order butter-worth filter was designed and used for the filtering.

For further improving the steady state analysis, averaged pressure signal over 100 engine cycles was used to reduce the effect of engine cyclic variations.

2.4.2.3 IMEP calculation

The IMEP is the engine's cyclic work done divided by the swept volume. It was calculated using the Equation (2.4), where V_{swept} is the swept volume over the engine cycle, P and dV are the instantaneous pressure and change in volume. The IMEP can be defined in two ways. Firstly, if the integral in the equation is carried over 0 CAD (End of Intake stroke) to 360 CAD (End of expansion stroke) then the IMEP is referred to as **Gross IMEP**. This just involves the work transfer during compression and expansion stroke. In the second case, where the integral is taken up-to 720 CAD, the complete engine cycle, the IMEP is referred as **Net IMEP**. The Net IMEP also takes pumping losses, that is the work done against piston during intake and exhaust stroke, into account. The testing was carried out at un-throttled and naturally aspirated conditions and thus does not have a lot of pumping work. Therefore, just the gross IMEP was calculated. Throughout this thesis, gross IMEP is referred as IMEP, else otherwise mentioned.

$$IMEP = \oint_0^\theta \frac{P(\theta)dV(\theta)}{V_{swept}} \quad (2.4)$$

where, $P(\theta)$ is the in-cylinder pressure and $dV(\theta)$ is the change in cylinder volume, at a given crank angle.

2.4.2.4 Heat release calculation

The heat release calculations are crucial for combustion performance analysis. The following Equation (2.5) was used for the heat release calculations, where the first two terms in the equation represent sensible energy change and work transferred to the piston and are termed as **Net heat release rate**, $\frac{dQ_{ht}}{d\theta}$ is the amount of heat loss to the walls and $\frac{dQ_{Crevice}}{d\theta}$ is the heat loss from the crevices. The crevice loss can be neglected [32].

$$\frac{dQ_{ch}}{d\theta} = \frac{\gamma}{\gamma - 1} P \frac{dV}{d\theta} + \frac{1}{\gamma - 1} V \frac{dP}{d\theta} + \frac{dQ_{ht}}{d\theta} + \frac{dQ_{Crevice}}{d\theta} \quad (2.5)$$

The main phenomenon for the heat loss to the surrounding is attributed to the convective heat transfer, which is represented by the Equation (2.6), where T is the instantaneous temperature of the charge inside the cylinder and T_w is the temperature of the cylinder wall. T in the Equation (2.6) was calculated using the ideal gas equation.

$$\frac{dQ_{ht}}{d\theta} = h_c(T(\theta) - T_w) \quad (2.6)$$

For calculating the h_c (heat transfer coefficient) in the Equation (2.6), a model was proposed by Woschini which was later modified by Chang [33] for LTC engines, owing to the fact that the total heat release in LTC engines happens at a higher rate compared to the conventional engines. The model is represented by the Equation

(2.7), where L is the instantaneous height of the cylinder and v_{tuned} is the mean gas velocity given by the Equation (2.8).

$$h_c = 3.4 * L(\theta)^{-0.2} T(\theta)^{-0.73} p(\theta)^{0.8} v_{tuned}^{0.8} \quad (2.7)$$

$$v_{tuned} = C_1 \overline{S_p} + \frac{C_2 V_s wept T_r}{6 P_r V_r} (P - P_m) \quad (2.8)$$

In the Equation (2.8) for mean gas velocity, $\overline{S_p}$ is the mean piston speed, P is the instantaneous pressure, T_r V_r P_r are the reference temperature, volume and pressure at the Intake Valve Closing (IVC) and P_m is the motoring pressure at that instant.

2.4.2.5 Mass fraction burn

For calculating the mass fraction burn, Rassweiler and Withrow [34] model was used, which is represented by the Equation (2.9), where x_b is the fuel mass fraction burn, P and V are the pressure and the volume at that crank angle, P_{soc} and V_{soc} are the pressure and the volume at the start of combustion and P_{eoc} and V_{eoc} are the pressure and the volume at the end of combustion. n_{comp} is the polytropic index of compression given by the Equation (2.11).

$$x_b = \frac{P^{1/n_{comp}} V - P_{soc}^{1/n_{comp}} V_{soc}}{P_{eoc}^{1/n_{comp}} V_{eoc} - P_{soc}^{1/n_{comp}} V_{soc}} \quad (2.9)$$

2.4.2.6 Polytropic index

For calculating combustion metrics like heat release, mass fraction burn, etc., value for γ is needed. Polytropic index value during compression is used for replacing γ [32]. Polytropic index is calculated using the Equation (2.11), which is derived from the Equation (2.10). Its value remains constant during compression and expansion, but changes during combustion.

$$PV^n = C \quad (2.10)$$

$$n = \frac{-VdP}{PdV} \quad (2.11)$$

2.5 Uncertainty analysis

With any measurement there are usually two factors involved, namely error and uncertainty. An error in measurement occurs owing to factors like human involvement, instrument wear and tear, etc. This can be minimized by adopting proper practices for measurement and calibrating the equipment at regular intervals. On the other hand, uncertainty is the confidence level of the instrument used for measurement, with which it reports the data. In this section, we look at the uncertainty involved in the measurement from a sensor and how it gets propagated to the calculation of other dependent parameters.

Table 2.5 shows uncertainty values pertaining to various measured inputs on the test setup. These measured inputs are defined as independent parameters.

Table 2.5
List of measured parameters and their associated uncertainties *

Parameter	Value	Uncertainty (\pm)
B [m]	0.086	0.001
S [m]	0.043	0.001
P _{In-cyl} [kPa]	2500 - 6000	1%
Crank Angle [deg]	0 - 720	1
T _{Int} [°C]	40 - 100	2 %
λ [-]	1 - 5.4	0.05
M _{Airflow} [g/s]	8.1 - 66.7	0.72 %
M _{Fuelflow} [mg/cycle]	7.4 - 48	0.1 %
P _{Manifold} [kPa]	95	0.5 %
T _{Exh} [°C]	215 - 450	2 %

(*Referred from Kannan [24])

The calculated dependent parameter, is represented in terms of independent measured parameters as per the Equation (2.12), where Y is the calculated parameter and X_i is the independently measured parameter [35]. For calculating propagation of uncertainty of independent parameters to the calculated parameters, Equation (2.13) is used, where U_Y is the propagated uncertainty and U_{X_i} is the uncertainty for i^{th} independently measured parameter involved in calculating Y [35].

$$Y = f(X_1, X_2, \dots, X_n) \tag{2.12}$$

$$U_Y = \sqrt{\sum_i^n \left(\frac{\partial Y}{\partial X_i}\right)^2 U_{X_i}^2} \quad (2.13)$$

Table 2.6 shows the uncertainty values for various calculated (dependent) performance parameters at a test condition, and the weight-age of various independently measured parameters, involved in each dependent parameter's uncertainty. The main source of uncertainty is found to be on part of the crank angle encoder with 1 CAD resolution.

Table 2.6
Uncertainty values for dependent parameters.*

	Value ±Uncert.	V_{Swept}	P_{In-cyl}	CAD	T_{Int}	λ	M_{Fuel}
					(%)		
IMEP [kPa]	383±31	17	0	83	0	0	0
ISFC [g/kWh]	376±28	0	0	98	0	0	2
$\eta_{Th,Ind}$ [%]	22.4±1.7	0	0	98	0	0	2
CA 50 [CAD aTDC]	21±1	0	0	100	0	0	0
EGR _{Fraction} [%]	19±0.3	0	0	0	0	100	0
T _{Max} [°C]	1264±74	0	6	93.4	0.6	0	0

(*Test reference EXP34–27)

An analysis for repeatability of the test setup was also carried out. All the test runs were carried out on the same day with different time stamps. The test condition is shown in Table 2.7. Table 2.8 shows the average and standard deviation values for three repeats, at the test condition in Table 2.7 .

Table 2.7
Test condition for the repeatability analysis

Parameter	Value
Intake Temperature (°C)	40
Engine Speed (RPM)	1000
Intake Pressure (kPa)	98
Fuel Qty (mg/cycle)	18
Premixed Ratio (-)	40
SOI (CAD bTDC)	33
EVC (CAD bTDC)	22
IVO (CAD bTDC)	25.5
Fuel(-)	n-heptane/iso-octane

Table 2.8
Test setup repeatability

Parameter	Average	Std Dev
Intake Temperature (°C)	40	1
Intake Pressure (kPa)	98	0
CA50 (CAD aTDC)	11	0
IMEP (kPa)	433	2
$\lambda(-)$	1.54	0
T_{max} (°C)	1280	2

Chapter 3

Engine mapping and parametric studies

The details about the steady state tests were described in the Section 2.4.1. In this chapter results are presented and discussed. The first part of the chapter will be concentrating on the engine maps, where as the last section will be describing the effects of various parameters, relevant in control of RCCI combustion.

3.1 Engine maps

In work by Kannan [24], steady state mapping of the current engine setup, using n-heptane (reactive fuel) and iso-octane was carried out. In this study, the engine mapping as mentioned previously, was carried out using conventional fuels, diesel (reactive fuel) and gasoline. As the study was being carried out on a GDI engine, with a stock compression ratio of 9.2:1, the efficiencies were not expected to be very high. The main concentration of the study was to understand various trends associated with RCCI combustion.

3.1.1 Mapping without EGR

This section, details the results from steady state tests as per the test matrix shown in the Table 2.3. For all the tests, SOI of the high reactivity fuel was adjusted to get a CA50 of around 5-10 CAD°aTDC [30].

Figure 3.1 shows the operating region for PR 20,40 and 60 fuel blends at intake temperatures of 40°C, 60°C, 80°C and 100°C for naturally aspirated conditions. It can be seen from the results, for any temperature condition, the maximum operating region is obtained for PR20. This is due to more reactive fuel being available, which acts as an ignition source for the charge [36]. Also for attaining the lower loads,

low PR values were needed. As the charge became lean, to sustain combustion, a higher reactivity fuel charge was required. This will be discussed further in this chapter. As the intake temperature was increased, the leaner limit increased for all the PR fuel blends. High temperature at Intake Valve Closing (IVC) results in a higher temperature at TDC, which aids autoignition [37]. The operating range over the higher engine speeds also increased, owing to the latter effect. Increase in TDC temperature reduces ignition delay [19][38], which in turn allows combustion to happen at the higher speeds, where the in-cylinder residence times are less compared to the lower speeds.

The four operating regions shown in Figure 3.1 were combined together by selecting the most optimum points, for a load at a given engine speed. The optimized maps are shown in Figure 3.2. As can be seen from the ISFC map, the optimum performance is achieved in the middle region, with the best operation shown by the blue island. This region mainly comprises of PR 40 fuel blend test runs. The low load range where the ISFC is higher are the test points at fuel blend PR20. When the PR value is low, combustion becomes more like conventional diesel, that is late fuel injection and highly stratified. Owing to this, mixing controlled or diffusion type combustion becomes prevalent, which in turn increases heat loss to the cylinder walls (due to heat release later during the expansion stroke) as well as reducing the combustion efficiency (due to improper mixing with air), thereby reducing the overall thermal efficiency [19]. For the higher loads, ISFC values increase. The test points comprising

this region are mainly operating at stoichiometric air-fuel ratios ($\lambda=1$). This reduces combustion efficiencies due to unavailability of air. Also, less dilution means higher in-cylinder temperatures, which eventually results in more heat loss to the cylinder walls. It can thus be concluded, for ideal operation of RCCI, the engine should be run at leaner charges as well as with higher PR fuel blends, to realize a more premixed type combustion [39]. The reactive fuel should only be injected in quantities such that enough reactivity gradient exists in the charge, to control the combustion phasing. The effects of PR as well other control parameters, are discussed in detail in the upcoming sections.

Figure 3.2(c) shows the variation of exhaust gas temperature over the combined optimized operating region. A trend for increase in temperature with increasing load over the speed range can be observed. The combustion efficiencies over the whole operating map were very low (50-80%). This could have caused the exhaust gas temperatures to go higher. From after-treatment system point of view, the points in lower load region will cause an issue for urea injection as well NO_x conversion efficiencies [12].

Figure 3.3 is an optimized map for $\eta_{Th,Ind}$ for the steady state tests carried out using n-heptane (reactive fuel) and iso-octane fuels. The performance metric in terms of efficiency is much better compared to the diesel-gasoline operation. Still, the trends are very similar. With this much difference in the performance, using different set of fuels, it is important to identify as to what are the main reasons causing

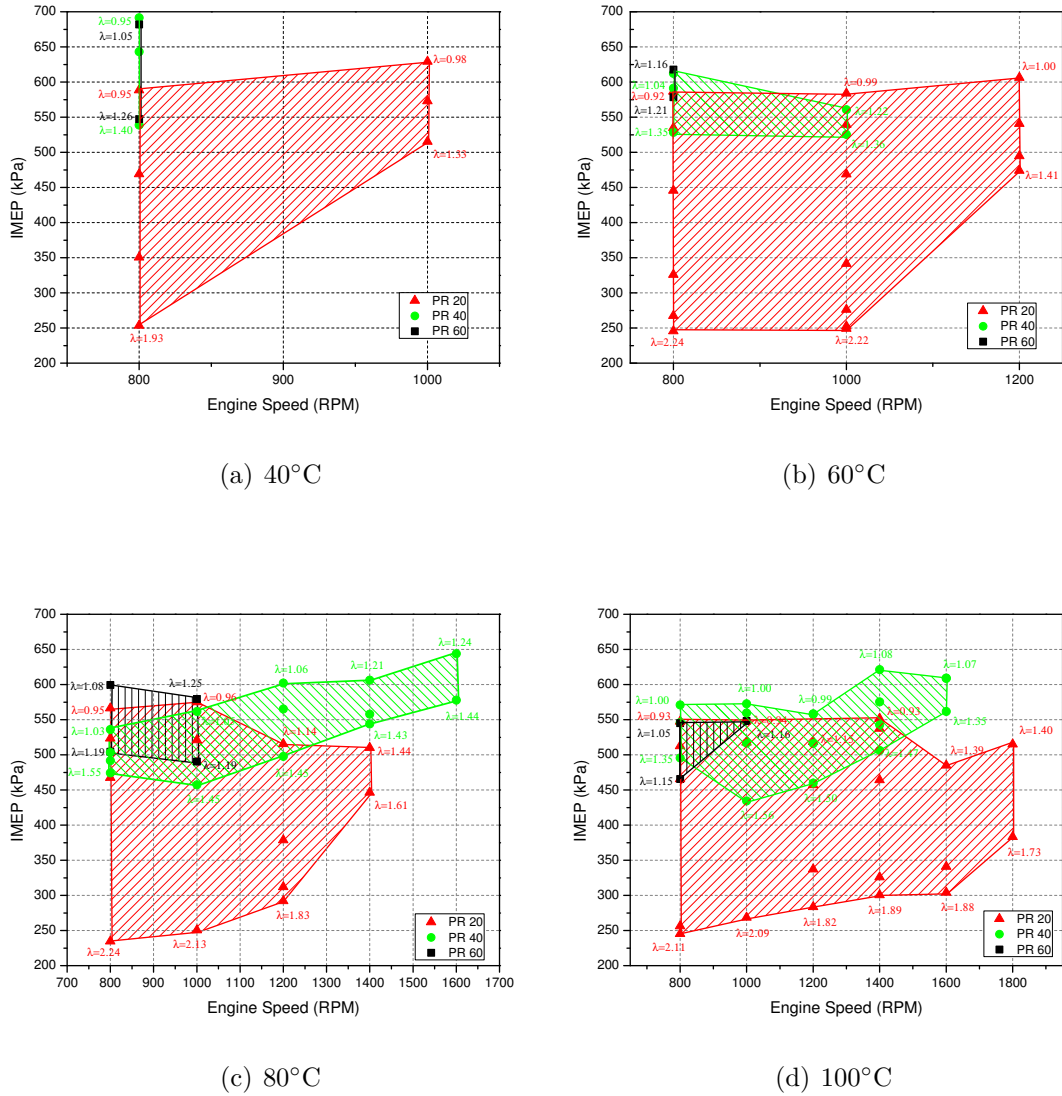


Figure 3.1: Operating region for different intake temperatures at intake pressure 95 kPa this. N-heptane and iso-octane have similar combustion characteristics [40] to diesel and gasoline and thus have been used for modeling purposes [41], with comparable experimental results [11].

The setup uses a GDI engine with stock injectors and rail, with an external high pressure pump. The tests were carried out at a DI rail pressure of 100 bar. Compared

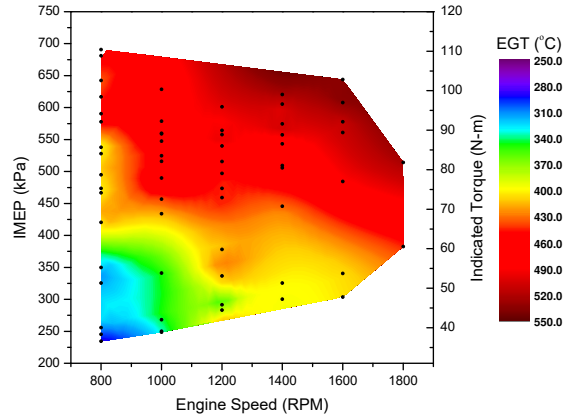
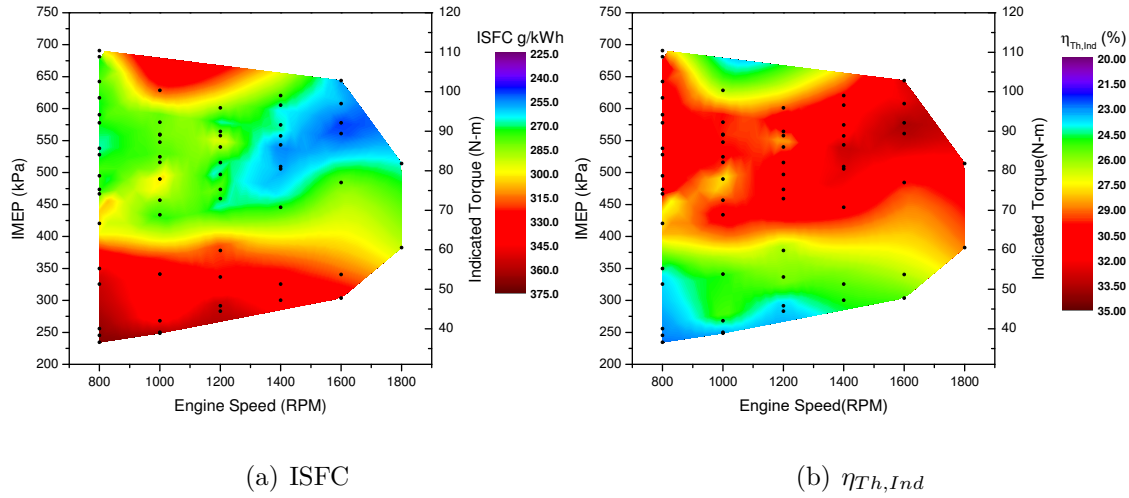


Figure 3.2: Engine map - intake temperature 40, 60, 80, 100 ($^{\circ}\text{C}$), MAP 95 kPa, PR 20, 40, 60 (-). Reference test conditions A.4 in appendix

to diesel, n-heptane is more volatile and thus mixes better with air [42]. To aid better mixing, the droplet size of diesel can be reduced. To achieve this, the fuel injection pressure can be increased. But, as we start to increase the rail pressure or reduce the droplet size, inertia of the droplet reduces too, which in turn reduces penetration of the diesel in the premixed gasoline charge [43]. Therefore, the rail pressure should be

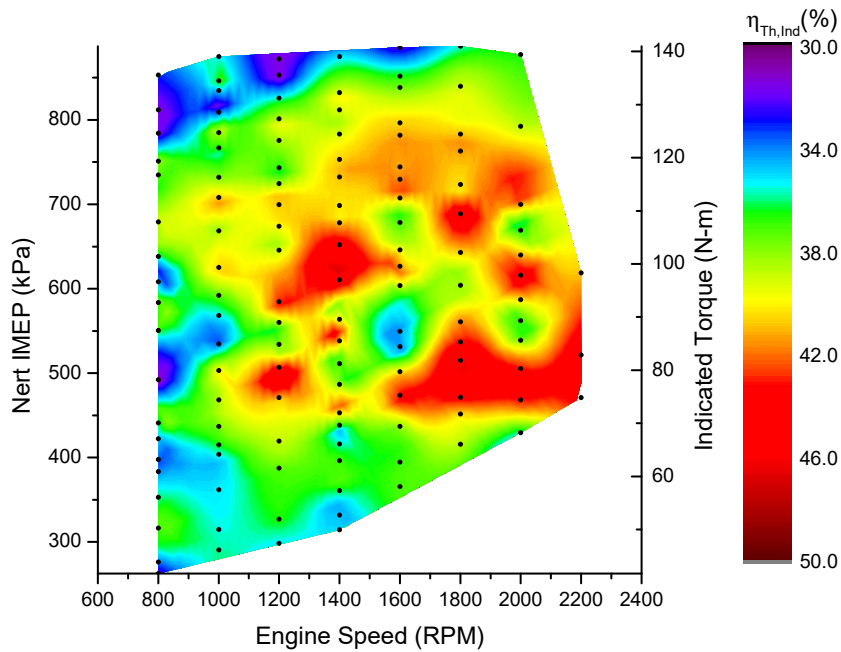


Figure 3.3: Engine Map - intake temperature 40, 60, 80, 100 (deg-C), MAP 95 kPa, PR 20, 40, 60 (-), n-heptane and iso-octane fuels (*Referred from work by Kaushik Kannan)

tuned to aid better mixing as well charge penetration of the fuel. In this thesis, the phenomenon was not studied due to limitation offered by the stock direct injection fuel system.

3.1.2 Mapping with EGR

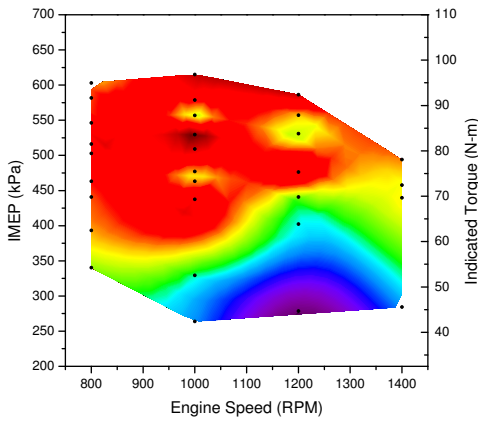
This section shows the results from steady state experiments, with the incorporation of EGR. The testing was carried out based on test matrix as shown in Table 2.3. The details about the EGR setup and measurement were mentioned in the Section 2.1.

In the test setup, as there was no turbocharger being used or any such restriction

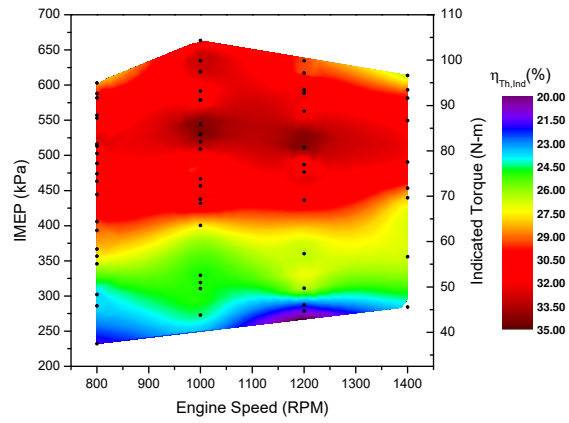
post-exhaust was offered, the exhaust manifold pressure was only 5-10 kPa higher than the intake manifold pressure. As the EGR flow was dependent on the difference between exhaust and intake manifold pressure, the amount of available EGR was very small. To counter this issue, a constant restriction was installed at the exhaust tail-pipe, so that the exhaust manifold pressure can be increased. Due to insertion of the fixed restriction, the volumetric efficiencies of the engine dropped by around 10%. Therefore, no results from the EGR steady state tests could be compared to the test results mentioned in the previous section. That is why testing was also carried out at 0% EGR fraction, so that we have a baseline map to compare with. The results are shown in Figure 3.4. The map optimization was carried out in the same way as it was done for the maps shown in the Section 3.1.1. As can be seen from Figure 3.4, that the engine operating range expanded for 0-15% compared to 0% EGR fraction. For lower loads, the range should not have expanded, as the EGR incorporation will have a negative effect on sustainable combustion. It was mentioned previously, that all the test runs in the optimized maps have a COV_{IMEP} less than 10%. Even though, at the lower loads (lean limit), with same fuel quantity as used for tests with EGR fraction 5 and 15%, test condition with EGR fraction 0% did give combustion, but with a higher COV_{IMEP} than the set limit. As the combustion efficiencies were very low, the re-breathed exhaust charge will have large amount of unburnt fuel/HC, which in turn will boost the lean operation limit. It has been shown that, above 1130°C

complete oxidation of the unburnt HC can occur [44]. Also oxidation of HC can occur for lower temperatures depending on the residence times [45], inside the cylinder. Even though, the LTC modes have comparatively lower in-cylinder temperatures due to dilution as well homogeneous nature, still some combustion of the unburnt HC is expected to happen, as they will have enough residence time when re-breathed into the cylinder. This effect is predominant at lower loads as the combustion efficiencies are very low compared to high loads, thus more unburnt HC will be re-breathed into the cylinder. Therefore, due to poor combustion efficiencies of the engine especially at lower engine loads, use of the EGR was advantageous. This won't be the case for the engines, where combustion efficiencies are very high.

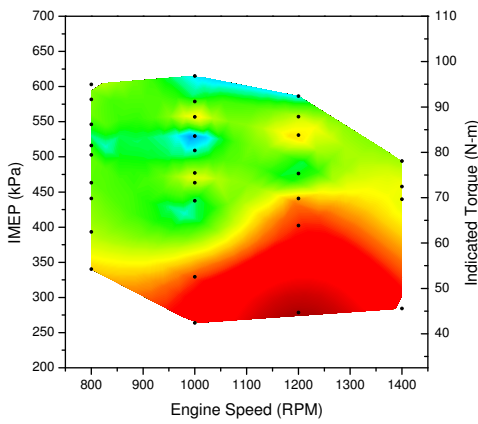
The rich limit expanded with the use of EGR. The increase in EGR fraction increases net specific heat capacity of the charge, which in turn reduces the in-cylinder temperatures and peak pressures. This reduction in the pressure allows to go to higher loads without getting any issue of engine knocking and high PRR. Also inducting more EGR allowed the SOI to be retarded (while maintaining CA50 between 5-10 CAD aTDC), which in turn allowed combustion to become more premixed, thereby improving thermal efficiency and thus the output. From the combustion performance point of view, a detailed study is shown in the Section 3.2.4. As for other trends, both the map without EGR (Fig 3.2(b)) as well as EGR incorporated map (Fig 3.4(b)) gave maximum efficiencies for the test runs with a higher PR fuel blend.



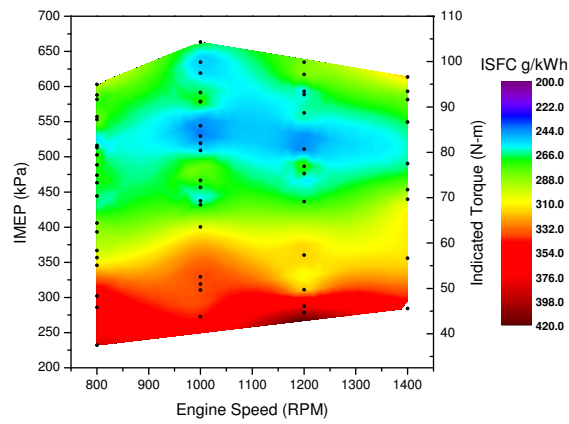
(a) $\eta_{Ind,Th}$ Map - EGR 0%



(b) $\eta_{Ind,Th}$ Map - EGR 0,5,15%



(c) ISFC Map - EGR 0%



(d) ISFC Map - EGR 0,5,15%

Figure 3.4: Engine maps - Intake temperature 60, 80 (°C), MAP 95 kPa, PR 20, 40 (-)

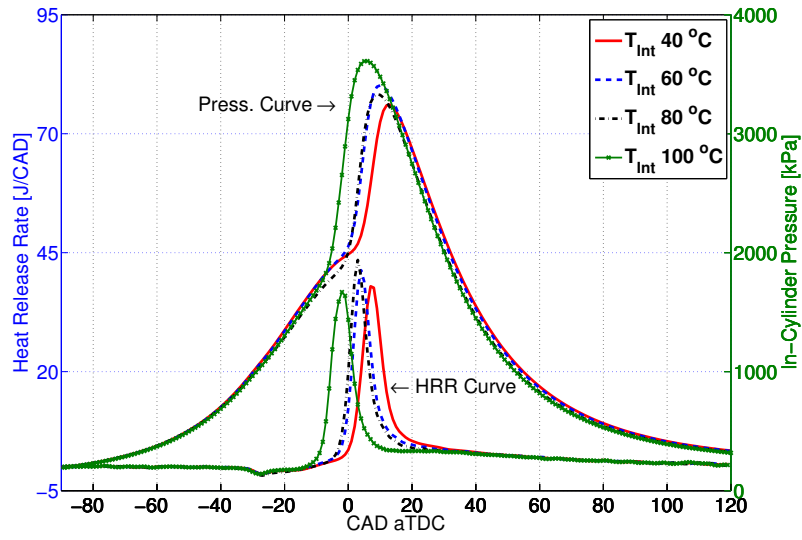
3.2 Parametric studies

3.2.1 Intake temperature

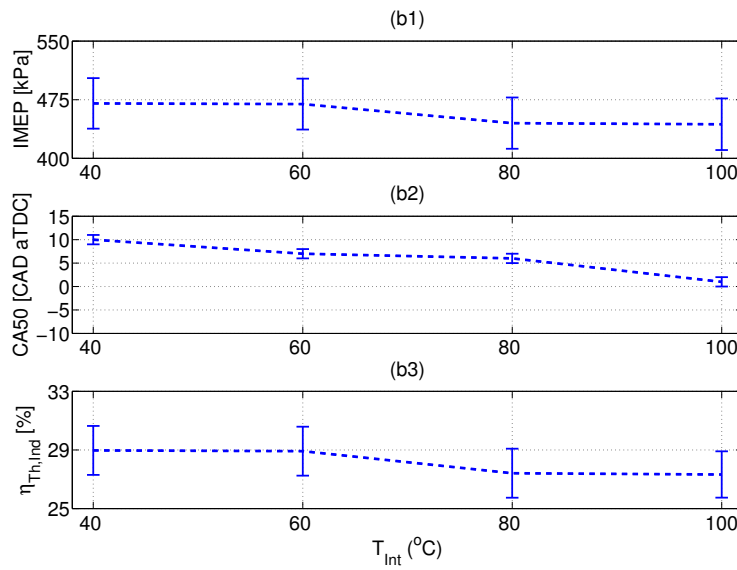
This section describes the effect of intake temperature on RCCI combustion. To isolate the effects of intake temperature in this study, experiments were carried out with fixed fuel quantity, PR and SOI. By keeping these factors constant, any effects that may be caused due to the fuel charge cooling effect, are neutralized. The conditions for the test are shown in Table 3.1. Figure 3.5 shows the effects of intake temperature on RCCI combustion.

Table 3.1
Engine test conditions to study the effect of intake temperature

Parameter	Value
Intake Temperature (°C)	40, 60, 80, 100
Engine Speed (RPM)	800
Intake Pressure (kPa)	95
Fuel Quantity (mg/cycle)	19
Premixed Ratio (-)	20
SOI (CAD bTDC)	30
EVC (CAD bTDC)	22
IVO (CAD bTDC)	25.5
Test reference (-)	EXP31 29, 55, 96



(a) HRR/Pressure vs CAD



(b) Effect on IMEP, SOI and $\eta_{Th,Ind}$

Figure 3.5: Effect of intake air temperature

As can be seen from the Figure 3.5(b2), that with increase in the intake temperature, CA50 gets advanced. As for the other combustion parameters, nothing much can be commented, as they strongly depend on the combustion phasing (CA50). To highlight

more on the later effect, we can refer to the Figure 3.5(a) and can observe as to how the heat release and the pressure curve gets shifted towards left. This clearly highlights the shift in onset of the start of combustion. Increasing the temperature of charge helps in achieving the autoignition earlier, by reducing the ignition delay [38][46]. This effect advances the combustion phasing. In RCCI, the start of combustion depends on the fuel injection quantity as well as injection timing of the reactive fuel. As the reactive fuel acts as an ignition source for the combustion initiation, therefore more reactive fuel % in the composition reduces ignition delay. On the other hand, the start of injection can affect the way mixing of directly injected (high reactive) fuel and premixed charge (air+low reactivity fuel) happens. Mixing of the charge affects local equivalence ratio, which in turn again controls the ignition delay [47]. Despite of the fact, that the injection timing was kept constant to neutralize the mixing effect, still the higher intake temperatures should aid better vaporization of diesel fuel and thus aid mixing. This effect will basically reduce stratification, thereby reducing the local equivalence ratio, which should increase the ignition delay [47] and thereby retard the combustion phasing. But as observed from the results, with increase in the intake temperature, phasing still gets advanced. Therefore we can conclude, the effect of intake temperature on reducing the ignition delay is more predominant compared to that of reduction in the charge stratification.

It is also important to look at other aspects of the increase in intake temperature. The experiments under study were carried out at naturally aspirated conditions. With

increase in the temperature at a constant pressure, the density of inducted charge decreases. Due to this effect, the mass inducted reduces. In this thesis, while going from an intake temperature of 40° C to 100° C, the intake charge reduced by 7%. This reduction in air quantity will affect the combustion efficiency. Also, reducing the air charge decreases the net specific heat capacity of the charge, which increases the peak in-cylinder temperatures and thereby aiding the NO_x formation. Other than these effects, the usage of intake charge heating won't be very helpful during transient operation, as the response for heating and cooling the charge is very slow. This effect was investigated (results not included in the study) during the transient study. Due to a very slow response, the intake temperature was kept constant during the transient operation.

We can conclude that the intake temperature can be used to control the combustion phasing as well help expand the low load range operation, by helping to achieve the autoignition temperatures for the lean charge. But other effects like the volumetric efficiency and the increase in in-cylinder peak temperatures, should also be taken into account.

3.2.2 Premixed Ratio

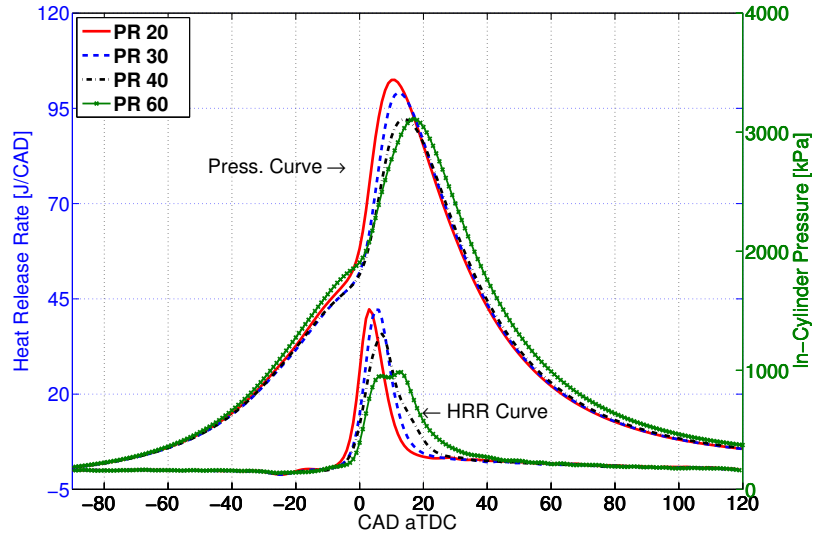
RCCI benefits from the fact that it offers a premixed combustion mode, which can be controlled by varying the reactivity of the fuel, utilizing an in-cylinder fuel blending

approach. Therefore it is important to study, how the ratio of fuel from DI and PFI affects the combustion process of the engine. In the current study a low Compression Ratio (CR) engine is used, owing to which low PR fuel blends were needed to achieve the charge autoignition. But despite this, the main concentration of the thesis was to observe, how good of a control parameter is the PR for controlling the combustion phasing. The experiments were carried out to capture the effect of PR. The

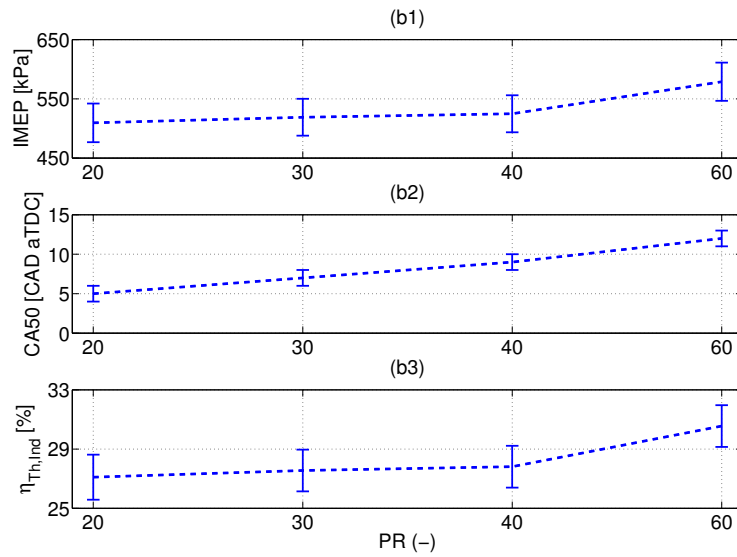
Table 3.2
Engine test conditions to study the effect of premixed ratio

Parameter	Value
Premixed Ratio (-)	20, 30 ,40 ,60
Engine Speed (RPM)	1000
Intake Pressure (kPa)	95
Intake Temperature (°C)	80
Fuel Qty (mg/cycle)	22
Start of Injection (CAD° bTDC)	30
EVC (CAD bTDC)	22
IVO (CAD bTDC)	25.5
Test Reference (-)	EXP31 149, 172, 163, 82

operating condition is specified in the Table 3.2. The results are shown in Figure 3.6. It can be seen from the results, that with increase in the PR, that is reducing reactive fuel, CA50 gets retarded. The main reason behind this can be attributed to the fact that with more diesel in the mixture, which initiates the ignition and thus providing with combustion front for the reactions to happen, is less in this case. Ra et al. [48] modeled the constant volume ignition delays for PRF fuels iso-octane and



(a) HRR/Pressure vs CAD



(b) Effect on IMEP, CA50 and $\eta_{Th,Ind}$

Figure 3.6: Effect of premixed ratio

n-heptane. The study showed that the ignition delay reduces with increase in the reactivity (more n-heptane). Therefore as the PR increases (reactivity reduces), the ignition delay increases too, which in turn retards the combustion phasing.

As mentioned before, the setup utilizes a low CR due to which a lower PR fuel blend

is needed. In case of higher CR engines, high PR values can be utilized. Ideally for RCCI combustion, the amount of reactive fuel should be injected in quantities so that enough reactivity gradient exists to control the combustion phasing. When the PR is high, combustion is highly premixed. This allows better mixing with air and hence result in higher heat release rates compared to conventional CI-mode, where lot of heat release happens in mixing-controlled environment (Diffusion type), which eventually causes a slow tail-type heat release profile later in the expansion cycle. This increases the heat loss to the cylinder walls, thereby decreasing the thermal efficiency. Also, better utilization of air gives higher combustion efficiencies. A detailed study was carried out by Kokjohn et al. [19] conforming the aforementioned factors. This effect was also observed in the optimized maps, where the best performance was achieved with the higher PR fuel blend test runs.

There is another parameter that can be used for controlling the phasing of reactions, the Start of Injection (SOI) of high reactivity fuel. Its effects are shown in the next section but it's worthwhile to mention here, that retarding CA50 due to increase in the PR can be optimized by advancing the SOI. Thus, it can be concluded that PR is a very effective parameter to control the combustion phasing as well optimize performance of the engine, especially in combination with SOI, as its control is independent of the resultant combustion constituents.

3.2.3 Start of injection

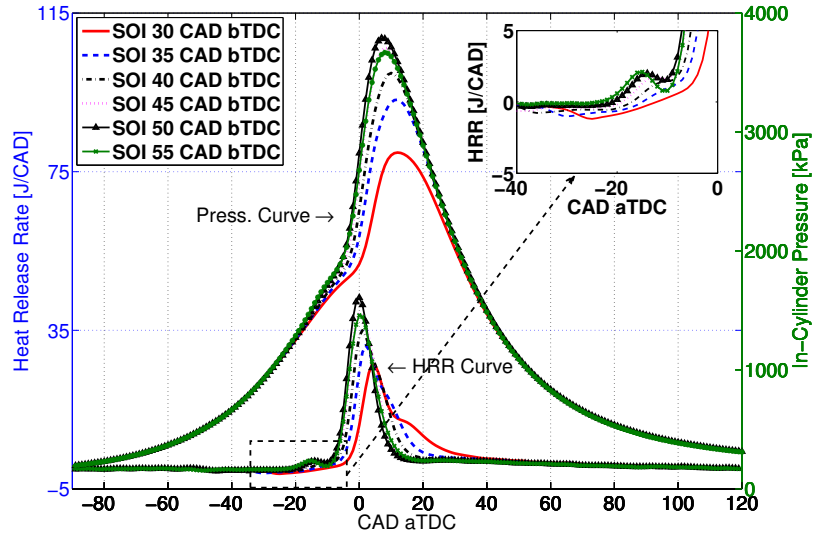
This section describes the effect of Start of Injection (SOI) of the high reactivity fuel on the RCCI combustion phasing. The experiments were carried out at a constant boundary condition with same PR and fuel quantity, to isolate the effects of SOI on combustion phasing and performance. The details are shown in Table 3.3.

The analysis results are shown in Figure 3.7. With advancing of SOI, the combustion

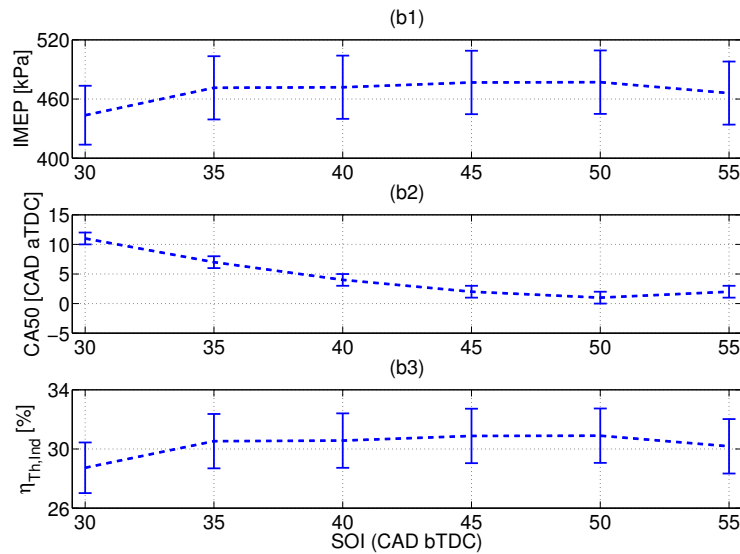
Table 3.3
Engine test conditions to study the effect of start of injection

Parameter	Value
Start of Injection (CAD bTDC)	30, 35, 40, 45, 50, 55
Engine Speed (RPM)	1000
Intake Pressure (kPa)	95
Intake Temperature (°C)	80
Fuel Qty (mg/cycle)	18
Premixed Ratio (-)	40
EVC (CAD bTDC)	22
IVO (CAD bTDC)	25.5
Test Reference (-)	EXP31 156, 157, 158, 159, 160, 161

phasing (CA50) advanced. Directly injected diesel fuel acts as the ignition source for the premixed gasoline charge [36], therefore advanced injection will cause the start of combustion to occur earlier. Also with an advanced SOI, Low-Temperature Heat Release (LTHR) increases, which raises the in-cylinder temperatures, thus onsetting the start of High Temperature Heat Release (HTHR) reactions, as seen in Figure



(a) HRR/Pressure vs CAD



(b) Effect on IMEP, CA50 and $\eta_{Th,Ind}$

Figure 3.7: Effect of start of injection

3.7(a). It can be observed that, by advancing the SOI beyond 50 CAD bTDC, the combustion phasing retarded. As the diesel gets more time to mix with gasoline premixed charge, the stratification reduces (local equivalence ratio reduces). This

increases the ignition delay and thereby retard the combustion phasing [47].

Another important trend can be seen in Figure 3.7(b1), for the IMEP. It follows the same trend as CA50 and increases with the advancing SOI. Advancing the SOI aids more premixed type combustion, which as discussed in the previous section, gives better thermal and combustion efficiency. In addition to that, as can be seen from the Figure 3.7(b1), IMEP does not improve drastically beyond 35 CAD bTDC. This is mainly because, more shift of the combustion phasing towards the TDC or before the TDC incurs negative work against the piston, which reduces the work output. Also the engine knocking starts to increase. Therefore, an optimum SOI strategy needs to be employed, considering noise constraints, performance and controllability in mind. But nonetheless, we can observe from the above findings that SOI is a very good control knob for controlling the combustion phasing (CA50).

Further effect of the SOI is shown on the combustion phasing (CA50) for different

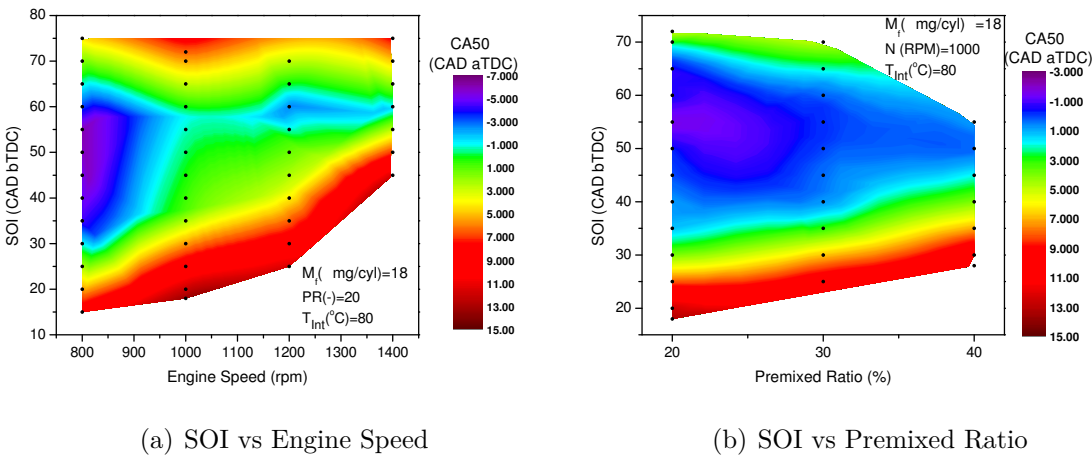


Figure 3.8: Maps for effect of start of injection

engine speeds at same PR value and fuel quantity in the Figure 3.8(a), and with different PR values for constant engine speed and fuel quantity in the Figure 3.8(b). The same trend is observed at different engine speeds as well at different PR values, as explained previously in this section.

3.2.4 EGR fraction

This section discusses regarding the effect of EGR on the combustion phasing and performance. In this study, effect of EGR is shown in two ways. Firstly, its effect on the combustion phasing. The details about the operating conditions are shown in Table 3.4, where the SOI was kept constant. In the second case, to look at the advantages of EGR fraction with respect to combustion performance, combustion phasing was kept constant.

Figure 3.9 shows the results for the first case. One can observe that, with the increase in EGR fraction, the combustion phasing gets retarded. More EGR fraction, that is reduced oxygen concentration, increases the ignition delay, which in turn retards the combustion phasing [46]. So, the EGR can be used to control the combustion phasing. But issue with the EGR is, that its constituents depend on the combustion itself. For the control purpose, we need a knob which is independent of the combustion like PR and SOI. EGR does not provide this feature and will cause difficulty for control, especially during the transients. Another test was carried out for looking at how

EGR can be used to improve the combustion performance. The test conditions are included in Table 3.5.

Table 3.4

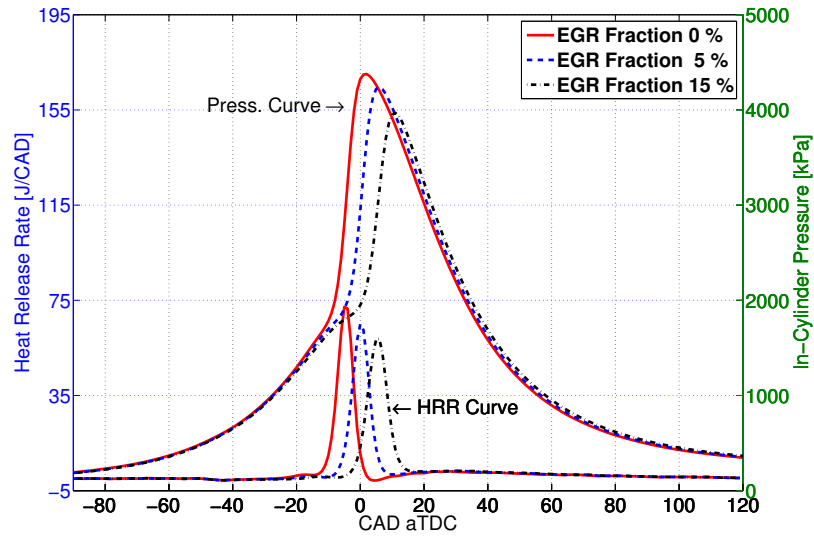
Engine test conditions to study the effect of EGR fraction with a fixed SOI

Parameter	Value
EGR Fraction (%)	0, 5, 15
Engine Speed (RPM)	1200
Intake Pressure (kPa)	95
Intake Temperature (°C)	80
Fuel Qty (mg/cycle)	21
Premixed Ratio (-)	40
Start of Injection (CAD bTDC)	50
EVC (CAD bTDC)	22
IVO (CAD bTDC)	25.5
Test Reference (-)	EXP32 165,164,163

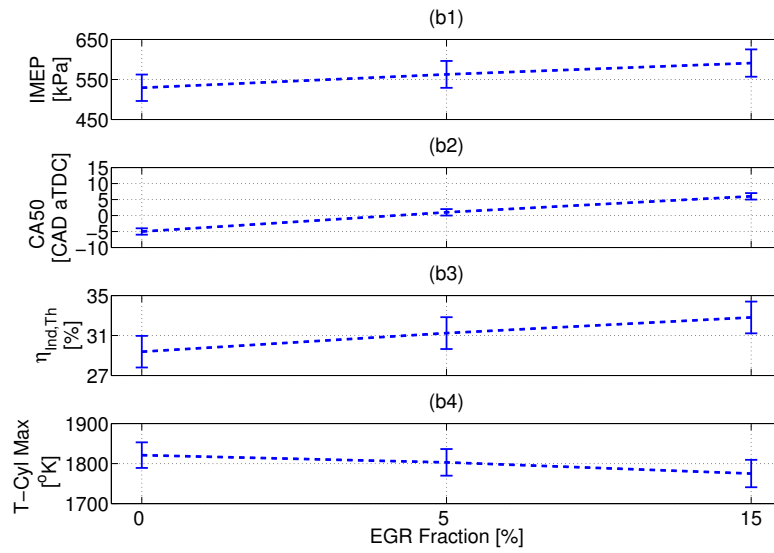
Table 3.5

Engine test conditions to study the effect of EGR fraction with fixed CA50

Parameter	Value
Load (Bar)	3.6
EGR Fraction (%)	0, 5, 15
Engine Speed (RPM)	1400
Intake Pressure (kPa)	95
Intake Temperature (°C)	80
Premixed Ratio (-)	20
CA50 (CAD aTDC)	14±1
EVC (CAD bTDC)	22
IVO (CAD bTDC)	25.5
Test Reference (-)	EXP32 95,97,102



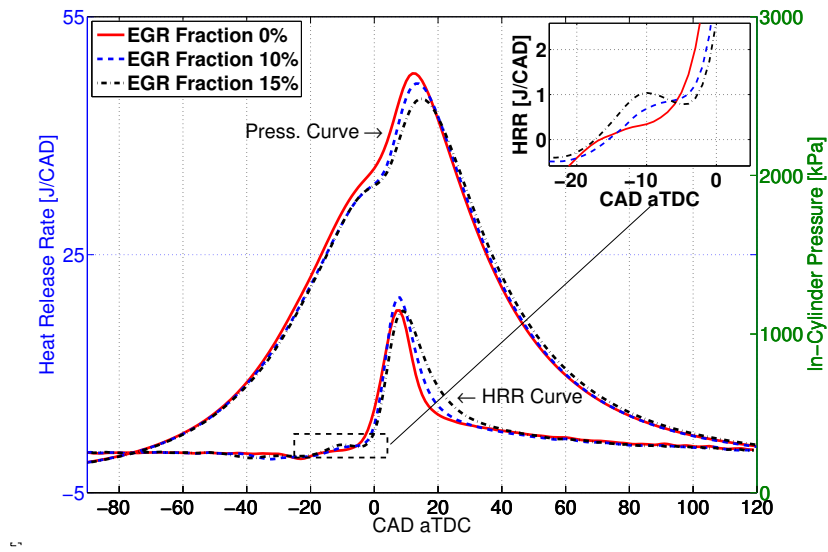
(a) HRR/Pressure vs CAD



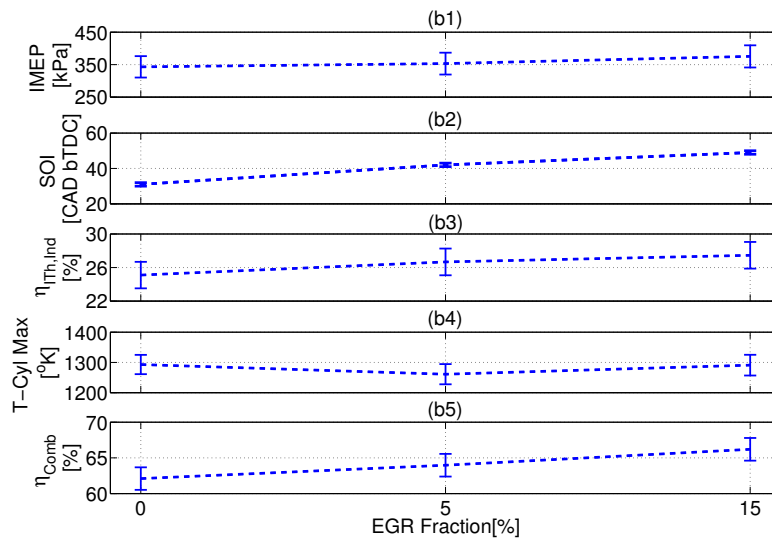
(b) Effect on IMEP, SOI, $\eta_{Th,Ind}$ and maximum in-cylinder temperature

Figure 3.9: Effect of EGR - SOI same

In this test, runs at similar loads and same CA50 were compared. With increasing in the EGR fraction, SOI was advanced, so as to keep the CA50 constant. For similar loads, maximum EGR fraction test condition gave the best $\eta_{Th,Ind}$, as is shown in



(a) HRR/Pressure vs CAD



(b) Effect on IMEP, SOI, $\eta_{Th,Ind}$, maximum in-cylinder temperature and η_{Comb}

Figure 3.10: Effect of EGR - CA50 same

Figure 3.10(b3). Increase in the EGR fraction delays the autoignition, therefore allowing advanced injection of the diesel fuel, which results in a more premixed type combustion. Additionally, with this advanced SOI, LTHR increases, as seen in Figure

3.10(a), which further aids the mixing of diesel with the premixed charge. This premixing helps to improve the combustion efficiency. Other important factor that can be noted here is the effect on emissions. In the CI-mode, the main cause of NO_x and soot emissions is combustion of a stratified charge, where occurrence of local rich regions which either cause high in-cylinder temperatures that increases the NO_x formation or increases the formation of soot. This can be seen in the Figure 1.1. In the case as mentioned above, with advancing of the SOI, stratification reduces, which thereby reduces the local rich regions and thus reducing soot and NO_x emissions [16]. Also it is important to note that, increasing the EGR fraction will reduce amount of oxygen, therefore at higher loads use of EGR will reduce combustion efficiency. This has been one of the limitations for RCCI high load operation, where more reliance on EGR to avoid engine knocking or high PRR, eventually leads to lower combustion efficiencies and higher HC and CO emissions. From a control prospective, being a quantity that depends on combustion, EGR is not a good combustion phasing control parameter compared to SOI and PR, especially during the transients.

Chapter 4

Transient study and combustion mode switching

RCCI combustion offers high thermal efficiencies with very low NO_x and soot emissions, as highlighted in the Chapter 1. Despite of these benefits, the challenges to realize RCCI combustion are its controllability and full-load range operation. For overcoming the challenge of control, we need to develop strategies which can respond to the changes by varying control knobs as discussed in Chapter 3, to achieve optimum combustion performance. As for the full load range operation, the engine can be switched over to a conventional DI or SI combustion mode. Techniques like this have been previously applied to HCCI combustion [49]. As in this study, experiments were carried out on a GDI engine, therefore an RCCI-SI combustion mode switch

was carried out. A study by Dempsey and Rietz [50] shows RCCI operation for a low CR of 11.6 at low and high loads (4-23 bar), with low NOx and soot formation and at the same time achieving comparable brake thermal efficiencies to that of a higher CR (16.1) RCCI engine operation. Also the higher loads were achieved using low compression ratio. As part of future work, the current setup CR of 9.2:1 is also planned to be changed to 12.3, therefore the study done in this thesis will be more relevant to that engine setup.

In realizing both the targets mentioned above, we need to control certain parameters which in turn are controlled by actuators. The first section in this chapter addresses various actuators and their responses that are relevant to the study. Also, a transient study has been carried out for observing the various trends during a step change, while operating in RCCI mode. Other than this, as previously discussed, to realize a full-load range operation, RCCI-SI combustion mode switching is done. The results are shown in the following sections.

4.1 Actuator dynamics

As mentioned before, the understanding of actuator dynamics is important for realizing successful combustion control strategies. Most of the actuators are mechanical, electrical or a combination of both. Every such device will have a response time to a certain input (step, impulse or ramp). For controlling the engine, ideally whenever an

actuator is commanded, it should reach the set point before the start of next engine cycle. But that is usually not the case. Any effective control strategy that is to be implemented on the engine needs to take care of this delayed response of actuators, especially during the transients, by predicting the effects that will be caused due to that actuator's delay. Therefore, as part of this thesis, actuator dynamics are characterized. Table 4.1 shows the various actuators available on the setup that are used for controlling RCCI and SI modes of combustion. For sending signals to the actuators, power electronics are involved, which can respond to the changes in an order of microseconds, so the delay caused due to them is neglected in the study.

Out of the actuators mentioned in Table 4.1 , effect of spark plug, air heater and fuel injectors have not been studied. The use of spark was involved in switching to the SI mode. To counter any delay due to them, their actuation was started 10-15 cycles before the start of SI mode (timing was kept such that it does not affect combustion). The fuel dynamics is one of the most important dynamic involved during transients but due to setup limitations it was not characterized in this thesis. Other than this, all the experiments were carried out at a constant intake temperature, thus not accounting for any delays due to the response of intake air heater. The response for the following actuators is characterized in this thesis:

1. Throttle
2. Cam phasors
3. Supercharger

Table 4.1

List of available actuators for controlling the engine operating conditions

Actuator	Control parameter
Throttle	Air flow
Cam phasors	Valve timing
Spark plug	Ignition timing
DI Fuel injector	Diesel fuel quantity
PFI Fuel injector	Gasoline fuel quantity
Intake air heater	Intake charge temperature
Supercharger	Intake charge pressure

4.1.1 Throttle

As mentioned in Section 4, that for realizing full load range operation it is necessary to switch the engine to SI mode. For RCCI mode, the operation is un-throttled but when the engine is switched to SI Mode, it will be going to a part load range of the mode and thus needing for the throttle to be partially closed.

Now, in case if the throttle response is too slow, we will run into issues of misfire or partial burns. In the first cycle, where the switch is activated, the engine controller based of a fuel map, will feed forward a value for fuel quantity based on the load requirement. Basically, the throttle opening will control the amount of air flowing into the engine. If it does not close to a required value by the next engine cycle, resulting air fuel mixture can be too lean to cause misfire or partial burn. This effect will magnify with increase in the engine speed. So as a requirement, the throttle should come to its position within 1-2 engine cycles of the switch being activated.

Keeping this in mind, the throttle response was improved, as shown in the Figure 4.1. A Proportional-Integral (PI) controller was designed for the throttle control with gain scheduling.

The throttle is a spring loaded butterfly valve, actuated using a DC Motor, which can be rotated in the either direction. The parking position of the throttle was found to be around 30% in terms of throttle opening. So above 30% the spring will get extended, whereas below 30% it will get compressed. So as expected, the behavior of throttle body above and below 30% was different. Initially, same set of PI gains were used for both the ranges of the throttle, and was found that the amount of resistance offered by the spring when it was being compressed was too high as compared to when it was getting extended Figure 4.1(a). So to attend this issue different PI gains were used for the both regions. A much aggressive PI controller was designed for the range of 0-30% throttle opening, compared to 30-100% throttle opening.

Response function for the throttle can be well described by a first order system given by Equation (4.1), where τ is the time taken to achieve 63% of the targeted value. The response time is not expected to change with speed between two set levels, even though it will be different for various set points. In this study as our main concentration was going from Wide Open Throttle (WOT) to partial opening, therefore the throttle response was characterized as shown in Figure 4.1. For an engine speed of 3000 RPM, engine cycle time (720 CAD rotation) will be 40 ms. In that case throttle will take up-to three engine cycles to come to its final position. In situations like these,

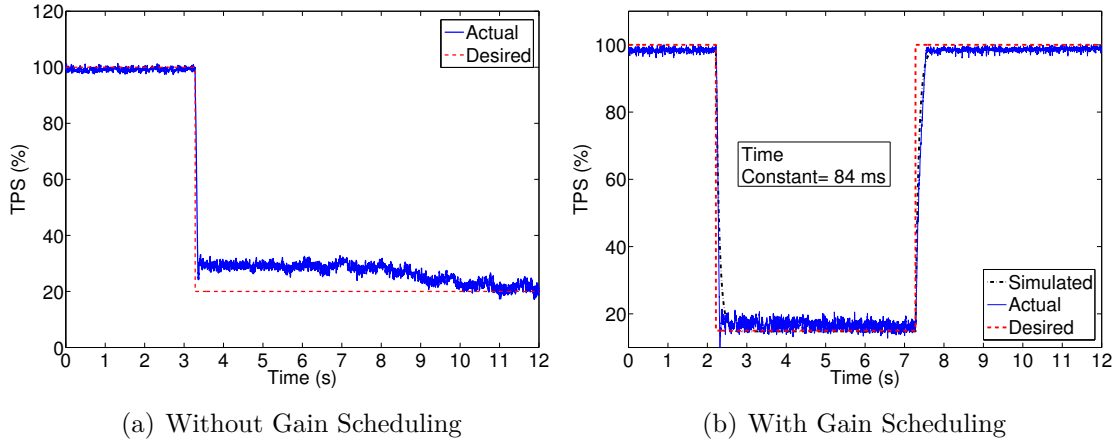


Figure 4.1: Throttle step response

the combustion controller strategies should counter this settling time of the throttle. This will be highlighted more while discussing RCCI-SI combustion mode switching.

$$G(s) = \frac{Output(s)}{Input(s)} = \frac{1}{\tau s + 1} \rightarrow \tau = 84 \text{ ms} \quad (4.1)$$

4.1.2 Cam phasor

Cam phasing is another control parameter involved in realizing LTC combustion. For all the tests in RCCI mode, cam phasing was kept constant, thus no actuation response was relevant. It was more relevant for RCCI-SI mode switching, as the cam phasing was different for the both modes. Cam phasing is used for exhaust gas trapping, to increase the charge temperature and thus help LTC combustion modes.

The engine setup in this study has a stock valve train with a fixed valve lift of 10.3 mm. For the LTC modes, charge trapping is done by negative valve overlapping, but due to this valve lift not much effect was observed. Instead, the Intake Valve Opening (IVO) was kept at the extreme position for RCCI modes, such that the intake valve closes just before intake BDC. This was mainly done to increase the effective compression ratio, thereby aiding TDC pressures. Figure 4.2 shows the response of intake valve to a step change. The response is divided into three sections and is represented by

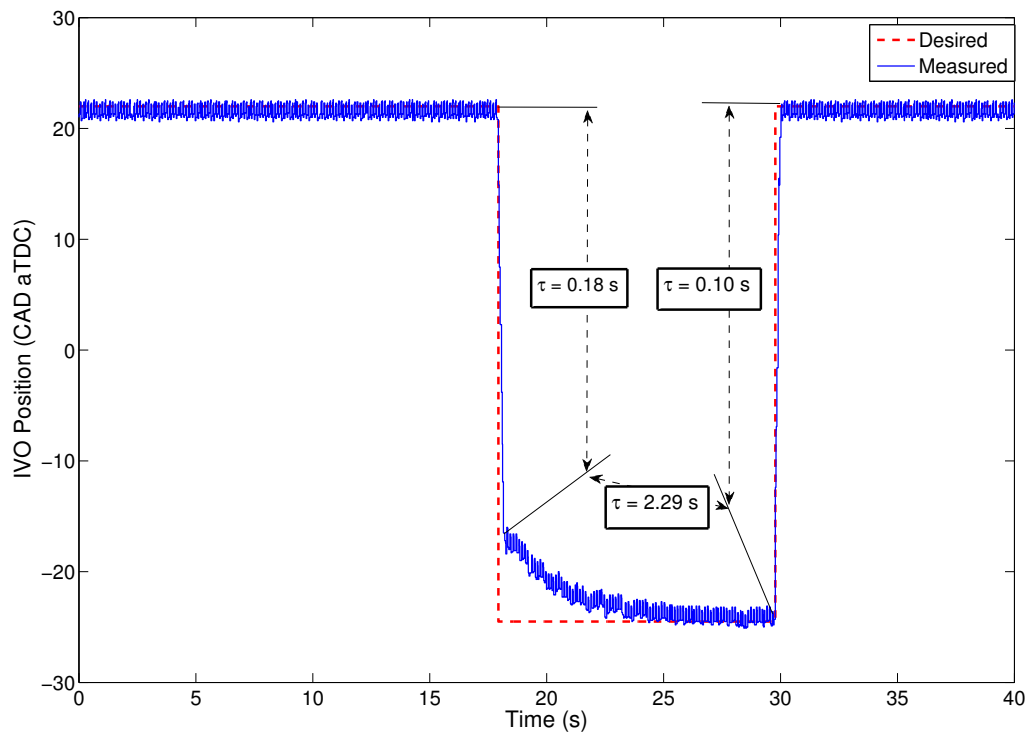


Figure 4.2: Intake cam phasor step response

the Equation (4.1). The time constants τ are highlighted in Figure4.2. The response during actuation from -20 to -24.5 CAD aTDC is too slow. This needs a better

investigation. The effect due to this delayed response is observed during RCCI-SI mode switch.

4.1.3 Supercharger

In the test setup, boosted conditions were achieved using an external supercharger. It is an electric motor, belt-driven, Eaton M62 supercharger. The specifications of the setup is given in Table 4.2. More details can be found in the previous work by Saigaonkar [2]. In this thesis, no tests were carried out at boosted conditions, but being a relevant control parameter, response was characterized for the actuator. To measure the response, couple of test conditions were carried out. Firstly, a switching from one boosted condition to another at a constant engine speed. Secondly, switching the engine speed at a constant boosted condition.

$$G(s) = \frac{Output(s)}{Input(s)} = \frac{1}{(\tau_w s)^2 + 2\zeta\tau_w s + 1} \quad (4.2)$$

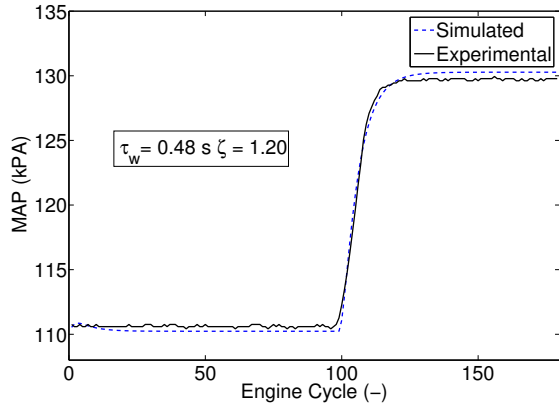
For capturing the effect of supercharger response for achieving the boost levels, tests were carried out at different engine speeds. The engine was motored. For characterizing the response of the supercharger, a 2nd model system was utilized and is represented by the Equation (4.2), where τ_w is the time constant representing 10-90% rise time and ζ is the damping factor. Matlab system identification toolbox was used

Table 4.2
Supercharger setup [2]

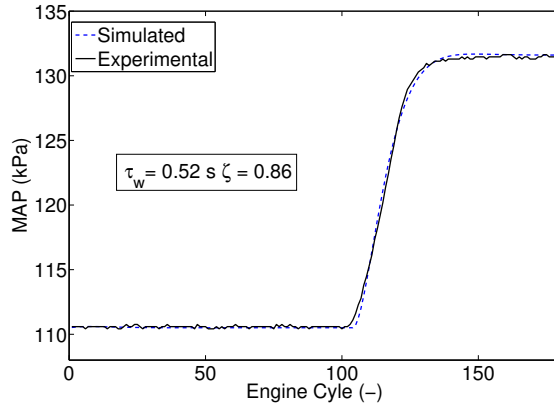
	Parameter	Specs
E-Motor	Make	Louis Allis Co
	Type	Induction (3 Phase)
	Rated Power	20 (hp)
	Rated Speed	3515 (RPM)
	Voltage Rating	220/440 (V)
	Current Rating	60/25 (A)
VFD	Make	Durapulse GS34040
	Model	GS34040
	Max power output	40 (hp)
	Rated output current	60 (A)
	Ramp up time	10 (s)
	Ramp down time	20 (s)
Supercharger	Make	Eaton
	Model	M62

for system characterization. The system response was found on an engine cycle basis and then later converted to the time domain (sec), to get a comparison between the two test conditions at different engine speeds. The results are highlighted in the Figure 4.3. It is important to note that the supercharger dynamics comprises of dynamics of the electric motor, air flow and the supercharger. The speed of the electric motor is controlled by a Variable Frequency Drive (VFD).

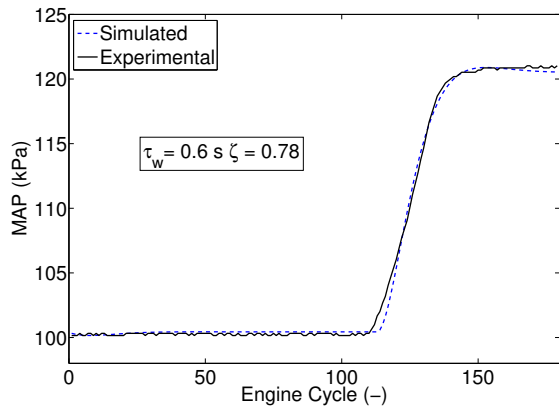
Figure 4.4 shows the map of supercharger, at different boost levels for the engine speed vs motor frequency. At a constant engine speed, change in the motor speed, for a boost of 10 kPa decreases as we go towards higher MAP or boost. This trend



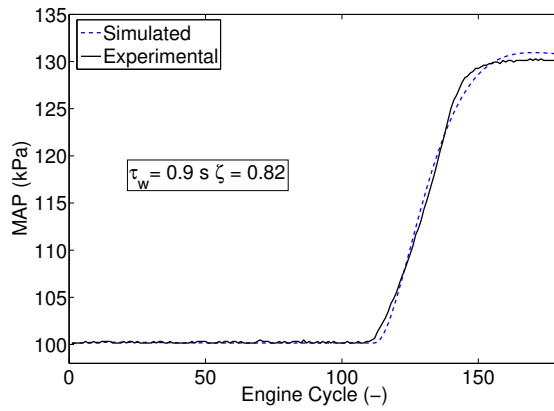
(a) 110-130 kPa/1000 RPM



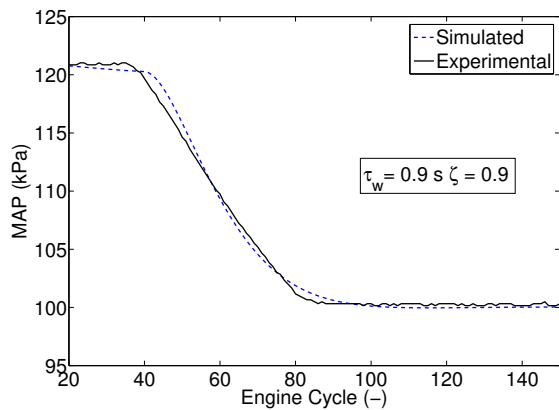
(b) 110-130 kPa/1600 RPM



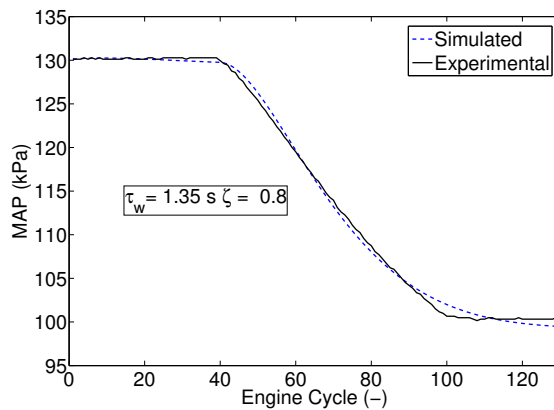
(c) 100-120 kPa/1600 RPM



(d) 100-130 kPa/1600 RPM



(e) 120-100 kPa/1600 RPM



(f) 130-100 kPa/1600 RPM

Figure 4.3: Supercharging dynamics: engine boost step-up and step-down response at constant engine speeds

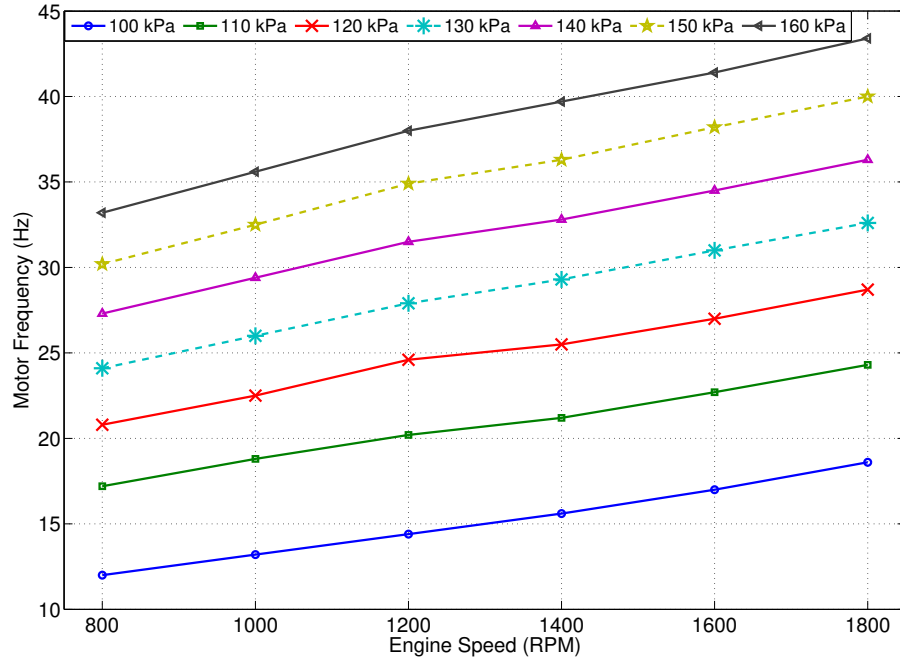


Figure 4.4: Supercharger map: engine speed vs motor frequency

is similar at all engine speeds. This can also be observed from the Figure 4.3(b) and (c), as τ_w for 110-130 kPa switch is less than that for 100-120 kPa. Other observation that can be made from the supercharger map is, the difference between motor speeds at two different boost levels for different engine speeds remains almost constant. For this we can refer to the Figure 4.3(a) and (b), where value of τ_w changes a little bit. Now for the last comparison, we can observe from the supercharger map, that with increase in the boost pressure from a certain lower level for a constant engine speed, the motor speed difference also increases. Figure 4.3(c) and (d) shows this effect, as τ_w increases for 100-130 kPa case compared to 100-120 kPa case. This is because the acceleration time of the motor is constant. Therefore, it takes more time

to switch between a larger speed step. The response for stepping down to a lower boost pressure level was also characterized. As the de-acceleration time of the motor is 20 secs, therefore it was expected that the response times for step down will also be lower. Figure 4.3(c),(d) and (e),(f) shows the comparison. T_w increases by about 1.35 times. This was found similar for all other test runs too. Other parameter that also needs to be taken into account is ζ . For switch from 100 to 120 kPa and from 100 to 130 kPa at different engine speeds, ζ was found to be decreasing with increase in the engine speed. This behavior was opposite for the case of 110 to 130 switch. ζ reduces with an increase in the engine speed, for the latter case. This behavior needs to be investigated, so that a proper model for the supercharger response can be made. But it can be concluded, that the supercharger response can be well represented as a 2nd order function at a constant engine speed.

The previous tests were carried out to observe the system response, when the boost pressure changes at a constant engine speed. The next test was carried out to characterize how the boost pressure levels respond to the engine speed changes. The switch was made from an engine speed of 1000 RPM to 1600 RPM, while keeping the MAP constant at 120 kPa. The control of supercharger was based of a feed-forward open loop control strategy. For feed-forward, the supercharger map as shown in Figure 4.4, was used. The results are shown in Figure 4.5. Not much change in the MAP value was observed during the switch. It is important to understand that as the supercharger is driven independently from the engine, therefore when a switch is made,

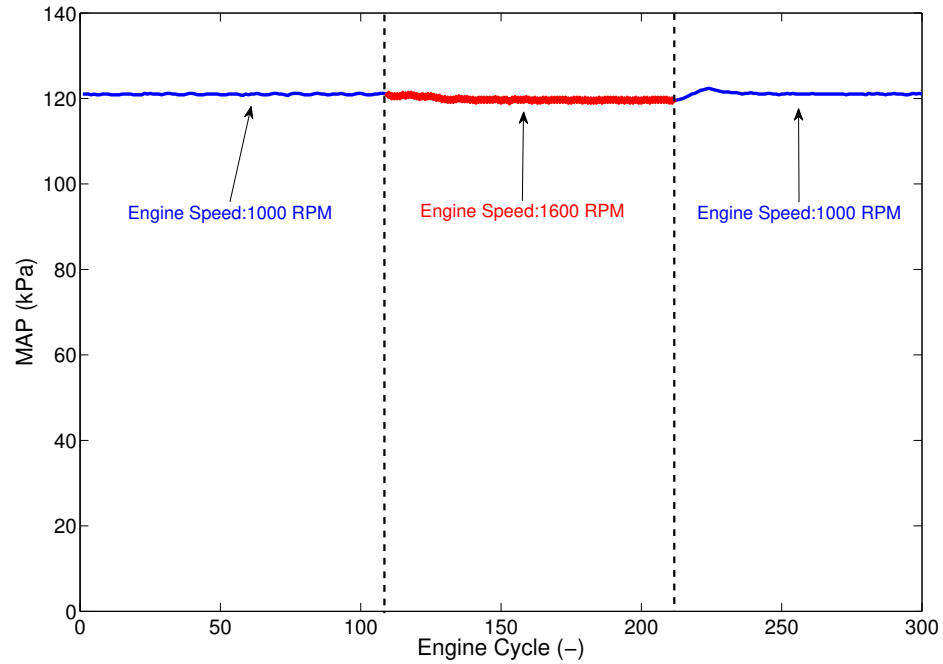


Figure 4.5: Supercharger Response: Engine Speed Switch $N(\text{RPM})=1000, 1600, 1000$, $\text{MAP}(\text{kPa})=120$

both the supercharger and the engine ramp up at different rates. Therefore, it was not possible to characterize the response. Due to the setup limitation, a simultaneous switch of both the boost pressure and the engine speed was not carried out, as the engine speed is controlled using LabView whereas the supercharger is commanded by dSPACE.

4.2 Transient response - RCCI domain

In this section, the results from transient operation of the engine, while operating in RCCI mode are presented. The only actuator dynamics involved in this study, was the fuel flow. The main control parameters, varied during operation of the engine were the PR, the SOI and the fuel quantity. In a conventional SI-mode or CI-mode engine control, maps for different parameters like fuel quantity, boost pressure, spark timing, etc. are used for feed-forward control in conjunction with feedback control. To improve the combustion performance in terms of work output as well as emissions, the engine combustion phasing is a very important control parameter. The main aim of this study was to observe and understand various transients in the combustion phasing and performance parameters.

For carrying out the study, step changes were made from one steady state condition to another. The steady state points were tuned for desired IMEP and combustion phasing, by adjusting the SOI and the fuel quantity. Two tests were carried out in this study. They are as follows:

1. PR step change
2. Fuel quantity step change

No step change on part of SOI was carried out, instead it was used as a control parameter, to stick to the required combustion phasing. This was mainly done because, SOI is dependent on the control signal coming from power electronics, which as discussed previously, are assumed to have no delay in response. The engine maps shown in Chapter 3, were based on fuel quantity and PR sweeps. For moving from one load condition to another condition in that map, either fuel quantity or PR or both can be changed. At the same time, SOI can be varied to achieve an optimum combustion phasing. Therefore, only step changes for the fuel quantity and the PR were made. The first test carried out was the PR switch. The test conditions are shown in the Table 4.3. As can be seen from the Figure 4.6, when the PR switch is made, it takes about two engine cycles for the IMEP to change from 500 kPa to 600 kPa. Another thing that is important to notice, is the CA50. The steady state points were tuned for a CA50 of 8 CAD aTDC. Still, we can observe that CA50 suddenly advances and takes around 50 engine cycles to stabilize at the set point. Before we look into the results, it is important to understand the different dynamics involved at the time of the switching. PR switch means changing the ratio of fuel coming from DI and PFI rails. As DI directly injects the fuel in the cylinder, therefore there will not be any delay owing to the wall wetting dynamics. For PFI as the fuel enters via a port, there will be wall wetting dynamics involved. Fuel transport response for wall wetting can be modeled [51] by the Equation (4.3), where both the factors, x -mass fraction for

percentage of injected fuel that is deposited on intake port wall and τ_f -time constant for fuel evaporation, are dependent on the fuel type, the coolant and intake temperature, MAP and the engine speed.

$$G(s) = \frac{m_{f,actual}}{m_{f,command}} = \frac{1 + \tau_f(1 - x)s}{1 + \tau_f} \quad (4.3)$$

RCCI combustion is also affected by factors like the wall and the residual gas temperatures [52]. So while going from a lower load to a higher load or vice-versa, these conditions will be different [53]. The test run can be divided into two parts. The first part is when switching to PR40. At that point of time when switch will be made, despite commanding a fuel blend of PR40, due to PFI fuel transport dynamics, actual PR of the fuel blend will be less. At the same time as the SOI was advanced too, therefore earlier SOI for a fuel blend having PR less than 40 (More reactive), will advance the CA50. Other effect that could retard combustion phasing would be the low wall and residual gas temperature. But looking at the results, effect of the SOI seems predominant in this case. Now moving to the second stage of results, that is switching back to PR20. Again when PR20 will be commanded, ratio of fuel coming from the DI rail will respond immediately but not the fuel from PFI, as it will take some time to stabilize. This can be confirmed by observing the IMEP curve, as it takes around 3-4 engine cycles to come down to the lower load set-point. This extra fuel will result in a blend with PR greater than 20. As the SOI was immediately retarded at the time of the switch, therefore for a fuel blend having a PR higher

than 20, the phasing should have retarded but there is no such affect observed. In this case, the reason for the CA50 not getting retarded could be attributed to higher cylinder wall-temperatures and residual gas temperatures, which in turn increases the charge temperatures and thus advancing the CA50. Both these effects, that is transient fueling delay and wall and residual gas temperature, could be neutralizing each other.

Table 4.3

Engine test conditions to study transient dynamics during premixed ratio switch

Parameter	Value
Premixed Ratio (-)	20 - 40
Engine Speed (RPM)	1200
Intake Pressure (kPa)	95
Intake Temperature (°C)	80
Fuel Qty (mg/cycle)	20
EVC (CAD bTDC)	22
IVO (CAD bTDC)	25.5
Test Reference (-)	EXP33 17

For the second test, a step change in fueling was executed. In this test, the SOI as well as the PR were kept constant. This was mainly done to isolate the effects of fueling on the the whole combustion process. The response was very slow for combustion phasing, as can be seen from the Figure 4.7, as it takes around 20-30 cycles for the CA50 to stabilize when the switch is made, and again around 20-30 cycles when the fuel is switched back to 18 mg/cyl. For RCCI combustion as previously discussed, combustion phasing depends on global fuel reactivity. As in this case the

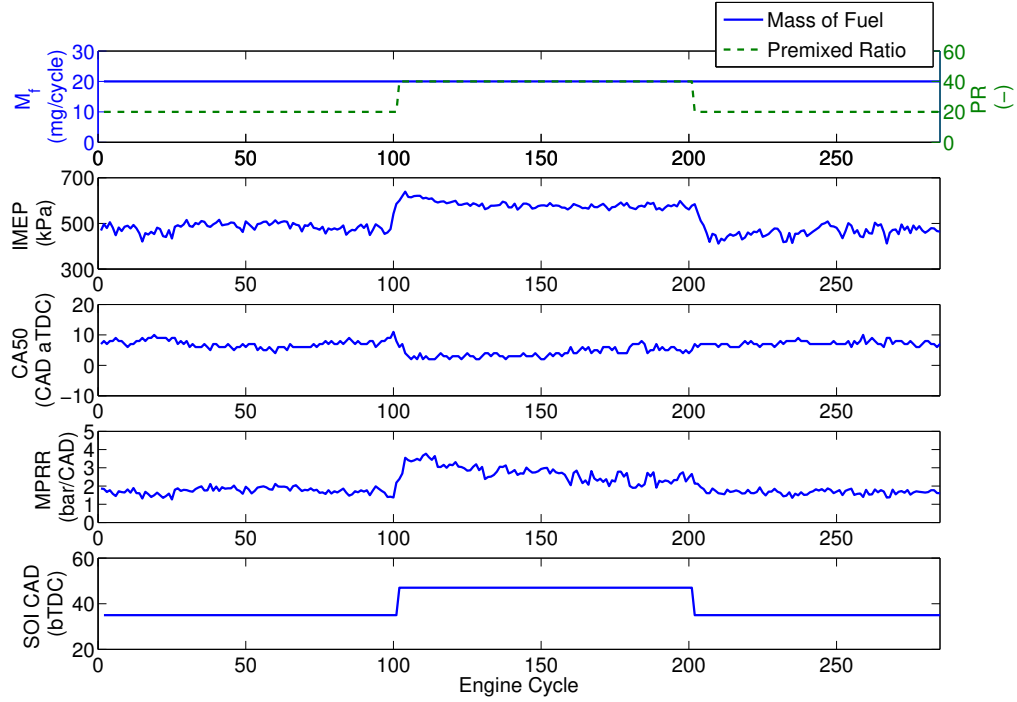


Figure 4.6: Combustion metrics of RCCI engine for premixed ratio step-change

PR was held constant thus the combustion phasing should also have remained constant. During the steady state mapping, it was observed that with increase in fuel quantity at constant PR and SOI for diesel/gasoline, the CA50 advanced. This effect could be mainly due to change in residual gas temperatures and wall temperatures as the engine load is varied. So in context to that trend, we expected the CA50 to advance. But as we will have a delay due to fuel response, when changing total fueling, CA50 also will take some time to stabilize. Observing from the IMEP plot, it takes around 2-3 engine cycles for the load to change. This delay is mainly due to lesser fuel reaching the cylinder. Therefore, we expected CA50 to be following IMEP's trend, if fueling was the only cause that departs operation from steady state conditions. But as mentioned before, a delayed response of around 20-30 engine cycles was observed

in CA50. Thus it can be confirmed that the fueling was not the only cause that will effect the transients. The wall and residual gas temperatures will also play an important factor during the transients and might even have a longer stabilization time, as it depends on the condition of the previous combustion cycle.

The above results necessitates that a proper model for transient fueling be character-

Table 4.4
Engine test conditions to study transient dynamics during mass of fuel switch

Parameter	Value
Fuel Qty (mg/cycle)	18 - 22
Engine Speed (RPM)	1400
Intake Pressure (kPa)	95
Intake Temperature (°C)	100
Premixed Ratio (-)	40
Start of Injection (CAD bTDC)	49
EVC (CAD bTDC)	22
IVO (CAD bTDC)	25.5
Test Reference (-)	EXP33 23

ized. Shahbakhti and Koch [51] used UEGO sensor to parameterize the fuel wetting model given by the Equation (4.3). The factors like fuel wetting and rail fluctuations need to be isolated, to attain a proper model for the fuel dynamics. After getting a proper model for transient fueling, wall and residual gas thermal dynamics also need to be studied. In Chapter 5, a closed-loop cycle-by-cycle combustion controller is designed and implemented on the engine, which compensates for these factors by varying SOI, to stick to a targeted combustion phasing.

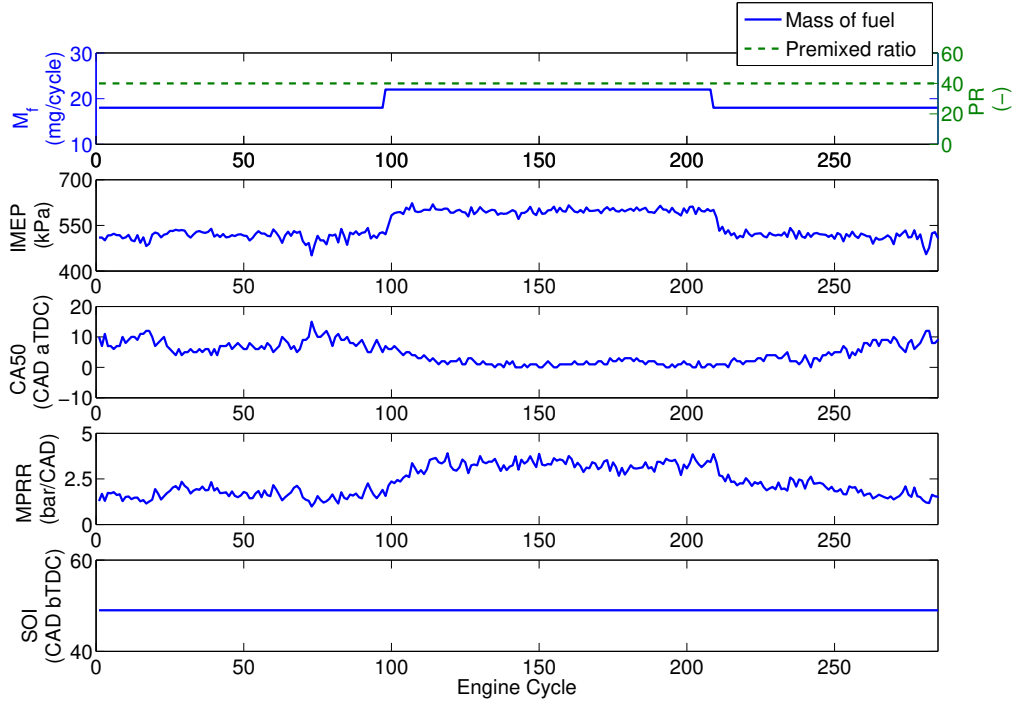


Figure 4.7: Combustion metrics of RCCI engine for mass of fuel step-change

4.3 Combustion mode switching

As discussed in the earlier, that the operation range of RCCI can be extended by switching to a conventional SI or CI combustion mode. In this section, basic strategies and factors involved in a combustion mode switching are explored. In this thesis, switch to SI-mode was carried out. Also for this experiment, n-heptane and iso-octane fuels were used for RCCI and gasoline for SI. This was done, because the engine map using diesel and gasoline for RCCI was not efficient compared to SI mode.

To carry out this study, first a simple open-loop feed-forward combustion control strategy was chosen. Basically, a switch to SI-mode will be needed at the point where

either SI mode is more efficient compared to RCCI mode or RCCI combustion is not possible. Based on this, an approximate load condition for RCCI was found and is shown in Table 4.5. The mode switching study was carried out at a constant load condition, therefore similar IMEP and optimum combustion phasing was set for the SI-mode by tuning the throttle position, fuel quantity and spark timing. This way, steady state points for each mode were found and fed as a feed-forward command. As soon as the switch was activated, the actuators namely throttle, fuel injectors and cam phasors, were varied to attain the required set-point. Misfire and partial burns for around 2-3 engine cycles were observed. The results are not included in the thesis. The main reasons attributed to this were, fuel dynamics[52] and air dynamics[49]. Air

Table 4.5
Engine test conditions for combustion mode switch from RCCI→SI→RCCI

Parameter	Value
Mode Switch (-)	RCCI - SI - RCCI
Engine Speed (RPM)	1400
Intake Temperature (°C)	60
Load Setpoint (kPa)	620
EVC - RCCI (CAD bTDC)	22
IVO - RCCI (CAD bTDC)	25.5
EVC - SI (CAD bTDC)	22
IVO - SI (CAD bTDC)	-24.5
Test Reference (-)	EXP33 30

dynamics is one of the main factors that caused misfires. When the engine operation switches from un-throttled RCCI operation to part-throttle SI operation, the air quantity took around 2-3 engine cycles to stabilize to a level where SI combustion was

possible. Similarly when switching back to RCCI mode, that is WOT, the air will again take some time to reach the required level. Due to the latter case, mixture will become rich and prevent autoignition to happen [45]. The part throttle operation will also reduce pressures at IVC, which will result in lower pressures near TDC and thus repress auto-ignition of the charge. This situation can be stabilized even faster, as shown by a study in [54], where by using an unconventional cam phasing, un-throttled SI operation was possible. Other dynamic that will cause issue is the fuel. In this test, for operation in SI-mode, PFI rails were used. So when the combustion mode will be switched to SI, where 100% fuel comes from the PFI rails, there will be a delay in the fuel flow, as discussed in the previous Section 4.2. Therefore, less fuel and more air will lead to misfires or partial burns.

Based on the aforementioned factors, a new strategy was devised. Firstly, for achieving SI to RCCI switch without any misfires, spark assist was provided for 2-3 engine cycles after the switch was activated, thus aid autoignition of the mixture. Secondly, for RCCI to SI switch, to avoid the mixture from becoming too lean, while the air condition stabilizes, a strategy for injecting extra fuel was devised. For realizing this a 2-D lookup table was created in simulink against MAP and cam phasing for air flow at 60°C. Based on the feedback from MAP sensor and cam positioning, an air flow value was given as an output from the table. This air flow value was used to calculate the amount of fuel that will be needed for maintaining a λ of 1.05. A value of 1.05 was taken for λ as the main aim behind this whole strategy was to just minimize the

engine misfire cycles while injecting minimum fuel, which was being possible using this value. This was done until the air flow stabilized to the steady-state values. The strategy is shown in Figure 4.8

The results for carrying out a switch with the aforementioned strategy is shown in

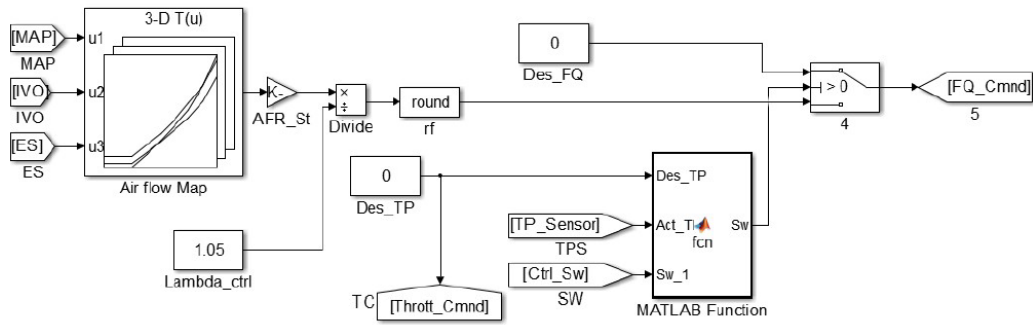


Figure 4.8: Fuel quantity calculation for switching to SI mode

Figure 4.7. As can be seen from the figure, when the switch is made from RCCI to SI there is one misfire cycle, post which the combustion starts again. Another interesting observation that can be made is, that despite of extra fuel being injected in the cycle where switch is made (misfire cycle), the next cycle where the fuel quantity is adjusted back to the steady state value, gets an overshoot and then undershoot. This is mainly due to the dynamics involved in the PFI fuel transport. Also the IMEP value takes around 20 engine cycles to reach the tuned steady state load condition. This can be attributed to lower wall temperatures during RCCI operation and delayed response of intake cam phasor as previously discussed in Section 4.1.2. The other part of this test was SI to RCCI switch. As can be seen in the figure, once the switch is made, with the aid of spark no misfire occurs. Instead, there is an overshoot in the IMEP values,

which eventually comes down to the tuned load level. When the engine comes out of the SI-mode where the operation is stoichiometric, wall and exhaust gas temperatures will be higher as compared to the RCCI mode. For a same fuel quantity we get more IMEP in RCCI because an increase in the wall and residual gas temperature causes the charge temperature to increase, which in turn aids higher temperature near TDC and thus improves the combustion efficiency. Even though this is beneficial, but it should be noted that as RCCI combustion is affected by chemical kinetics, increase in temperature will depart the operation from optimum steady state condition. The current test setup uses a stock GDI engine. As we are using stock pistons with a low CR, the combustion efficiency of the engine for RCCI combustion is poor. The increase in charge temperature in this case improved the combustion efficiency and that is why an improved combustion performance. For the engines where combustion efficiency is already very high, this factor might not play a very important role in improving performance. Instead it might lead the combustion phasing to advance thereby causing knock or even unstable combustion.

The reason for having one misfire cycle was mainly due to the fuel supply delay on part of the PFI rails as well as stabilization of the air flow, which will eventually increase with increase in engine speed. To counter this, another strategy was devised. When the switch was made from RCCI to SI, for that particular engine cycle both the fuels were injected at the same time, that is PR60 fuel blend using DI and 1st PFI rail and gasoline using 2nd PFI rail. The strategy gave no misfires but incurred a high

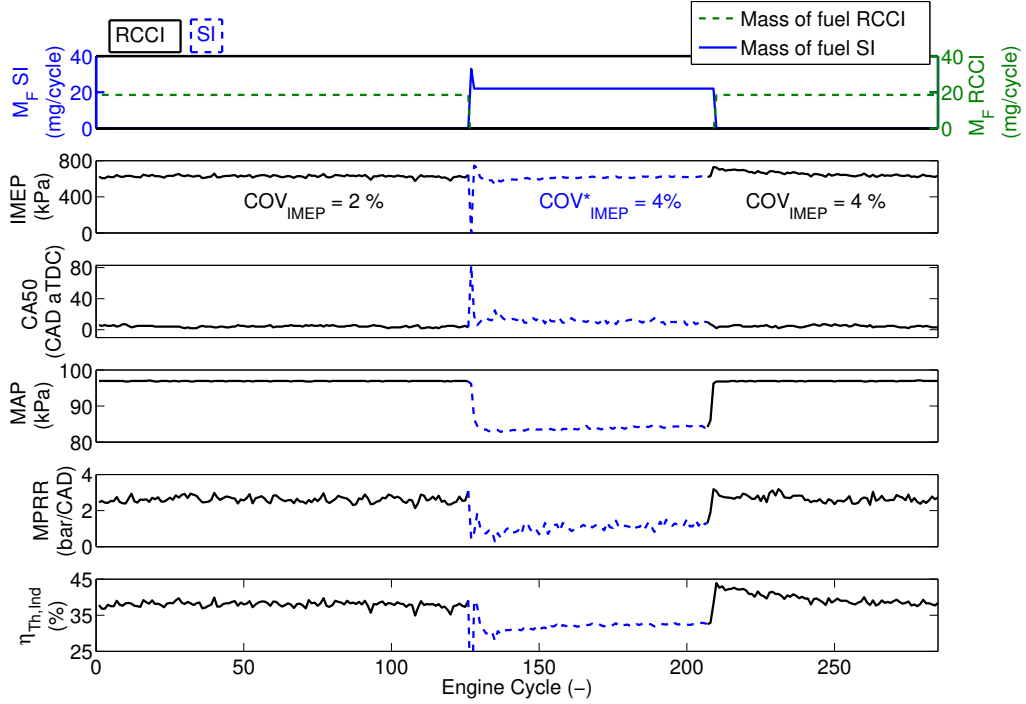


Figure 4.9: Combustion metrics for RCCI→SI→RCCI mode switching (* COV_{IMEP} calculation for SI mode does not include the misfire cycle)

audible knock and PRR. It was used for HCII-SI mode switching. The test condition is given in Table 4.6 and the results are shown in Figure 4.10. The strategy was not used further, as the previous strategy was enough to attain a COV_{IMEP} condition of less than 10%. But as already discussed, previous switching strategy will start to fail with increasing engine speed. For that purpose strategy of inducting both the fuels will be necessary. This strategy can be improved such that knock and PRR be reduced by tuning the quantity of fuel being injected and inducting EGR.

As in this thesis, main aim was to identify various factors involved on part of switching, therefore just an open loop strategy was designed and implemented on the engine. Nonetheless, performance can be improved by use of combustion feedback closed-loop

Table 4.6

Engine test conditions for combustion mode switch from SI→HCCI→SI

Parameter	Value
Mode Switch (-)	SI - HCCI - SI
Engine Speed (RPM)	1000
Intake Temperature (°C)	60
Engine Load Indicated (kPa)	440
EVC - HCCI (CAD bTDC)	22
IVO - HCCI (CAD bTDC)	25.5
EVC - SI (CAD bTDC)	22
IVO - SI (CAD bTDC)	-24.5
Test Reference (-)	EXP38 12

strategies. The main dynamics identified were related to air and fuel. In terms of practical application, for making a switch to LTC mode and initiating combustion, exhaust gas trapping is also a very important factor, as it is used to heat up the charge [55]. In this test scenario, it was neglected as we did not have enough residual gas trapping possible owing to the valve lift and thus intake charge was heated by in-line heaters to compensate for that factor. But in real-world applications, the factor of exhaust gas trapping will play a very important role for switching to RCCI mode, as the air heaters don't have a fast response for heating up the charge and thus will be an important transient factor to look into.

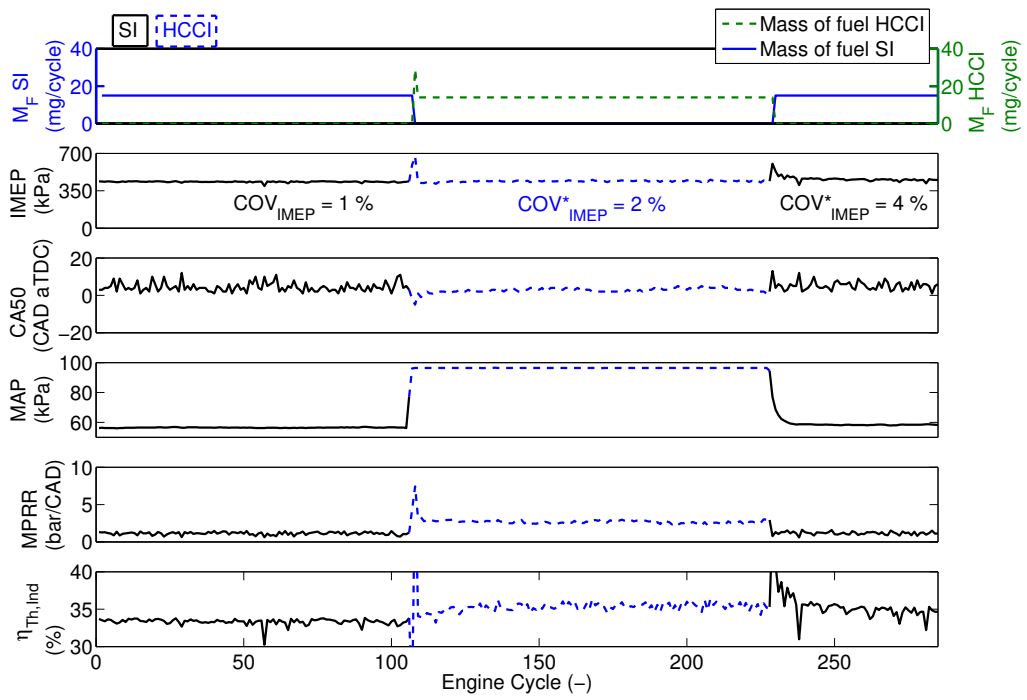


Figure 4.10: Combustion metrics for HCCI→SI→HCCI mode switching (* COV_{IMEP} are calculated for the steady-state engine cycles)

Chapter 5

Combustion feedback for real-time engine control

In Chapter 4, it was shown that despite implementing an engine map based feed-forward control strategy, the engine operation departed from the optimized steady state conditions, especially during the transient phase. This was mainly due to the parameters or boundary conditions, like wall temperature, residual gas fraction, transient fueling, etc., which are difficult to control. To counter these effects, we need to vary the parameters like fuel quantity, SOI, PR, cam phasing, etc., which can be directly controlled and thus achieve optimum combustion phasing. But for executing this, we need to have feedback from the combustion process, thus a real-time combustion feedback system is required. The key variables that can be used for feedback

purposes, are also needed to be identified.

The engine combustion is a thermo-chemical process where fuel energy is converted to heat energy. This brings us to a conclusion, that these combustion timing events will be one of the most important feedback information in controlling the engine combustion. The engine combustion timing or phasing is represented by CA50 defined as crank angle of 50% heat release [30] and can be used as a feedback parameter.

One of the main aim of the combustion control is to increase the work output of the engine. This is represented by IMEP defined as the work transferred to the piston over an engine cycle divided by the swept volume. This can also be a very important feedback parameter while optimizing combustion.

Pressure related parameters like the peak pressure and its location can also be key feedback information. Even though they are not robust enough for combustion control but they can still characterize the combustion process and its variability [32].

5.1 Hardware and setup

In the setup, a Field Programmable Gate Array (FPGA) was utilized to carry out the real-time calculations for the combustion parameters - CA50, IMEP, peak cyclic pressure, location of peak cyclic pressure. As part of this thesis, a combustion feedback system has been designed and embedded on an FPGA for RCCI combustion feedback, utilizing MATLAB and Xilinx Simulink Generator (XSG). The programming

of the FPGA has been done using the aforementioned simulink based tools and not the VHSIC Hardware Description Language (VHDL). MATLAB code and simulink model are shown in Appendix B.

FPGAs are not very flexible for rapid prototyping, but they are very cost-effective compared to a real-time processor, especially for a task that requires a very high throughput and performance. So a solution was provided by dSPACE, so that one can utilize high throughput of an FPGA and flexibility of a real time processor. As can be seen in Figure 5.1, the hardware layer, that is the FPGA as well as a real time processor are embedded into one single hardware, where they can communicate via a serial bus. Owing to this, we can take advantage of a cost-effective FPGA to calculate some standard algorithms at a very high speed and send over the required feedback parameters to the processor, where a real-time cycle-by-cycle closed-loop combustion controller can be embedded. In this section, we will be concentrating on how the FPGA is utilized to implement those standard algorithms.

For carrying out calculations for the combustion parameters as identified before, we need two main inputs from the engine. Firstly, the in-cylinder pressure and secondly, the crank angle of the engine. The pressure signal was read using the in-cylinder pressure transducers and fed to the FPGA via an A/D Converter whereas the angle was measured by counting angular pulse A and cyclic pulse Z, generated by the shaft encoder, and then sent over to the FPGA digital input ports. The details about the pressure transducer and the encoder is included in the experimental setup Section

2.2. The details regarding the FPGA and the I/O board are shown in the Table 5.1. In the current setup, calculations were carried out on the 1st cylinder, therefore only one A/D converter was utilized. A more detailed description about the resource utilization is provided in the resource allocation Section 5.4

Table 5.1
FPGA board and I/O Specification

	Component	Specification
FPGA	Xilinx Spartan-6 LX150	
	Logical cells (nos)	147443
	Slice registers (nos)	184304
	Slice LUT (nos)	92152
	Block RAM blocks (kB)	4824
	Clock speed(MHz)	80
I/O Board	dSPACE DS1552	
	A/D converter	
	Sampling frequency (MSPS)	1
	Resolution (Bit)	16
	Input (V)	± 10
	Digital input	
	Update rate (MHz)	80
	Input (V)	± 40
	Threshold level L \Rightarrow H (V)	3.6
	Threshold level H \Rightarrow L (V)	1.2

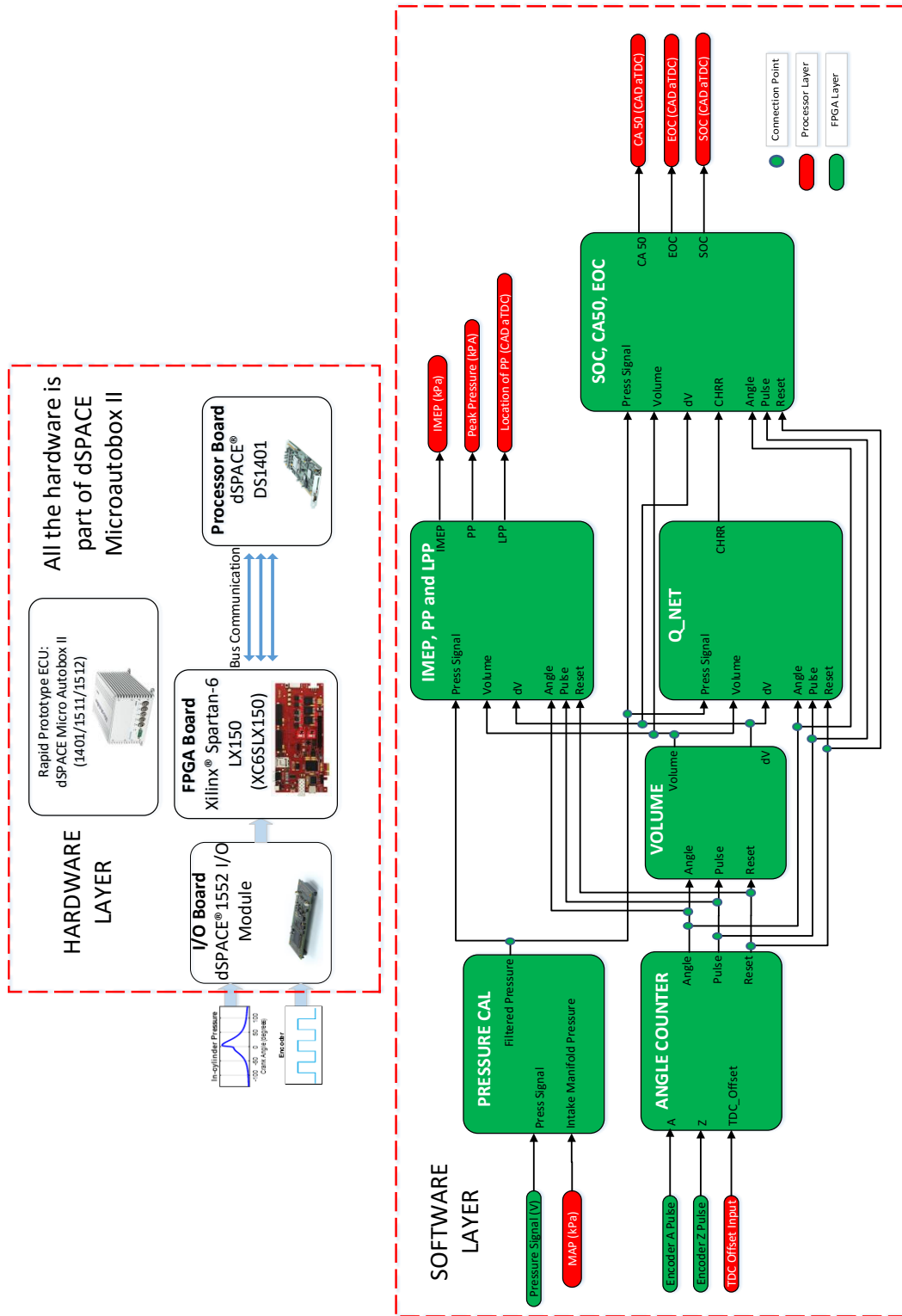


Figure 5.1: FPGA - setup and the software model designed and implemented in this thesis

5.2 Algorithms and calculations

This section will be concentrating on the concept behind the algorithms designed in this thesis, for calculation of the combustion parameters that can be used for the engine combustion control.

5.2.1 Pressure measurement and conditioning

The in-cylinder pressure was measured using piezoelectric sensors. They generate a voltage proportional to the pressure applied on them. A charge amplifier was used to amplify the signal coming from the sensors, which was then sent to the FPGA.

Furthermore, these pressure transducers need an absolute pressure reference. This process is known as pegging [32]. There are many ways to carry out pegging [56]. In the setup, pegging was done using manifold absolute pressure reading at -180 CAD bTDC.

The other issue that arises in the cylinder pressure measurement is noise. But before we look into that, it is important to select as to how we sample our data based on the Analog Digital Converter (ADC) capability. As an example, if we need 1 CAD resolution pressure measurement at 2000 RPM, we will require an A/D converter with a sampling frequency of

$$(2000 \text{ rev/min} * 360 \text{ CAD/rev}) / (60 \text{ s/min} * 1 \text{ CAD/sample}) = 12 \text{ KSPS}$$

This value is significantly below the maximum capability of the A/D converter available on the setup and thus there won't be any data loss, instead we will be oversampling. With this we can look at the following two methods to carryout sampling:

Triggered Sampling [57]: In this type of sampling, the A/D conversion will be triggered by the encoder pulse every CAD, thus not oversampling.

Equidistant Sampling [58]: In this case, we let the sampling happen at the maximum rate and just pick up the data synchronous to the crank angle.

In this thesis, equidistant sampling was carried out.

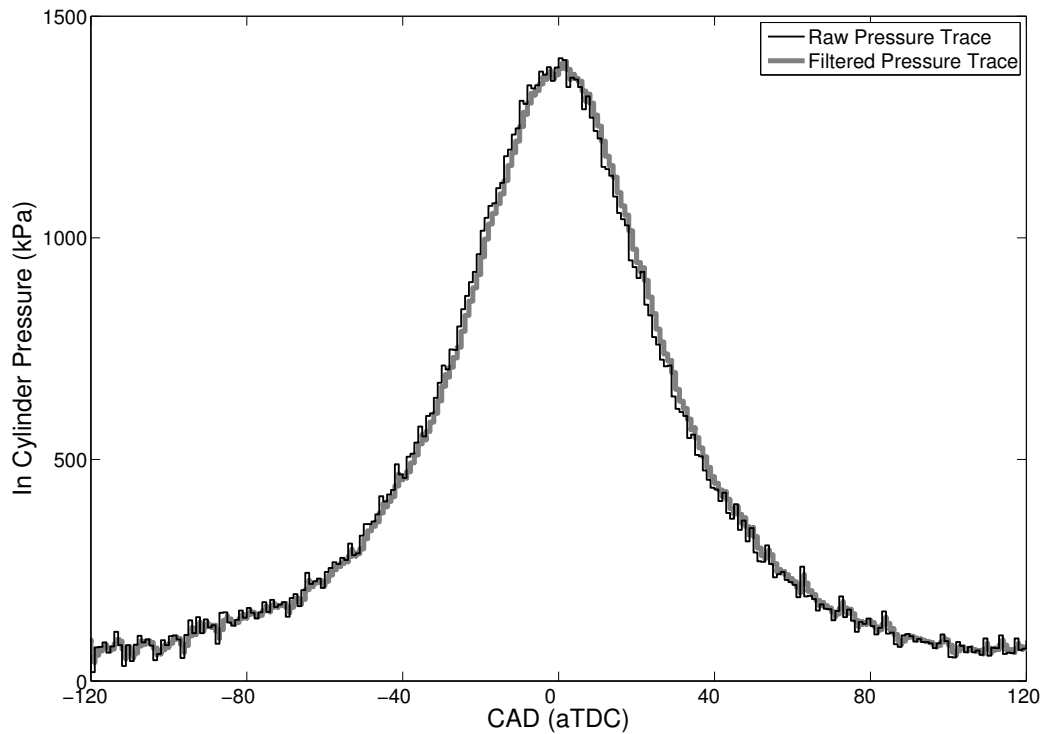


Figure 5.2: Comparison of raw and filtered pressure trace

As mentioned before, the pressure signal received can have noise in it. There are many ways to filter it out. We can either use an analog filter or carry out on-line digital filtering or both. In the setup, a digital filter was implemented. Digital filtering was done post angle-synchronous sampling of the data. A first-order low pass butterworth filter was used to filter the data. A comparison of the on-line pressure signal for raw vs filtered trace is shown in Figure 5.2. The main points that were analyzed while selecting the coefficients of the filter were, shift in the location of peak pressure and attenuation in the magnitude of peak pressure, for the motoring curves, in comparison to the data collected by a commercial combustion analyzer i.e. ACAP.

5.2.2 IMEP, PP, LPP calculation

Calculation of the IMEP was done using the following equation:

$$IMEP = \frac{\int_0^{360} P(\theta)dV(\theta)}{V_{swept}} \quad (5.1)$$

The calculation was carried out from the start of compression stroke (0°) to the end of expansion stroke (360°). Another parameter that was needed for this calculation was volume and change in volume. Instead of calculating the volume on-line, the values were fed to a RAM and extracted based on an angular trigger. This method was computationally effective and was used for providing V and dV values where ever

needed throughout the FPGA model [58].

For calculation of the peak pressure and the location of peak pressure, values for the filtered pressure trace were compared every CAD, to identify the peak pressure and its location.

5.2.3 Heat release calculation

While carrying out the on-line heat release calculations, the main challenge was the computation capabilities of the hardware as well as the implementation simplicity of the algorithm. Keeping this in mind, the algorithm for on-line heat release was selected.

The following Equation (5.2) shows the conventional way of calculating heat release, based on the pressure signal [59]. This model, henceforth, is referred to as **conventional model** through the thesis.

$$\frac{dQ_{ch}}{d\theta} = \frac{\gamma}{\gamma - 1} P \frac{dV}{d\theta} + \frac{1}{\gamma - 1} V \frac{dP}{d\theta} + \frac{dQ_{ht}}{d\theta} + \frac{dQ_{Crevice}}{d\theta} \quad (5.2)$$

In the Equation (5.2), $\frac{dQ_{ch}}{d\theta}$ is the gross heat release rate, $\frac{dQ_{ht}}{d\theta}$ is the heat transfer to the wall, $\frac{dQ_{Crevice}}{d\theta}$ is the heat loss due to flow through crevices and γ is the ratio of specific heats $\frac{C_p}{C_v}$.

For simplification $\frac{dQ_{ht}}{d\theta}$ and $\frac{dQ_{Crevice}}{d\theta}$ were neglected, as shown in the study by Bengtsson et al. [60], that the model, without these two terms was accurate enough for real-time combustion control. The model without the last two factors is called Apparent Heat Release Rate (AHRR) [61]. Equation (5.2) has a derivative of pressure and as we expect the signal for pressure trace could be noisy, a derivative of it could amplify the noise. To avoid this issue, a simplified model was suggested by Wilhelmsson et al. [58] and is represented by the Equation (5.3). This model will henceforth be referred to as **reduced model**. In this equation θ_{start} is the crank angle from where the calculation of heat release is started. In this thesis, θ_{start} was taken at IVC.

$$Q_{net} = \frac{1}{\gamma - 1} P(\theta) V(\theta) + \int_{\theta_{start}}^{\theta} P(\theta) \frac{dV}{d\theta} d\theta - \frac{1}{\gamma - 1} P(\theta_{start}) V(\theta_{start}) \quad (5.3)$$

A post processed comparison of both models is shown in Figure 5.3. It can be seen from the figure that curve for the reduced model departs from conventional model post TDC. This is attributed to the heat transfer to the cylinder walls [32]. Therefore, using the absolute values from the reduced model heat release curve, to locate CA50 crank angle may incorporate an error. Instead, as can be observed, both the curves even after departure, tend to follow the same trend. Thus, the reduced model heat release curve was used to identify the End of Combustion (EOC). Also, there is another factor that affects the calculation of heat release; that is, γ . The effect of γ on the heat release calculations is shown in Figure 5.4. With change in the γ there is a significant change in the net heat release, which can be another

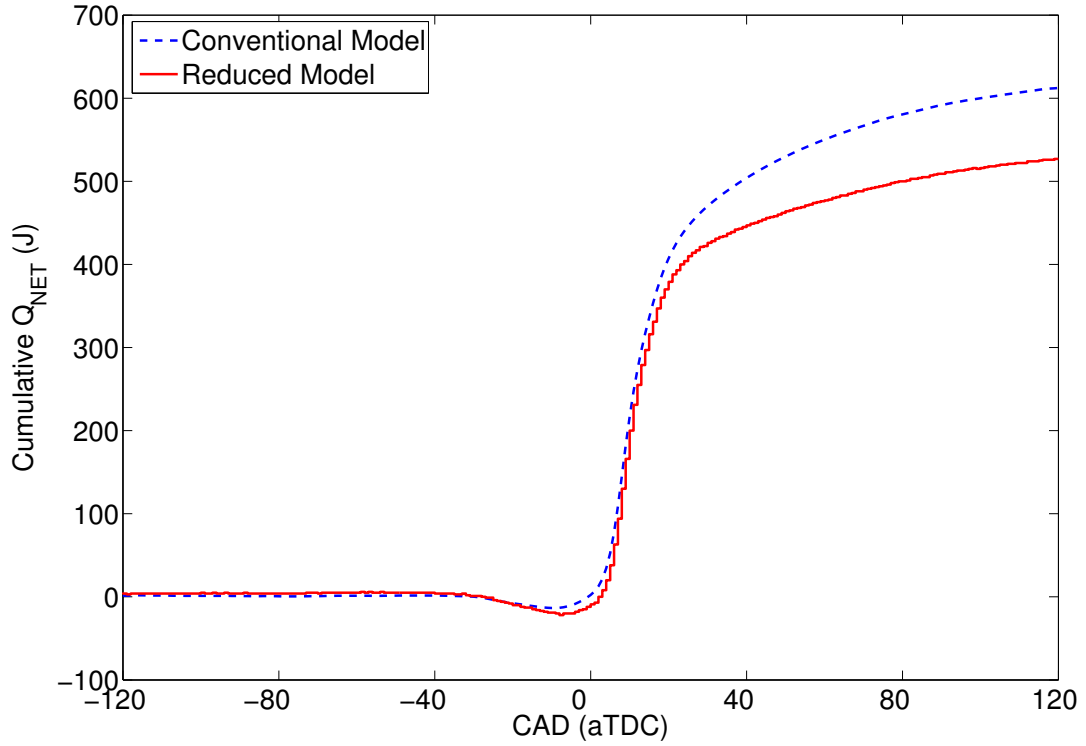


Figure 5.3: Comparison of conventional model and reduced model for calculating the net cumulative heat release

source of error while doing combustion parameter calculations; However, the trend remains the same. As suggested before, this curve was only used to identify the end of combustion and no absolute values of the net heat release curves were used. For algorithmic calculations, a constant $\gamma = 1.35$ was selected. As part of future work (Chap 6), it is recommended to utilize heat release model for CA50 calculations. In that scenario, the current algorithm will need to be modified so as to calculate γ real-time. Asad and Zheng [62] recommended using a mean cylinder temperature dependent specific heat ratio to minimize the error caused due to a constant γ value.

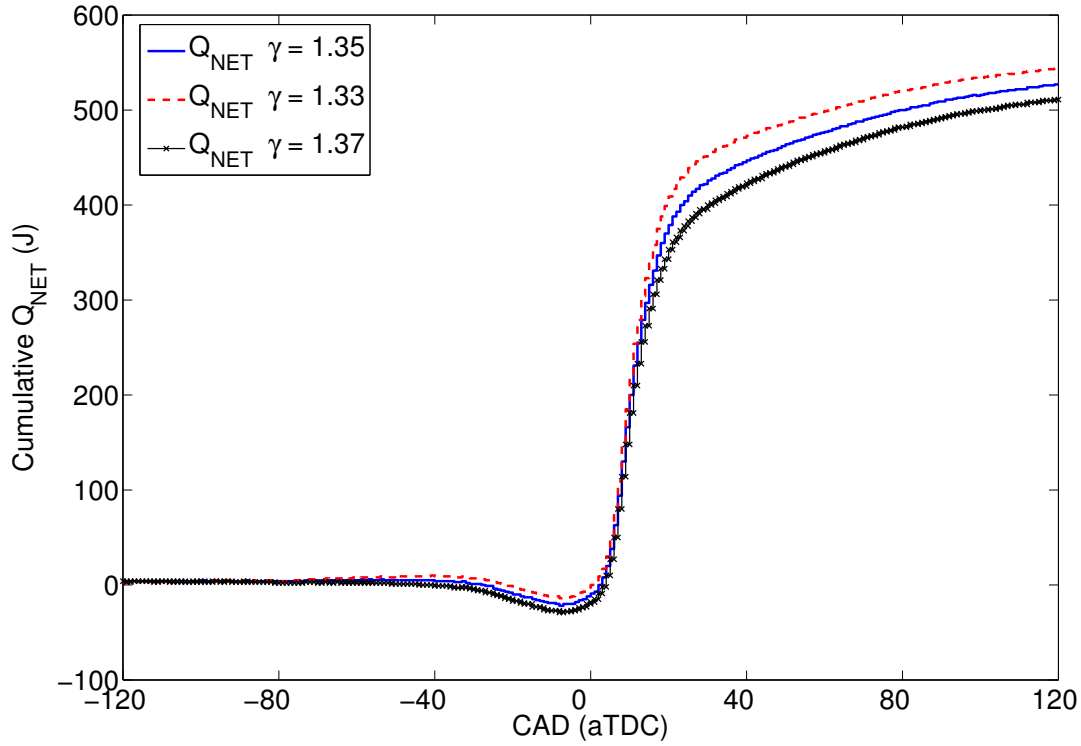


Figure 5.4: Effect of γ on reduced HRR model

5.2.4 CA50 calculation

For the combustion feedback control, combustion phasing related parameters are very crucial, as discussed previously. The Rassweiler-Withrow [34] model based Mass Fraction Burn (MFB) algorithm was used to calculate the CA50, as it is computationally efficient and easier to implement on a FPGA [63]. Even though the CA50 is 50% heat release location, it can still be represented by the half burn location (See Fig.5.5). Figure 5.5 shows that the results from reduced heat release model and mass fraction

burn model are matching very closely. The Rassweiler-Withrow model for mass fraction burn estimation is represented by the Equation (5.4), where x_b is the MFB, soc denotes the start of combustion, eoc is the end of combustion, n is the polytropic index and P and V are pressure and volume.

$$x_b = \frac{P^{1/n}V - P_{soc}^{1/n}V_{soc}}{P_{eoc}^{1/n}V_{eoc} - P_{soc}^{1/n}V_{soc}} \quad (5.4)$$

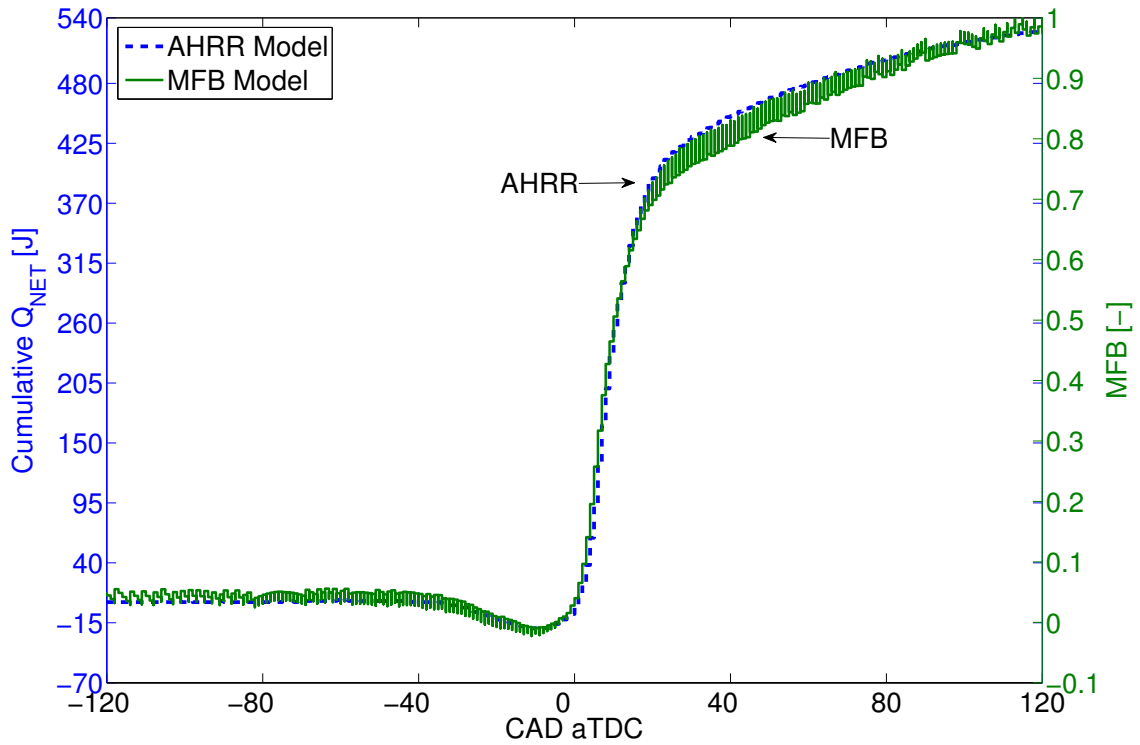


Figure 5.5: Comparison of reduced heat release model and Rassweiler–Withrow Model

As explained earlier, Rassweiler-Withrow model is an estimate for MFB rather than

heat release, so it is necessary to analyze for what conditions this model will calculate CA50 with less error. A study by Asad and Zheng [62], showed an error between the CA50 calculated using reduced heat release model and Rassweiler-Withrow for different combustion strategies. The maximum error occurred when multiple fuel injections were carried out, especially with few very late fuel injections for enabling after-treatment or soot destruction. The type of combustion mode in this thesis that compare to the modes in the aforementioned study, gave very small error in calculating real-time CA50 utilizing MFB model in comparison to heat release based model . The Rassweiler-Withrow model, as shown in the Equation (5.4), requires a SOC as well as an EOC for calculating the fuel mass burn profile. As discussed in the Section 5.2.3, heat release curve was used to identify the EOC. This will be explained later in this section.

The other parameter needed for Rassweiler-Withrow model, as highlighted above, is the SOC. In conventional approaches, the start of combustion is identified as the crank angle where the heat release curve rises to positive values [62]. In the current study, the algorithms have been developed for calculating combustion metrics of an LTC mode of operation, where fuel injection occurs very early. Owing to this early injection, we might observe a two-stage heat release phenomenon, as shown in Figure 5.6. It can be seen that there are two peaks in the heat release curve, a Low Temperature Heat Release (LTHR) and a High Temperature Heat Release (HTHR). If the conventional way is used, it will identify the start of LTHR to be the SOC. As

per the control requirement, we needed to identify the SOC for HTHR (Main-stage). It should be noted that the FPGA algorithm calculates main-stage CA50. Thus all the results shown for the FPGA are for the main-stage heat release. There is another case, where we might not get any two-stage heat release. As shown for RCCI type combustion, in the Figure 3.7, where with retarding SOI, the heat release curve changed from a two-stage to a single-stage curve. Therefore, it was necessary to come up with an algorithm which can address both the heat release behaviors.

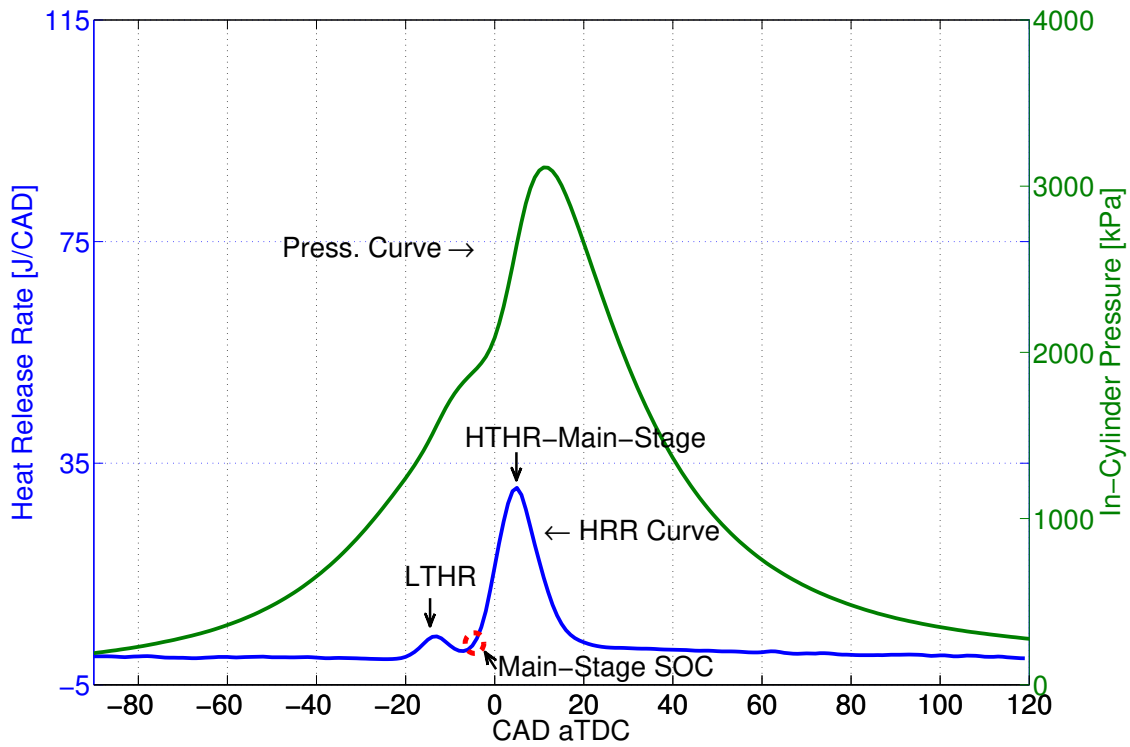


Figure 5.6: Two-stage RCCI heat release for test condition EXP31 201 Appendix A.2

As shown in the log-PV Figure 5.7(a), the curve departs from a straight line during

the combustion period. The SOC can be identified as a point where this departure happens, that is where the magnitude of slope increases [32]. The slope of this straight line is the polytropic index of compression (n_{comp}), which can be calculated using the Equation 5.5

$$n_{comp} = \frac{-VdP}{PdV} \quad (5.5)$$

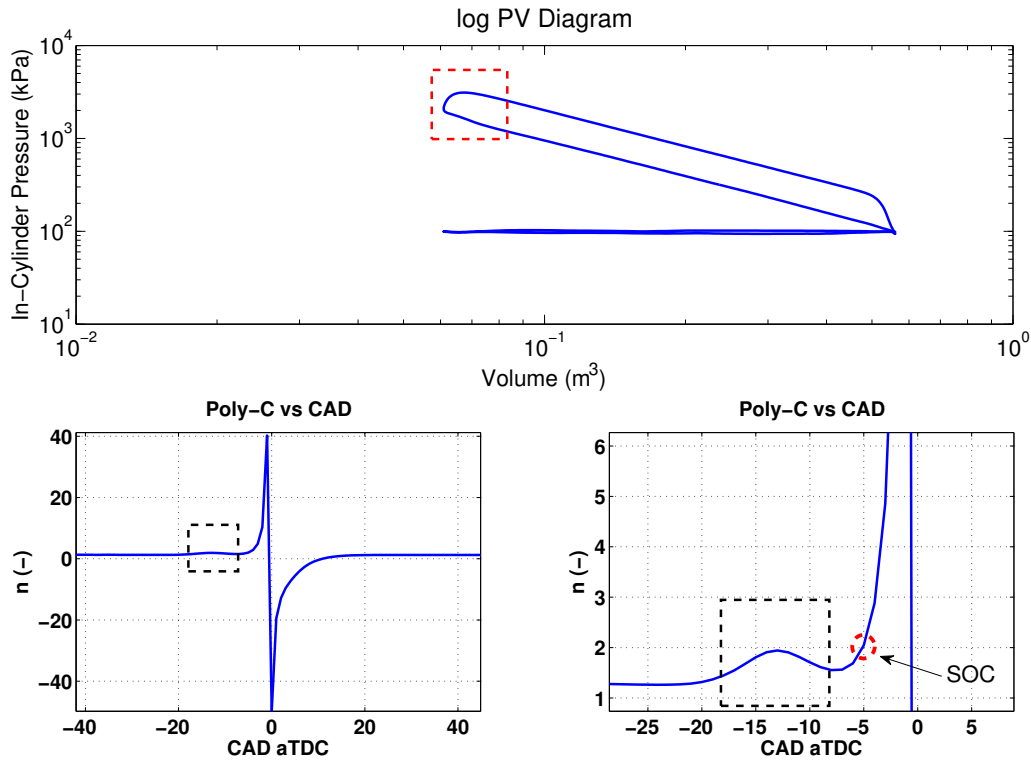


Figure 5.7: SOC identification for two-stage heat release

For identifying the SOC, a certain value of threshold for polytropic index of compression was selected based on the experimental data. This approach also had a shortcoming. As seen from the Figure 5.7 (b) and (c), when we get a two-stage heat

release, the polytropic index values also increase during the LTHR region. So to address this issue, a window-based algorithm was made such that this LTHR peak was bypassed. A window of three CAD was taken such that if the value of polytropic index of compression was higher than the threshold values for those consecutive crank angles, then the point will be identified as the SOC. Using this approach, the LTHR peak was bypassed. The algorithm was tested off-line for both the single-stage and the two-stage heat release behaviors.

Other than the SOC, identification of EOC was also required for CA50 calculation. EOC is defined as the first zero crossing of heat release curve, after maximum peak of heat release is achieved. Estimation of the EOC, utilizing this approach, gave an error for the CA50 calculation in cases where high diffusion type combustion occurred [62]. To avoid this, an approach similar to the SOC identification algorithm was used. A three-CAD window based algorithm was written such that if the rate of heat release goes below 0.5 J/CAD, the first instance was identified as the EOC. This algorithm was tested and validated off-line.

5.3 Validation and results

In the previous Section 5.2, the details about algorithms were provided. This section shows the results obtained for the combustion parameters during the engine operation, utilizing the FPGA and how they compare against the results from a commercial

combustion analyzer.

To execute this, steady state tests were carried out in RCCI mode. All the analysis was carried out on the 1st cylinder. So, the signals coming from the in-cylinder pressure transducer could either have been tapped into the FPGA module for getting on-line combustion feedback or acquired by the commercial combustion analyzer, from where the recorded pressure data was used for post processing the combustion parameters. Due to this limitation, the test runs were repeated so as to get the data from the FPGA and the combustion analyzer. The boundary conditions were kept as close possible, so that a comparison would be meaningful.

Figure 5.8(a) shows a comparison for main-stage CA50 from the FPGA and post processing. The average, minimum and maximum errors are shown in the Figure 5.8. The average error as shown is 1 CAD. As already mentioned, the resolution for all the calculations was 1 CAD. In addition to this, the data for these points was not collected parallelly. Also the algorithm used for the post processed CA50 was based on AHRR model, whereas the FPGA calculation was based of MFB model. A comparison with AHRR model was done, as the commercial combustion analyzers also utilize this AHRR model for CA50 calculations and thus this approach gave a more realistic validation to the results calculated real-time using the FPGA. The aforementioned factors could have contributed to the error shown in the plot. Figure 5.8(b), (c) and (d) shows a comparison for the IMEP, the peak pressure and its location. Again, as mentioned above, this small error could be attributed to the fact that the data was

not collected simultaneously.

One of the main purpose of this work is to send the combustion feedback to the

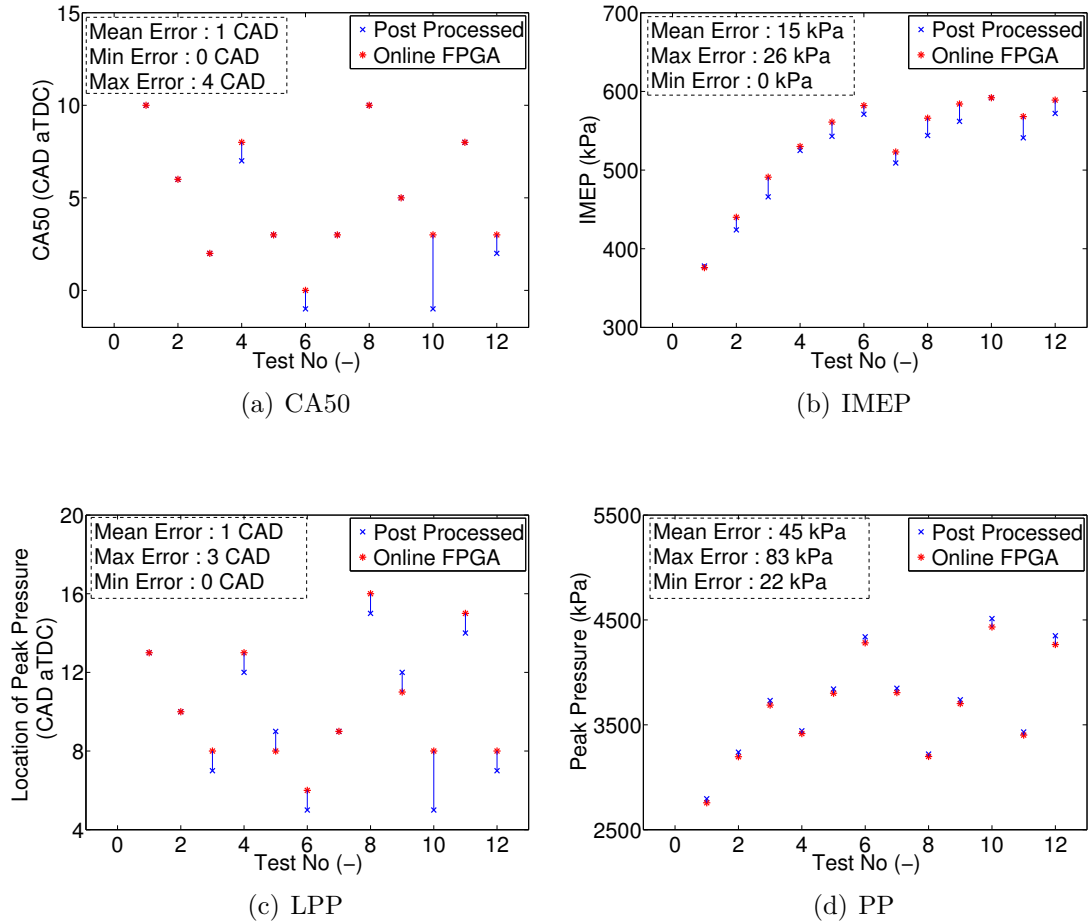


Figure 5.8: Comparison of on-line FPGA and post-processed combustion parameters

engine controller, especially when the engine operating conditions are changed. For RCCI these conditions can be changed by varying the fuel quantity, SOI, PR, etc. To validate the calculations done by FPGA, in respect to this, transient experiments were carried out. The test conditions are listed in Tables 5.2 and 5.3. Firstly, the Figure 5.10 shows the change in CA50 with the switching of PR. Similarly, Figure

5.11 shows the change in CA50, with advancing of SOI from 30-50 CAD bTDC. The trends shown in Figures 5.95.10, match with the findings of Chapters 3 and 4.

Table 5.2
Engine test conditions for premixed ratio switch

Parameter	Value
Premixed Ratio (-)	20 - 40
Engine Speed (RPM)	1000
Intake Pressure (kPa)	95
Intake Temperature (°C)	40
Fuel Qty (mg/cycle)	21
SOI (CAD bTDC)	35
EVC (CAD bTDC)	22
IVO (CAD bTDC)	25.5
Fuel	n-heptane/iso-octane

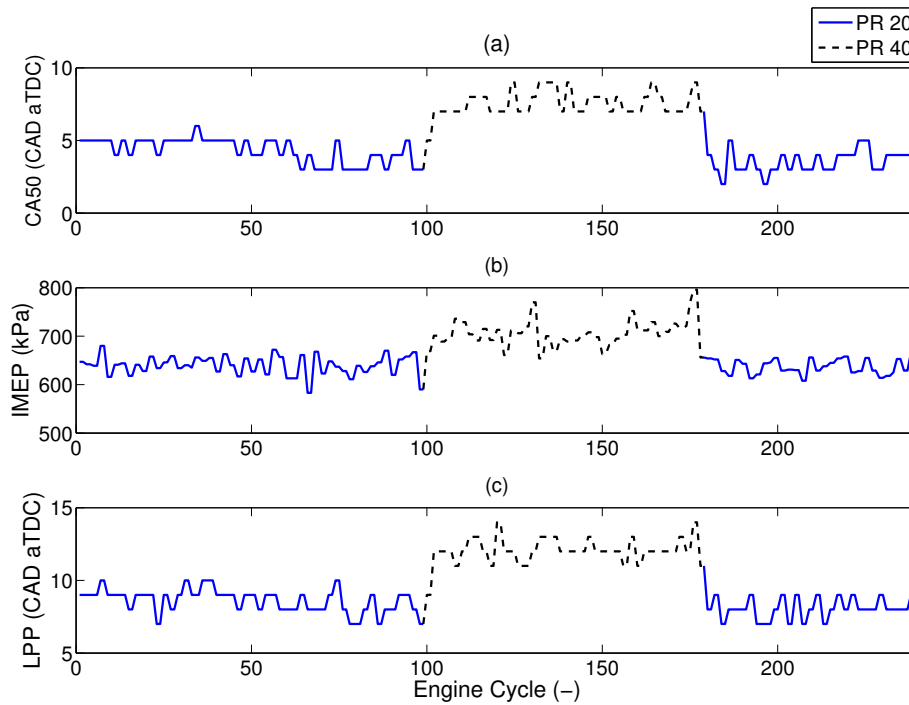


Figure 5.9: Real-time calculated combustion metrics during the PR switch

Table 5.3
Engine test conditions for SOI switch

Parameter	Value
Start of Injection (CAD bTDC)	30 - 50
Engine Speed (RPM)	1000
Intake Pressure (kPa)	95
Intake Temperature (°C)	40
Fuel Qty (mg/cycle)	15
Premixed Ratio (-)	20
EVC (CAD bTDC)	22
IVO (CAD bTDC)	25.5
Fuel	n-heptane/iso-octane

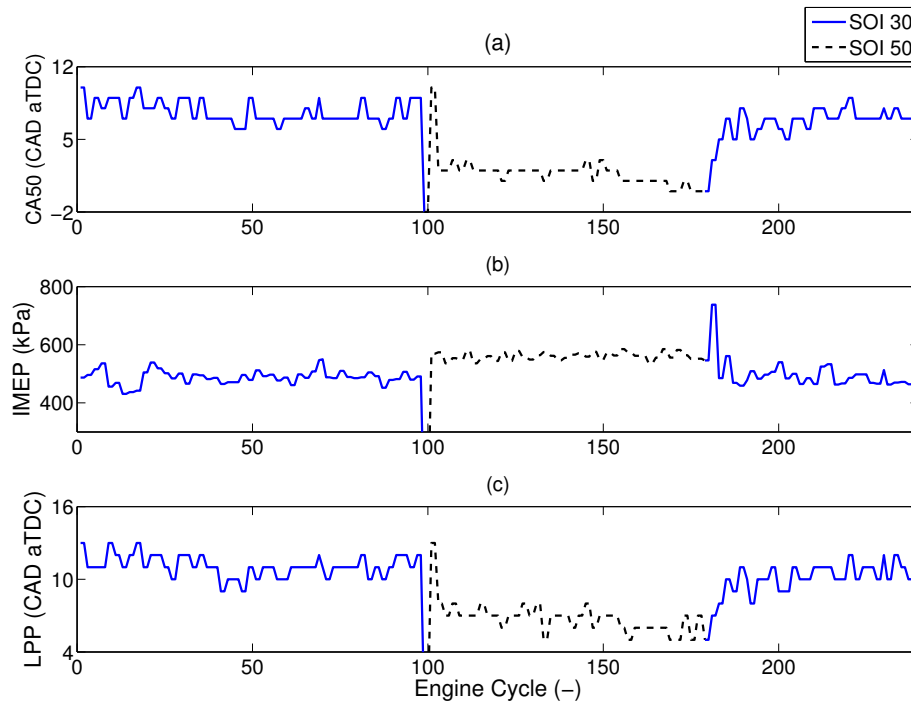


Figure 5.10: Real-time calculated combustion metrics during the SOI switch

It can be concluded from the results, the on-line calculation of combustion feedback parameters is very close to the post processing results. As the encoder resolution is 1 CAD, there is by default an uncertainty of 1 CAD involved in any calculation. But

more importantly, from a control point of view, not just the steady state values are important but also the change in feedback parameter value when a certain engine operating condition is varied, which is highlighted by the transient test results.

5.4 Resource allocation

An FPGA has limited number of resources on board. A brief summary of resource allocation is shown in Table 5.4. As can be seen from the percentages, more than 90% of the resources are still available. As of now the algorithms mentioned in the previous sections were implemented just on the 1st cylinder. In future, the algorithms can be implemented on the other three cylinders too, as there are enough resources left on the FPGA board. In this thesis, no analysis was done in selection of the FPGA

Table 5.4
FPGA resource allocation*

Component	Available	Used
Slice Registers (nos)	184304	8459 (4 %)
Slice LUT (nos)	92152	8646 (9 %)
Memory (kB)	4824	900 (18 %)

* Implemented on the 1st cylinder

hardware as the board, Xilinx Spartan-6 LX150, came as a standard module included as part of dSPACE MicroAutobox. Otherwise, looking at the resource allocation, one

can also go for a much smaller board which would be cheaper. Xilinx offers tools which help one to carry out off-line resource estimations and timing analysis for the necessary algorithms to be embedded on the board. Based on this, one can decide as to what hardware will be sufficient for the required application.

5.5 Closed-loop combustion control - IMEP and CA50

In the Section 4.2, results for the transient RCCI operation were shown. The engine was operated based on a feed-forward open-loop combustion control strategy. As it was seen, when the switch was carried out, the IMEP and the CA50 values stabilized after a few engine cycles. An open loop or map based strategy is good for steady state engine control but they don't capture the transient or boundary condition factors correctly, thus it necessitates to have some other strategy such that engine sticks to an optimum combustion phasing or performance even during transients. In light of this, a feedback combustion controller was designed and implemented in addition to the feed-forward control strategy. For a proper control strategy, it is necessary that a controller provides good disturbance rejection as well tracking capability. Owing to this reason, a feed-forward strategy was used in combination with PI controllers. The control strategy is shown in the Figure 5.11. Two PI controllers were implemented for

tracking. The first controller was used to tune the engine load (IMEP) by controlling the fuel quantity. The second controller adjusted SOI, to achieve a targeted CA50 value. Both the PI controllers were back-calculation anti-windup controllers. It is important to note that the control algorithm was triggered once every engine cycle. The PI gain values are shown in Table 5.5. The base values for the PI were based on sensitivities of the IMEP and the CA50 for the fuel quantity and the SOI respectively, which were then tuned to get the values in the table while operating the engine.

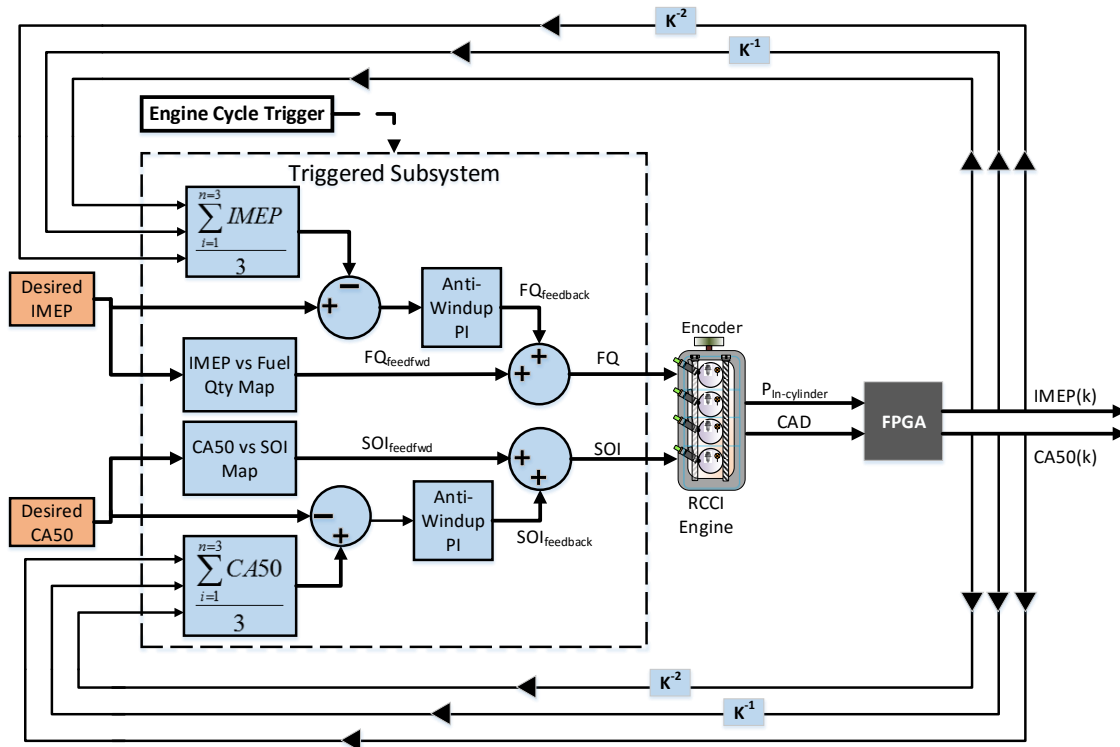


Figure 5.11: RCCI combustion control strategy to obtain desired engine load and combustion phasing

Table 5.5
PI controller gains for the designed RCCI combustion controller

	K_P	K_I
Fuel Qty	0.01	0.005
SOI	1	0.1

The test condition is shown in the Table 5.6. The results are shown in Figure 5.12. A three cycle running average value was used as feedback for both the CA50 and the IMEP, to avoid un-stability due to engine cyclic variations. The results shown in Figure 5.12 are cycle-by-cycle based. Figure 5.12 (c) and (d) shows the SOI and the fuel quantity, respectively.

Table 5.6
Engine test conditions for IMEP-CA50 control

Parameter	Value
Engine Speed (RPM)	1000
Intake Pressure (kPa)	95
Intake Temperature ($^{\circ}$ C)	60
Premixed Ratio (-)	40
EVC (CAD $^{\circ}$ bTDC)	22
IVO (CAD $^{\circ}$ bTDC)	25.5
Fuel	n-Heptane/Iso-Octane
CA50 Target (CAD $^{\circ}$ aTDC)	10
Load Change (kPa)	620-530-620-560

In contrast to the transient operation results shown in the Chapter 3, the CA50, as shown in Figure 5.12 sticks to the targeted value of 9 CAD aTDC. Even with the

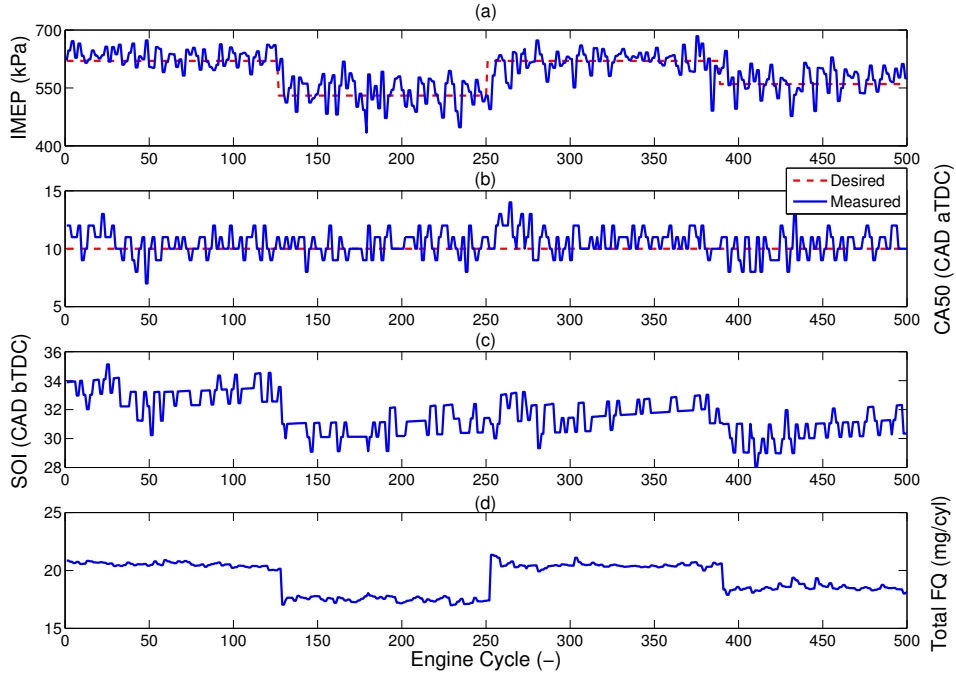


Figure 5.12: IMEP-CA50 closed-loop combustion control for the RCCI engine

feedback combustion controller the IMEP takes around 2-3 engine cycles to reach the desired value. This is due to the delay in fuel transport. Nonetheless, CA50 sticks to the target as SOI was varied to achieve that. This highlights the benefits of closed-loop cycle-by-cycle combustion control enabled through the FPGA based online combustion feedback system that was designed in this chapter.

Chapter 6

Conclusion and future work

This chapter summarizes work done as part of this thesis as well as results obtained from that. Recommendations for future work have also been laid out.

6.1 Summary and conclusion

As part of the thesis three main tasks were carried out. Firstly, steady state mapping of the engine was done to look at various performance metrics and identify control knobs for optimizing and controlling RCCI combustion. Secondly, experiments for transient RCCI operation and combustion mode switching to SI mode for full load

range operation were carried out. The main aim was to identify various engine dynamics involved during transient operation and their effects on combustion phasing. The third part of the thesis involved design and development of a real-time combustion feedback system using cost effective FPGA hardware. This was then used to implement a closed loop combustion control strategy for controlling load and CA50. The main conclusions of the work are listed below:

- † At constant engine speeds, lean limit expanded with increase in intake temperature. At rich limit, points with lower intake temperature gave better indicated efficiencies due to higher volumetric efficiencies.
- † The Low load limit was achieved using low PR fuel blends (PR20), where as the high load limit was achieved using high PR fuel blends (PR40) for the studied range.
- † Lower PR values were needed at higher engine speeds. Low PR fuels have a smaller ignition delay. As the engine speed increases, time available for autoignition decreases, therefore low PR fuels which auto-ignite faster are needed.
- † Highest indicated efficiency was found to be for the points with higher PR and advanced SOI. Test runs were mainly in the middle of lean and rich limits. These test runs were highly premixed thus having better η_{comb} and $\eta_{Ind,Th}$.
- † The load range expanded by utilizing EGR. Test runs with EGR fraction gave better $\eta_{Ind,Th}$. This was mainly due to the possibility of advancing SOI which results in more premixed type combustion.

- † Increase in intake temperature leads to advanced combustion phasing. High intake temperatures result in higher temperatures near TDC thereby reducing ignition delay and thus advancing the start of combustion.
- † Increase in Premixed Ratio (PR) retarded combustion phasing. As PR increases, amount of non-reactive fuel increases. This increases ignition delay of the charge thereby retarding CA50.
- † Advancing Start of Injection (SOI) for the reactive fuel (diesel) advanced CA50. Reactive fuel acts as an ignition front for the charge thereby advancing its injection, which will make combustion occur earlier. With advancing of SOI beyond a certain limit, CA50 starts to retard. This was mainly due to a decrease in stratification of charge (local equivalence ratio) which thereby increases ignition delay, thus retarding combustion phasing.
- † Increase in EGR fraction retarded combustion phasing. Increase in EGR fraction reduces oxygen concentration of the charge which thereby increases ignition delay thus retarding combustion.
- † During transients within RCCI domain, combustion phasing did not remain constant when switching was done using open-loop control strategy. Factors like wall and residual gas temperature and fuel transport dynamics depart the operation from optimum combustion phasing.
- † For combustion mode switching (RCCI-SI-RCCI), main dynamics were involved on part of air and fuel. It took around 2-3 cycles for both fuel and air to stabilize.

This caused very lean mixtures when switching to SI and globally rich mixtures when switching to RCCI mode.

† A combined PI + feed-forward control was designed and implemented to maintain optimum cycle by cycle CA50 during engine load transients.

† The FPGA based combustion feedback system in this thesis provides an economical way to realize cycle by cycle combustion control. The hardware being used in the setup, if needed, can carry out calculations with a resolution of 0.1 CAD @ 8000RPM.

† The SOC algorithm, if proper n_{comp} threshold values were applied, was able to bypass LTHR peaks and thus provided SOC for just HTHR.

† The algorithm based on mass fraction burn gave comparable results to that of heat release based algorithm for calculating CA50. MFB algorithm was preferred as it is computationally efficient and easier to implement.

6.2 Future work

Future work has been outlined here mainly under three categories. The first is in regard to changes that can be incorporated on the setup configuration so as to expand its operation range as well as testing capability. Another important part of this thesis was transient analysis. The second part lays out the work requirements where improvements can be made in terms of testing as well as understanding engine

dynamics during transients. Moving towards closed loop combustion control of an RCCI engine was one of the main aims of this thesis. FPGA has been utilized to calculate and provide combustion feedback for closed loop control. The third part recommends various improvements and additions that can be implemented on the existing FPGA hardware in context to combustion control.

1. Engine and measurement setup

- (a) The current study was carried out on a very low CR of 9.2:1. New pistons with higher CR of 12.31:1 were designed as part of previous work [2]. By increasing CR we will be able to expand the operation range of the engine.
- (b) The current engine crank angle encoder has a resolution of 1 CAD. To improve data analysis, an encoder with a higher resolution should be used.
- (c) EGR is very important in realizing RCCI (or LTC) operation especially at higher loads. The current setup does not allow high EGR quantities even at naturally aspirated conditions due to less ΔP between exhaust and intake port. For increasing ΔP , a small e-motor driven supercharger should be installed on the engine setup.
- (d) The main advantage of LTC modes is low emissions. The current setup does not have any emissions analyzer, therefore engine out emissions were not studied. An economic option would include use of after-market NOx

and PM sensor modules for measuring NO_x and PM emissions. Additionally from a control point of view, these parameters can be implemented as part of the control strategy.

2. Transient testing

- (a) Current tests were carried out at constant engine speeds. The speed of the engine is controlled using dynamo-meter which in turn is controlled by labview and NI system. This works independent of dSPACE hardware, which is used to control load and other engine operating parameters. For realizing proper transient testing, control of dynamo-meter should also be integrated in dSPACE so that both engine speed and load can be controlled simultaneously.
- (b) Dynamics of fuel transport need to be characterized to design injection strategies for RCCI combustion control.
- (c) EGR can be used to control combustion phasing. In the setup it was measured using UEGO sensors, which have a very slow response owing to its installation. Installation configuration of the sensor can be modified to improve the measurement response time. This would also help in utilizing lambda values for AFR control.
- (d) Integration of air heater control can be done in dSPACE so that intake temperature can also be controlled during transients.

3. Combustion feedback

- (a) Current CA50 calculation is based on mass fraction burn model. This can be modified to the heat release based model (AHRR). This is expected to reduce error on the part of calculations. This was discussed in section 5.2.3, where CA50 calculated by the burn model have higher error.
- (b) Currently, combustion feedback algorithms are implemented on the 1st cylinder only. This can be extended to the other three cylinders also. This provides the possibility of conducting cylinder to cylinder control.
- (c) Other combustion metric algorithms like COV_{IMEP} , knock intensity, etc can also be added on the existing hardware. Thus RCCI combustion can be controlled to operate within desired engine combustion limits.

References

- [1] A. Paykani, A. Kakaee, P. Rahnama, and R.D. Reitz. Progress and recent trends in reactivity-controlled compression ignition engines. *International Journal of Engine Research*, 17(5):481–524, 2016.

- [2] H.A. Saigaonkar. “An investigation of variable valve timing effects on HCCI engine performance”. Master’s thesis, Michigan Technological University, 2014.

- [3] U.S. Energy Information Administration. “International Energy Outlook 2016 <http://www.eia.gov/todayinenergy/detail.cfm?id=26212>”. 2016, Date accessed: 07/08/16.

- [4] United States E.P.A. “EPA and NHTSA Set Standards to Reduce Greenhouse Gases and Improve Fuel Economy for Model Years 2017-2025 Cars and Light Trucks”. Office of Transportation and Air Quality, August 2012.

- [5] Energy and Inc. an ICF International Company Environmental Analysis. “Technologies to improve light-duty vehicle fuel economy <http://www.hdsystems.com/TechnologyandStrategy.html>”. 2007, Date accessed: 07/08/2016.
- [6] M.A. Kromer. “Electric powertrains: opportunities and challenges in the US light-duty vehicle fleet”. Master’s thesis, Massachusetts Institute of Technology, 2007.
- [7] J.B. Heywood. “*Internal combustion engine fundamentals*”. chpt:15, Mcgraw-hill New York, 1988.
- [8] R.H. Thring. “Homogeneous-charge compression-ignition (HCCI) engines”. SAE Technical paper 892068, 1989.
- [9] K. Inagaki, T. Fuyuto, K. Nishikawa, and I. Nakakita, K.and Sakata. “Dual-fuel PCI combustion controlled by in-cylinder stratification of ignitability”. SAE Technical Paper 2006-01-0028, 2006.
- [10] J.E. Dec and Y. Yang. “Boosted HCCI for high power without engine knock and with ultra-low NOx emissions-using conventional gasoline”. *SAE International Journal of Engines*, 3(1):750–767, 2010.
- [11] S.L. Kokjohn, R.M. Hanson, D.A. Splitter, and R.D. Reitz. “Experiments and modeling of dual-fuel HCCI and PCCI combustion using in-cylinder fuel blending”. *SAE International Journal of Engines*, 2(2):24–39, 2010.

- [12] T.V. Johnson. “Diesel emissions in review”. *SAE International Journal of Engines*, 4(2011-01-0304):143–157, 2011.
- [13] P.M. Najt and D.E. Foster. “Compression-ignited homogeneous charge combustion”. SAE Technical Paper 830264, 1983.
- [14] J.O. Olsson, P. Tunestål, and B. Johansson. “Closed-loop control of an HCCI engine”. SAE Technical Paper 2001-01-1031, 2001.
- [15] K. Okude, K. Mori, S. Shiino, and T. Moriya. “Premixed compression ignition (PCI) combustion for simultaneous reduction of NO_x and soot in diesel engine”. SAE Technical Paper 2004-01-1907, 2004.
- [16] R.M. Hanson, S.L. Kokjohn, D.A. Splitter, and R.D. Reitz. “An experimental investigation of fuel reactivity controlled PCCI combustion in a heavy-duty engine”. *SAE international journal of engines*, 3(1):700–716, 2010.
- [17] P.W. Bessonette, C.H. Schleyer, K.P. Duffy, W.L. Hardy, and M.P. Liechty. “Effects of fuel property changes on heavy-duty HCCI combustion”. SAE Technical Paper 2007-01-0191, 2007.
- [18] D. Splitter, S. Kokjohn, K. Rein, R. Hanson, S. Sanders, and R. Reitz. “An optical investigation of ignition processes in fuel reactivity controlled PCCI combustion”. *SAE International Journal of Engines*, 3(1):142–162, 2010.
- [19] S.L. Kokjohn, R.M. Hanson, D.A. Splitter, and R.D. Reitz. “Fuel reactivity

- controlled compression ignition (RCCI): a pathway to controlled high-efficiency clean combustion”. *International Journal of Engine Research*, 12(3):209–226, 2011.
- [20] M. Wissink and R.D. Reitz. “Direct dual fuel stratification, a path to combine the benefits of RCCI and PPC”. *SAE International Journal of Engines*, 8(2):878–889, 2015.
- [21] D Kothari. “Experimental setup and controller design for an HCCI engine”. Master’s thesis, Michigan Technological University, 2014.
- [22] V.S. Thakkar. “Modeling and experimental setup of an HCCI engine”. Master’s thesis, Michigan Technological University, 2014.
- [23] K.K. Sadabadi. “Modelling and Control of Combustion Phasing of an RCCI Engine”. Master’s thesis, Michigan Technological University, 2015.
- [24] K. Kannan. “An experimental investigation of low temperature combustion regimes in a light duty engine”. Master’s thesis, Michigan Technological University, 2016.
- [25] C.S. Lee, K.H. Lee, and D.S. Kim. “Effect of premixed ratio on nitric oxide emission in diesel engine”. SAE Technical Paper 2008-01-1392, 2001.
- [26] O. Welling and N. Collings. “UEGO based measurement of EGR rate and residual gas fraction”. SAE Technical Paper 2011-01-1289, 2011.

- [27] K. Owen and T. Coley. “*Automotive fuels reference book*”. Society of Automotive Engineers, Warrendale, PA (United States), 1995.
- [28] K.G. Raghavan. “An experimental investigation into the effect of NO₂ and temperature on the passive oxidation and active regeneration of particulate matter in a diesel particulate filter”. Master’s thesis, Michigan Technological University, 2015.
- [29] M. Yao, Z. Zheng, B. Zhang, and Z. Chen. “The effect of PRF fuel octane number on HCCI operation”. SAE Technical Paper 2004-01-2992, 2004.
- [30] J. Klimstra. “The optimum combustion phasing angle—a convenient engine tuning criterion”. SAE Technical Paper 852090, 1985.
- [31] J.B. Heywood. “*Internal combustion engine fundamentals*”. chpt:2, Mcgraw-hill New York, 1988.
- [32] J.B. Heywood. “*Internal combustion engine fundamentals*”. chpt:9, Mcgraw-hill New York, 1988.
- [33] J. Chang, O. Güralp, Z. Filipi, D.N. Assanis, T. Kuo, P. Najt, and R. Rask. “New Heat Transfer Correlation for an HCCI Engine Derived from Measurements of Instantaneous Surface Heat Flux”. SAE Technical Paper 2004-01-2996, 2004.
- [34] G.M. Rassweiler and L. Withrow. “Motion pictures of engine flames correlated with pressure cards”. SAE Technical Paper 380139, 1938.

- [35] International Organization for Standardization Geneva. “Guide to the Expression of Uncertainty in Measurement”. Technical report, ISBN 92-67-10188-9, 1995.
- [36] S. Singh, L. Liang, S.C. Kong, and R.D. Reitz. “Development of a flame propagation model for dual-fuel partially premixed compression ignition engines”. *International Journal of Engine research*, 7(1):65–75, 2006.
- [37] M. Sjöberg and J.E. Dec. “An investigation of the relationship between measured intake temperature, BDC temperature, and combustion phasing for premixed and DI HCCI engines”. SAE Technical Paper 2004-01-1900, 2004.
- [38] J.B. Heywood. “*Internal combustion engine fundamentals*”. chpt:10, McGraw-hill New York, 1988.
- [39] R. Hanson, S.L. Kokjohn, D. Splitter, and R.D. Reitz. “Fuel effects on reactivity controlled compression ignition (RCCI) combustion at low load”. *SAE International Journal of Engines*, 4(1):394–411, 2011.
- [40] J. Weber, H.W. Won, and N. Peters. “Experimental validation of a surrogate fuel for diesel”. SAE Technical Paper 2007-01-1842, 2007.
- [41] Y. Ra, J.E. Yun, and R.D. Reitz. “Numerical parametric study of diesel engine operation with gasoline”. *Combustion Science and Technology*, 181(2):350–378, 2009.

- [42] K. Tong, B.D. Quay, J.V. Zello, and D.A. Santavicca. “Fuel volatility effects on mixture preparation and performance in a GDI engine during cold start”. SAE Technical Paper 2001-01-3650, 2001.
- [43] M. Nazemi. “Modeling and analysis of Reactivity Controlled Compression Ignition (RCCI) combustion”. Master’s thesis, Michigan Technological University, 2015.
- [44] S.C. Medina, R.M. Green, and J.R. Smith. “Optical measurements of hydrocarbons emitted from a simulated crevice volume in an engine”. Technical report. SAE Technical Paper 840378, 1984.
- [45] J.B. Heywood. “*Internal combustion engine fundamentals*”. chpt:11, McGraw-hill New York, 1988.
- [46] A. Andree and S.J. Pachernegg. “Ignition conditions in diesel engines”. SAE Technical Paper 690253, 1969.
- [47] S. Kokjohn, R.D. Reitz, D. Splitter, and M. Musculus. “Investigation of fuel reactivity stratification for controlling PCI heat-release rates using high-speed chemiluminescence imaging and fuel tracer fluorescence”. *SAE International Journal of Engines*, 5(2012-01-0375):248–269, 2012.
- [48] Y. Ra and R.D. Reitz. “A reduced chemical kinetic model for IC engine combustion simulations with primary reference fuels”. *Combustion and Flame*, 155(4):713–738, 2008.

- [49] N. Milovanovic, D. Blundell, S. Gedge, and J. Turner. “SI-HCCI-SI mode transition at different engine operating conditions”. SAE Technical Paper 2005-01-0156, 2005.
- [50] A.B. Dempsey and R.D. Reitz. “Computational optimization of reactivity controlled compression ignition in a heavy-duty engine with ultra low compression ratio”. *SAE International Journal of Engines*, 4(2011-24-0015):2222–2239, 2011.
- [51] M. Shahbakhti and C.R. Koch. “Dynamic modeling of HCCI combustion timing in transient fueling operation”. *SAE International Journal of Engines*, 2(2009-01-1136):1098–1113, 2009.
- [52] R. Hanson and R. Reitz. “Transient RCCI operation in a light-duty multi-cylinder engine”. *SAE International Journal of Engines*, 6(3):1694–1705, 2013.
- [53] C. Wilhelmsson, A. Vressner, P. Tunestål, B. Johansson, G. Särner, and M. Aldén. “Combustion chamber wall temperature measurement and modeling during transient HCCI operation”. SAE Technical Paper 2005-01-3731, 2005.
- [54] J. Szybist, M. Foster, W.R. Moore, K. Confer, and R. Youngquist, A. and Wagner. “Investigation of knock limited compression ratio of ethanol gasoline blends”. SAE Technical Paper 2005-01-0156, 2010.
- [55] H. Xu, S. Rudolph, Z. Liu, S. Wallace, S. Richardson, M. Wyszynski, and

- A. Megaritis. “An investigation into the operating mode transitions of a homogeneous charge compression ignition engine using EGR trapping”. SAE Technical Paper 2004-01-1911, 2004.
- [56] K. Lee, M. Yoon, and M. Sunwoo. “A study on pegging methods for noisy cylinder pressure signal”. *Control Engineering Practice*, 16(8):922–929, 2008.
- [57] M. Larsson. “Combustion Sensing Methods-in Theory and Practice”. Master’s thesis, Chalmers University of Technology,, 2007.
- [58] C. Wilhelmsson, P. Tunestål, and B. Johansson. “Fpga based engine feedback control algorithms”. *FISITA 2006 World Automotive Congress*, 2006.
- [59] J.A. Gatowski, N Balles, K.M. Chun, F.E. Nelson, J.A. Ekchian, and J.B. Heywood. “Heat release analysis of engine pressure data”. SAE Technical Paper 841359, 1984.
- [60] J. Bengtsson, P. Strandh, R. Johansson, P. Tunestål, and B. Johansson. “Closed-loop combustion control of homogeneous charge compression ignition (HCCI) engine dynamics”. *International journal of adaptive control and signal processing*, 18(2):167–179, 2004.
- [61] R.K.Y.G. Borman. “The Computation of Apparent Heat Release for Internal Combustion Engines”. *American Society of Mechanical Engineers. ASME*, 1966.

- [62] U. Asad and M. Zheng. “Real-time heat release analysis for model-based control of diesel combustion”. SAE Technical Paper 2008-01-1000, 2008.
- [63] K. Telborn. “A real-time platform for closed-loop control and crank angle based measurement”. Master’s thesis, Linköping University, 2002.

Appendix A

Experimental Data Summary

Details about all steady state test runs are given in this appendix.

Table A.1
Operating Conditions for RCCI Mapping Data - Naturally Aspirated

Exp #	T_{in} (°C)	P_{man} (kPa)	N (rpm)	PR (-)	λ (-)	SOI (°bTDC)	IMEP (kPa)	CA50 (°aTDC)	$\eta_{ind.th}$ (%)	MPPR (bar/CAD)	ISFC (g/kWh)
31 1	40	95	806	20	2.21	21	234	14	20	0.56	432
31 2	40	95	806	20	2.10	21	253	13	20	0.64	418
31 3	40	95	806	20	1.79	21	350	11	24	1.13	350
31 4	40	95	807	20	1.44	21	469	8	26	1.88	323
31 5	40	95	806	20	1.03	21	588	6	24	2.75	356
31 6	40	96	1008	20	1.43	45	515	11	29	1.61	294
31 7	40	96	1008	20	1.25	45	572	7	28	2.57	302
31 8	40	96	1007	20	1.06	45	629	7	26	3.17	321
31 9	40	95	806	40	1.70	30	435	13	28	0.93	298
31 10	40	95	805	40	1.53	30	538	11	31	1.75	268
31 11	40	95	806	40	1.21	30	642	7	30	3.08	280
31 12	40	95	806	40	1.04	30	691	8	28	3.60	303
31 13	40	95	808	60	1.37	24	547	20	29	0.75	290
31 14	40	95	807	60	1.14	24	681	13	30	1.99	275
31 15	60	95	808	20	2.44	18	245	12	23	0.72	367
31 16	60	95	807	20	2.16	18	267	11	22	0.86	378
31 17	60	95	807	20	1.87	18	326	11	24	1.06	354
31 18	60	95	808	20	1.49	18	445	9	26	1.70	324
31 19	60	95	808	20	1.22	18	534	7	26	2.26	324
31 20	60	95	807	20	1.01	18	586	5	24	2.94	357
31 21	60	96	1008	20	2.39	25	249	15	23	0.43	362
31 22	60	96	1010	20	2.29	25	252	16	23	0.43	372
31 23	60	96	1010	20	2.11	25	276	14	23	0.59	366
31 24	60	96	1007	20	1.85	25	341	13	25	0.92	338

continued on next page...

Exp #	T_{in} (°C)	P_{man} (kPa)	N (rpm)	PR (-)	λ (-)	SOI (°bTDC)	IMEP (kPa)	CA50 (°aTDC)	$\eta_{ind,th}$ (%)	MPPR (bar/CAD)	ISFC (g/kWh)
31 25	60	96	1008	20	1.47	25	468	11	27	1.55	308
31 26	60	96	1008	20	1.27	25	539	9	27	1.94	308
31 27	60	97	1008	20	1.07	25	583	8	25	2.23	334
31 28	60	96	1211	20	1.63	40	426	13	28	0.97	305
31 29	60	96	1220	20	1.51	40	474	10	29	1.43	289
31 30	60	96	1209	20	1.45	40	494	8	29	1.40	292
31 31	60	96	1201	20	1.24	40	540	8	27	1.34	307
31 32	60	96	1199	20	1.07	40	605	6	26	1.93	321
31 33	60	96	808	40	1.69	20	419	11	28	1.23	301
31 34	60	96	807	40	1.47	20	528	8	31	1.75	273
31 35	60	96	807	40	1.26	20	590	5	30	2.44	281
31 36	60	96	817	40	1.14	20	611	6	29	2.57	295
31 37	60	97	1010	40	1.46	30	525	13	31	1.34	275
31 38	60	97	1006	40	1.32	30	560	13	30	1.31	283
31 39	60	97	1006	40	1.15	30	597	12	28	1.52	302
31 40	60	96	807	60	1.33	20	578	13	30	1.12	274
31 41	60	96	807	60	1.27	20	617	10	31	1.54	269
31 42	80	96	807	20	2.45	15	234	10	23	0.91	369
31 43	80	96	808	20	2.16	15	262	9	23	0.97	371
31 44	80	96	807	20	1.92	15	309	10	24	1.06	350
31 45	80	96	807	20	1.44	15	467	9	27	1.78	309
31 46	80	96	807	20	1.24	15	523	6	27	2.33	317
31 47	80	96	807	20	1.04	15	566	5	25	3.00	344
31 48	80	97	1008	20	2.31	20	250	13	23	0.56	360
31 49	80	97	1008	20	1.29	20	520	9	28	1.79	305
31 50	80	97	1008	20	1.04	20	574	8	25	2.48	339
31 51	80	97	1008	20	1.55	20	405	12	26	1.26	320

continued on next page...

Exp #	T_{in} (°C)	P_{man} (kPa)	N (rpm)	PR (-)	λ (-)	SOI (°bTDC)	IMEP (kPa)	CA50 (°aTDC)	$\eta_{ind,th}$ (%)	MPPR (bar/CAD)	ISFC (g/kWh)
31 52	80	97	1009	20	1.88	20	304	12	24	0.78	356
31 53	80	96	1209	20	1.87	30	327	11	26	0.79	330
31 54	80	96	1210	20	1.65	30	382	11	26	0.99	321
31 55	80	96	1209	20	1.46	30	422	11	26	1.09	324
31 56	80	96	1212	20	1.23	30	515	7	27	1.63	308
31 57	80	96	1413	20	1.41	40	465	10	27	1.17	310
31 58	80	96	807	40	1.61	23	420	6	29	1.35	291
31 59	80	95	806	40	1.69	23	474	4	32	1.84	259
31 60	80	96	807	40	1.51	23	491	3	30	2.01	279
31 61	80	96	807	40	1.27	23	535	1	28	2.45	296
31 62	80	96	807	40	1.13	23	503	8	23	1.22	358
31 63	80	96	999	40	1.28	36	497	9	26	1.36	319
31 64	80	97	1008	40	1.57	36	457	6	30	1.55	284
31 65	80	97	981	40	1.14	36	561	7	26	1.58	321
31 66	80	96	1210	40	1.31	50	565	1	31	3.25	268
31 67	80	96	1209	40	1.55	50	497	5	32	1.88	261
31 68	80	96	1208	40	1.14	50	601	7	29	1.99	288
31 69	80	96	1414	40	1.43	60	557	5	32	2.37	259
31 70	80	96	1414	40	1.52	60	543	5	33	1.98	252
31 71	80	96	1415	40	1.29	60	606	0	32	3.89	262
31 72	80	95	1615	40	1.44	60	578	9	34	1.70	249
31 73	80	95	1615	40	1.24	60	644	3	33	3.69	257
31 74	80	96	1210	20	1.89	30	312	9	24	0.98	347
31 75	80	96	1210	20	1.96	30	292	9	24	0.88	358
31 76	80	96	1210	20	1.66	30	378	9	26	1.21	324
31 77	80	96	1415	20	1.72	50	446	6	31	1.46	275
31 78	80	96	1414	20	1.53	50	509	3	31	2.18	269

continued on next page...

Exp #	T_{in} (°C)	P_{man} (kPa)	N (rpm)	PR (-)	λ (-)	SOI (°bTDC)	IMEP (kPa)	CA50 (°aTDC)	$\eta_{ind,th}$ (%)	MPPR (bar/CAD)	ISFC (g/kWh)
31 79	80	96	807	60	1.30	17	504	18	27	0.75	315
31 80	80	96	805	60	1.18	17	599	10	29	1.68	289
31 81	80	97	1009	60	1.36	30	490	19	27	0.65	309
31 82	80	97	1008	60	1.28	30	579	12	31	1.10	274
31 83	100	95	807	20	2.30	15	245	6	23	0.99	368
31 84	100	96	807	20	2.20	15	256	6	23	0.99	366
31 85	100	96	807	20	1.77	15	338	7	25	1.24	341
31 86	100	96	807	20	1.41	15	465	6	27	1.88	310
31 87	100	96	807	20	1.22	15	512	4	26	2.63	324
31 88	100	96	807	20	1.02	15	547	4	24	3.05	356
31 89	100	97	1008	20	2.26	22	268	6	25	1.01	336
31 90	100	97	1008	20	1.86	22	321	37	25	1.11	337
31 92	100	97	1008	20	1.26	22	517	6	28	0.92	307
31 93	100	97	1008	20	1.02	22	550	7	24	1.09	354
31 94	100	96	1212	20	1.81	27	337	11	26	0.17	321
31 95	100	96	1210	20	1.95	27	283	13	24	0.10	356
31 96	100	96	1209	20	1.44	27	456	12	28	0.31	300
31 97	100	96	1210	20	1.23	27	518	9	28	0.44	306
31 98	100	96	1210	20	0.99	27	420	12	18	0.15	463
31 99	100	96	1413	20	2.01	35	300	10	25	0.12	336
31 100	100	96	1414	20	1.88	35	326	10	25	0.13	332
31 101	100	96	1414	20	1.48	35	464	9	29	0.27	295
31 102	100	96	1408	20	1.17	35	537	7	27	0.37	309
31 103	100	96	1410	20	1.00	35	551	10	24	0.32	353
31 104	100	96	1614	20	2.00	45	304	11	25	0.06	332
31 105	100	96	1614	20	1.88	45	340	12	27	0.08	318
31 106	100	96	1616	20	1.47	45	485	10	30	0.20	283

continued on next page...

Exp #	T_{in} (°C)	P_{man} (kPa)	N (rpm)	PR (-)	λ (-)	SOI (°bTDC)	IMEP (kPa)	CA50 (°aTDC)	$\eta_{ind,th}$ (%)	MPPR (bar/CAD)	ISFC (g/kWh)
31 107	100	96	1614	20	1.17	45	317	13	16	0.06	524
31 108	100	97	1815	20	1.84	53	383	12	29	0.06	292
31 109	100	97	1817	20	1.48	53	514	8	32	0.17	266
31 110	100	97	1809	20	1.25	53	345	7	18	0.07	460
31 111	100	96	808	40	1.71	17	396	12	28	0.55	300
31 112	100	96	807	40	1.48	17	495	7	30	0.85	277
31 113	100	96	807	40	1.27	17	545	5	29	1.31	291
31 114	100	96	805	40	1.09	17	570	7	27	1.56	316
31 115	100	97	1006	40	1.69	27	434	10	31	0.38	274
31 116	100	97	1008	40	1.46	27	516	6	32	0.60	265
31 117	100	97	1010	40	1.20	27	559	5	30	0.75	284
31 118	100	97	1007	40	1.09	27	572	8	27	0.74	315
31 119	100	96	1208	40	1.61	35	459	7	31	0.32	267
31 120	100	96	1216	40	1.38	35	516	4	32	0.41	266
31 121	100	96	1218	40	1.20	35	558	3	30	0.50	284
31 122	100	96	1200	40	1.07	35	557	8	26	0.35	323
31 123	100	96	1413	40	1.57	48	506	7	33	0.25	256
31 124	100	96	1414	40	1.48	48	542	4	33	0.40	253
31 125	100	96	1402	40	1.25	48	575	5	30	0.41	276
31 126	100	96	1404	40	1.15	48	621	3	30	0.63	279
31 127	100	96	1614	40	1.43	58	561	6	34	0.33	250
31 128	100	96	1614	40	1.25	58	608	3	32	0.69	261
31 129	100	96	1614	40	1.14	58	609	5	30	0.47	284
31 130	100	96	807	60	1.26	15	465	20	25	0.20	341
31 131	100	96	807	60	1.15	15	545	15	26	0.38	318
31 132	100	97	1007	60	1.26	29	548	13	29	0.26	290
31 133	80	97	1008	20	1.59	18	366	15	24	0.21	355

continued on next page...

Exp #	T_{in} (°C)	P_{man} (kPa)	N (rpm)	PR (-)	λ (-)	SOI (°bTDC)	IMEP (kPa)	CA50 (°aTDC)	$\eta_{ind,th}$ (%)	MPPR (bar/CAD)	ISFC (g/kWh)
31 134	80	97	1008	20	1.59	20	393	13	26	0.32	330
31 135	80	97	1008	20	1.59	25	442	7	29	0.58	293
31 136	80	97	1008	20	1.60	30	454	4	30	0.77	286
31 137	80	97	1008	20	1.60	35	457	2	30	0.97	284
31 138	80	97	1013	20	1.57	40	459	2	30	0.90	283
31 139	80	97	1015	20	1.59	45	464	1	30	0.95	279
31 140	80	97	1002	20	1.61	50	480	1	31	1.09	270
31 141	80	97	1009	20	1.60	55	480	-2	31	1.47	270
31 142	80	97	1008	20	1.60	60	477	-1	31	1.02	272
31 143	80	97	1015	20	1.59	65	471	-1	31	1.25	275
31 144	80	97	1008	20	1.60	70	469	2	31	0.66	276
31 145	80	97	1008	20	1.62	72	478	6	31	0.43	271
31 146	80	97	1008	20	1.28	17	475	15	25	0.26	334
31 147	80	97	1016	20	1.28	20	521	10	28	0.54	304
31 148	80	97	1006	20	1.28	25	524	6	28	0.77	302
31 149	80	97	1008	20	1.28	30	509	5	27	0.81	311
31 150	80	97	1009	20	1.27	35	517	4	28	0.95	306
31 151	80	97	1001	20	1.30	40	522	1	28	1.45	304
31 152	80	97	1015	20	1.27	45	386	-2	21	0.76	411
31 153	80	97	1004	20	1.26	50	535	-4	28	2.57	296
31 154	80	97	1009	20	1.26	55	519	-4	28	2.06	306
31 155	80	97	1009	40	1.57	28	447	11	29	0.29	290
31 156	80	97	1010	40	1.58	30	444	11	29	0.36	292
31 157	80	97	1009	40	1.57	35	471	7	31	0.55	275
31 158	80	97	1008	40	1.57	40	472	4	31	0.65	275
31 159	80	97	1008	40	1.57	45	477	2	31	0.81	272
31 160	80	97	1008	40	1.57	50	477	1	31	0.91	272

continued on next page...

Exp #	T_{in} (°C)	P_{man} (kPa)	N (rpm)	PR (-)	λ (-)	SOI (°bTDC)	IMEP (kPa)	CA50 (°aTDC)	$\eta_{ind,th}$ (%)	MPPR (bar/CAD)	ISFC (g/kWh)
31 161	80	97	1008	40	1.58	55	466	2	30	0.75	278
31 162	80	97	1006	40	1.26	29	411	18	22	0.08	385
31 163	80	97	1007	40	1.26	30	525	9	28	0.43	302
31 164	80	97	1008	40	1.24	35	496	7	26	0.49	320
31 165	80	97	1008	40	1.27	40	530	5	28	0.74	299
31 166	80	97	1007	40	1.26	45	550	0	29	1.86	288
31 167	80	97	1020	40	1.24	50	550	0	29	1.82	288
31 168	80	97	1008	40	1.25	55	551	-5	29	3.11	288
31 169	80	97	1008	40	1.25	60	542	-4	29	3.21	293
31 170	80	97	1021	30	1.23	22	398	17	21	0.13	399
31 171	80	97	1009	30	1.24	25	342	20	18	0.10	463
31 172	80	97	1009	30	1.25	30	519	7	28	0.70	306
31 173	80	97	1003	30	1.28	35	533	4	28	0.96	298
31 174	80	97	1007	30	1.28	40	414	3	22	0.66	383
31 175	80	97	1016	30	1.26	45	524	1	28	1.73	302
31 176	80	96	1001	30	1.28	50	562	-5	30	2.47	282
31 177	80	97	1014	30	1.26	55	543	-5	29	3.01	292
31 178	80	97	1008	30	1.27	60	529	-6	28	3.03	299
31 179	80	97	1009	30	1.56	25	430	10	28	0.37	302
31 180	80	97	1008	30	1.58	30	459	7	30	0.58	283
31 181	80	97	1008	30	1.58	35	472	3	31	0.78	275
31 182	80	97	998	30	1.59	40	480	1	31	1.07	270
31 183	80	97	1008	30	1.57	45	478	1	31	1.10	272
31 184	80	97	1008	30	1.58	50	479	0	31	1.26	271
31 185	80	97	1008	30	1.58	55	478	0	31	1.26	271
31 186	80	97	1008	30	1.58	60	477	0	31	1.20	272
31 187	80	97	1008	30	1.58	65	472	2	31	0.96	275

continued on next page...

Exp #	T_{in} (°C)	P_{man} (kPa)	N (rpm)	PR (-)	λ (-)	SOI (°bTDC)	IMEP (kPa)	CA50 (°aTDC)	$\eta_{ind,th}$ (%)	MPPR (bar/CAD)	ISFC (g/kWh)
31 188	80	97	1006	30	1.59	70	474	5	31	0.36	273
31 189	80	96	807	20	1.60	15	376	10	24	0.54	345
31 190	80	96	807	20	1.61	20	419	5	27	1.10	309
31 191	80	96	806	20	1.61	25	436	0	28	1.45	298
31 192	80	99	806	20	1.61	30	444	-3	29	1.80	292
31 193	80	96	807	20	1.61	35	429	-3	28	2.00	302
31 194	80	96	806	20	1.61	40	423	-5	27	2.40	307
31 195	80	96	807	20	1.60	45	413	-6	27	2.61	314
31 196	80	96	815	20	1.59	50	406	-6	26	2.54	319
31 197	80	96	803	20	1.62	55	411	-6	27	2.64	316
31 198	80	96	805	20	1.62	60	423	-6	28	2.57	306
31 199	80	96	808	20	1.62	65	390	-4	25	2.29	332
31 200	80	96	808	20	1.62	70	387	-2	25	1.58	335
31 201	80	96	815	20	1.64	75	393	5	26	0.52	330
31 202	80	96	1202	20	1.58	25	386	13	25	0.10	336
31 203	80	96	1210	20	1.56	30	450	8	29	0.25	288
31 204	80	96	1211	20	1.56	35	450	6	29	0.28	288
31 204	80	96	1211	20	1.56	35	450	6	29	0.28	288
31 205	80	96	1205	20	1.57	40	455	4	30	0.32	285
31 206	80	96	1210	20	1.56	45	464	3	30	0.34	280
31 207	80	96	1209	20	1.56	50	455	2	30	0.39	285
31 208	80	96	1213	20	1.56	55	463	-1	30	0.33	280
31 209	80	96	1209	20	1.57	60	435	-3	28	0.65	298
31 210	80	96	1210	20	1.56	65	441	-1	29	0.85	294
31 211	80	96	1210	20	1.57	70	442	2	29	0.52	294
31 212	80	96	1414	20	1.60	45	414	12	27	0.09	313
31 213	80	96	1414	20	1.60	50	481	5	31	0.29	270

continued on next page...

Exp #	T_{in} (°C)	P_{man} (kPa)	N (rpm)	PR (-)	λ (-)	SOI (°bTDC)	IMEP (kPa)	CA50 (°aTDC)	$\eta_{ind,th}$ (%)	MPPR (bar/CAD)	ISFC (g/kWh)
31 214	80	96	1414	20	1.60	55	495	2	32	0.54	262
31 215	80	96	1413	20	1.62	60	503	-2	33	0.71	258
31 216	80	96	1413	20	1.61	65	458	0	30	0.55	283
31 217	80	96	1413	20	1.62	70	456	2	30	0.37	284
31 218	80	96	1416	20	1.62	75	432	7	28	0.10	300

Table A.2
Optimized map Test points without EGR

RPM	800	1000	1200	1400	1600	1800
Test ID	31 42	31 21	31 95	31 99	31 104	31 108
	31 15	31 48	31 75	31 100	31 105	31 109
	31 84	31 89	31 94	31 77	31 106	
	31 17	31 24	31 76	31 123	31 127	
	31 3	31 115	31 119	31 78	31 72	
	31 58	31 64	31 29	31 70	31 128	
	31 45	31 81	31 67	31 69	31 73	
	31 59	31 116	31 120	31 125		
	31 112	31 37	31 31	31 71		
	31 34	31 132	31 121	31 126		
	31 10	31 117	31 66			
	31 40	31 38	31 68			
	31 35	31 82				
	31 41	31 8				
	31 11					
	31 14					
	31 12					

Table A.3
Operating Conditions for RCCI Mapping Data - NA with EGR

Exp #	T_{in} (°C)	P_{man} (kPa)	N (rpm)	EGR (%)	PR (-)	λ (-)	SOI (°bTDC)	IMEP (kPa)	CA50 (°aTDC)	$\eta_{ind,th}$ (%)	MPPR (bar/CAD)	ISFC (g/kWh)
32 1	60	94	784	0	20	1.69	19	347	9	24	0.61	353
32 2	60	94	784	0	20	1.41	19	461	7	27	1.18	313
32 3	60	94	784	0	20	1.17	19	527	6	26	1.59	328
32 4	60	94	784	0	20	1.00	19	569	5	24	2.44	355
32 5	60	94	785	5	20	1.55	22	340	9	23	0.55	360
32 6	60	94	784	5	20	1.37	22	425	7	26	0.96	322
32 7	60	94	784	5	20	1.16	22	515	4	27	1.56	315
32 8	60	94	783	5	20	0.96	22	562	3	24	2.79	346
32 9	60	98	784	15	20	1.42	27	393	6	27	0.82	312
32 10	60	94	783	15	20	1.38	27	414	6	28	0.99	305
32 11	60	94	784	15	20	1.13	27	501	5	28	1.49	302
32 12	60	94	784	15	20	0.91	27	560	4	25	2.67	335
32 13	60	95	984	0	20	2.25	22	264	13	24	0.10	355
32 14	60	95	984	0	20	1.89	22	330	12	25	0.21	339
32 15	60	95	984	0	20	1.45	22	477	10	28	0.57	302
32 16	60	95	984	0	20	1.17	22	557	6	27	0.98	317
32 17	60	95	984	0	20	1.02	22	592	6	25	1.33	341
32 18	60	95	984	5	20	2.02	26	277	11	24	0.14	351
32 19	60	95	984	5	20	1.81	26	319	11	25	0.21	339
32 20	60	95	983	5	20	1.42	26	466	9	29	0.57	294
32 21	60	95	984	5	20	1.16	26	548	6	28	0.93	302
32 22	60	95	984	5	20	1.02	26	578	6	26	1.31	324
32 23	60	95	983	12	20	1.70	37	311	11	25	0.15	336
32 24	60	95	983	14	20	1.39	37	446	9	30	0.48	283

continued on next page...

Exp #	T_{in} (°C)	P_{man} (kPa)	N (rpm)	EGR (%)	PR (-)	λ (-)	SOI (°bTDC)	IMEP (kPa)	CA50 (°aTDC)	$\eta_{ind,th}$ (%)	MPRR (bar/CAD)	ISFC (g/kWh)
32 25	60	95	984	15	20	1.14	37	529	8	29	0.88	286
32 26	60	95	983	15	20	0.95	37	581	8	27	1.26	310
32 27	60	94	1184	0	20	1.99	32	298	13	24	0.05	351
32 28	60	94	1185	0	20	1.85	32	334	13	25	0.07	335
32 29	60	94	1186	0	20	1.44	32	441	9	26	0.35	327
32 30	60	94	1184	0	20	1.23	32	557	6	28	0.57	298
32 31	60	94	1185	5	20	1.68	39	360	14	26	0.09	320
32 32	60	94	1184	5	20	1.39	39	487	11	30	0.30	281
32 33	60	94	1184	5	20	1.14	39	566	7	29	0.48	293
32 34	60	95	1188	5	20	0.99	39	592	6	27	0.59	316
32 35	60	95	1184	15	20	1.27	50	521	10	32	0.40	263
32 36	60	95	1184	15	20	1.14	50	563	9	31	0.63	269
32 37	60	94	1184	15	20	0.95	50	617	9	29	1.06	292
32 38	60	95	1179	15	20	0.79	50	625	13	24	0.93	346
32 39	60	94	1387	0	20	1.57	38	440	12	28	0.11	303
32 40	60	94	1385	0	20	1.45	38	494	9	29	0.19	292
32 41	60	94	1388	5	20	1.43	44	484	12	30	0.14	283
32 42	60	94	1383	5	20	1.17	44	582	10	30	0.34	285
32 43	60	94	784	0	40	1.63	16	441	13	29	0.61	286
32 44	60	94	783	0	40	1.46	16	503	9	30	0.84	279
32 45	60	94	782	0	40	1.23	16	494	10	25	0.78	336
32 46	60	94	782	5	40	1.57	22	422	11	29	0.54	290
32 47	60	94	782	5	40	1.43	22	464	10	29	0.74	287
32 48	60	94	783	5	40	1.13	22	542	7	27	1.38	306
32 49	60	94	784	15	40	1.42	37	441	10	30	0.50	277
32 50	60	94	783	15	40	1.19	37	515	9	30	1.10	280
32 51	60	94	782	15	40	0.98	37	578	7	28	2.28	299

continued on next page...

Exp #	T_{in} (°C)	P_{man} (kPa)	N (rpm)	EGR (%)	PR (-)	λ (-)	SOI (%bTDC)	IMEP (kPa)	CA50 (°aTDC)	$\eta_{ind,th}$ (%)	MPRR (bar/CAD)	ISFC (g/kWh)
32 52	80	94	783	0	20	1.97	15	243	12	20	0.21	415
32 53	80	94	783	0	20	1.78	15	294	12	22	0.30	380
32 54	80	94	784	0	20	1.39	15	443	9	26	0.96	325
32 55	80	94	778	0	20	1.18	15	496	6	25	1.91	342
32 56	80	94	782	5	20	1.72	17	302	10	24	0.53	358
32 57	80	94	784	5	20	1.27	17	448	8	26	1.01	322
32 58	80	94	779	5	20	1.06	17	518	4	25	2.13	334
32 59	80	94	783	5	20	0.93	17	545	5	24	2.41	357
32 60	80	94	784	12	20	1.94	17	232	10	22	0.28	388
32 61	80	94	783	15	20	1.29	17	402	12	26	0.58	323
32 62	80	94	782	15	20	1.33	17	264	11	17	0.33	492
32 63	80	94	784	15	20	1.14	17	469	10	27	0.84	315
32 64	80	94	782	15	20	0.90	17	532	7	24	1.94	352
32 65	80	94	783	15	20	1.02	17	500	8	25	1.26	332
32 66	80	95	983	0	20	1.56	21	417	11	27	0.47	311
32 67	80	95	984	0	20	1.44	21	463	8	28	0.61	303
32 68	80	95	983	0	20	1.20	21	530	5	26	1.13	320
32 69	80	95	984	0	20	1.02	21	557	6	24	0.88	349
32 70	80	95	984	5	20	1.97	23	268	11	23	0.19	363
32 71	80	95	983	5	20	1.77	23	313	11	24	0.28	345
32 72	80	95	983	5	20	1.43	23	450	9	28	0.56	296
32 73	80	95	982	5	20	1.19	23	516	6	27	0.87	307
32 74	80	95	983	5	20	0.96	23	560	5	24	0.89	347
32 75	80	95	983	12	20	1.85	27	273	10	25	0.18	343
32 76	80	95	984	13	20	1.40	27	401	10	28	0.36	306
32 77	80	95	983	13	20	1.15	27	492	7	28	0.68	300
32 78	80	95	984	14	20	0.99	27	526	6	26	0.59	322

continued on next page...

Exp #	T_{in} (°C)	P_{man} (kPa)	N (rpm)	EGR (%)	PR (-)	λ (-)	SOI (°bTDC)	IMEP (kPa)	CA50 (°aTDC)	$\eta_{ind,th}$ (%)	MPRR (bar/CAD)	ISFC (g/kWh)
32 79	80	95	975	15	20	0.84	27	563	7	24	0.54	358
32 80	80	94	1181	0	20	1.73	23	279	18	21	0.04	401
32 81	80	94	1184	0	20	1.41	23	402	15	25	0.17	340
32 82	80	94	1184	0	20	1.19	23	531	11	26	0.37	319
32 83	80	94	1184	0	20	1.02	23	564	9	24	0.49	345
32 84	80	94	1185	5	20	2.03	27	238	14	21	0.05	393
32 85	80	94	1185	5	20	1.76	27	288	14	22	0.08	376
32 86	80	94	1183	5	20	1.38	27	446	12	27	0.25	307
32 87	80	94	1184	5	20	1.15	27	517	9	27	0.38	314
32 88	80	94	1186	5	20	1.05	27	526	10	26	0.32	329
32 89	80	94	1187	10	20	1.77	43	311	12	27	0.09	313
32 90	80	94	1185	13	20	1.44	43	437	9	31	0.32	272
32 91	80	94	1185	13	20	1.17	43	513	7	30	0.61	281
32 92	80	94	1185	15	20	1.01	43	561	7	29	0.80	295
32 93	80	94	1182	15	20	0.83	43	595	8	25	0.51	339
32 94	80	94	1387	0	20	2.03	31	284	13	24	0.04	355
32 95	80	94	1388	0	20	1.75	31	346	13	25	0.05	333
32 96	80	94	1385	0	20	1.42	31	458	12	27	0.17	307
32 97	80	94	1388	5	20	1.74	42	356	13	27	0.07	314
32 98	80	94	1388	5	20	1.49	42	454	10	29	0.19	286
32 99	80	94	1386	5	20	1.17	42	551	5	29	0.54	288
32 100	80	94	1388	5	20	0.98	42	593	5	27	0.65	316
32 101	80	94	1386	5	20	0.99	42	596	5	27	0.61	314
32 102	80	94	1385	15	20	1.49	49	379	15	28	0.05	304
32 103	80	94	1387	15	20	1.32	49	490	11	32	0.19	264
32 104	80	94	1389	15	20	1.15	49	549	7	31	0.46	269
32 105	80	94	1387	15	20	1.00	49	593	6	30	0.53	286

continued on next page...

Exp #	T_{in} (°C)	P_{man} (kPa)	N (rpm)	EGR (%)	PR (-)	λ (-)	SOI (%bTDC)	IMEP (kPa)	CA50 (°aTDC)	$\eta_{ind,th}$ (%)	MPRR (bar/CAD)	ISFC (g/kWh)
32 106	80	94	1388	15	20	0.86	49	614	6	27	0.64	317
32 109	60	95	787	0	40	1.91	20	340	15	26	0.21	318
32 110	60	95	786	0	40	1.59	20	516	9	33	0.93	251
32 111	60	95	785	0	40	1.28	20	582	6	31	1.78	273
32 112	60	95	786	0	40	1.11	20	603	5	28	2.34	299
32 113	60	95	787	5	40	1.92	23	286	15	24	0.12	353
32 114	60	95	787	5	40	1.79	23	355	13	28	0.36	305
32 118	60	95	786	5	40	1.20	23	580	6	31	1.79	273
32 119	60	95	784	13	40	1.73	28	367	13	29	0.34	295
32 120	60	95	786	15	40	1.43	28	513	9	33	1.06	253
32 121	60	95	786	15	40	1.15	28	588	8	31	1.81	270
32 122	60	95	786	15	40	1.00	28	603	8	28	2.17	299
32 123	60	96	987	0	40	1.62	34	530	11	34	0.48	245
32 124	60	96	986	0	40	1.30	34	615	6	33	1.48	258
32 125	60	96	989	5	40	1.49	37	517	13	34	0.34	251
32 126	60	96	986	5	40	1.21	37	619	8	33	1.27	256
32 127	60	96	986	5	40	1.22	37	616	7	33	1.45	257
32 128	60	96	985	15	40	1.44	44	544	10	35	0.57	238
32 129	60	96	985	15	40	1.17	44	635	5	34	2.17	250
32 130	60	96	985	15	40	1.02	44	663	5	31	2.84	272
32 131	80	94	784	0	40	1.75	17	393	14	29	0.58	293
32 132	80	94	785	0	40	1.55	17	463	12	30	0.79	280
32 133	80	94	785	0	40	1.25	17	546	8	29	1.46	290
32 134	80	94	785	0	40	1.09	17	585	8	27	1.91	308
32 135	80	94	788	5	40	1.73	19	357	13	28	0.47	303
32 136	80	94	787	5	40	1.61	19	406	14	30	0.50	284
32 137	80	94	785	5	40	1.44	19	489	10	32	0.87	266

continued on next page...

Exp #	T_{in} (°C)	P_{man} (kPa)	N (rpm)	EGR (%)	PR (-)	λ (-)	SOI (%bTDC)	IMEP (kPa)	CA50 (%aTDC)	$\eta_{ind,th}$ (%)	MPRR (bar/CAD)	ISFC (g/kWh)
32 138	80	94	786	5	40	1.44	19	474	10	31	0.83	274
32 139	80	94	785	5	40	1.17	19	557	7	30	1.52	284
32 140	80	94	786	5	40	1.03	19	578	7	27	1.77	312
32 141	80	94	787	15	40	1.67	21	346	19	27	0.47	312
32 142	80	94	784	15	40	1.56	21	444	12	32	0.66	259
32 143	80	94	786	15	40	1.38	21	488	10	32	0.86	266
32 144	80	94	786	15	40	1.12	21	553	7	29	1.36	287
32 145	80	94	785	15	40	0.98	21	582	8	27	1.61	310
32 146	80	96	988	0	40	1.76	27	438	13	32	0.33	263
32 147	80	96	986	0	40	1.57	27	509	9	33	0.55	255
32 148	80	96	985	0	40	1.26	27	579	6	31	0.99	274
32 149	80	96	985	5	40	1.65	30	432	13	31	0.31	267
32 150	80	96	986	5	40	1.45	30	505	11	33	0.54	257
32 151	80	96	986	5	40	1.19	30	578	6	31	1.08	274
32 152	80	96	987	15	40	1.55	34	457	13	33	0.34	253
32 153	80	96	987	15	40	1.37	34	519	10	34	0.56	250
32 154	80	96	986	15	40	1.12	34	592	8	31	1.01	268
32 155	80	96	986	15	40	0.97	34	609	7	28	1.36	296
32 156	80	95	1184	0	40	1.65	38	476	13	33	0.19	257
32 157	80	95	1188	0	40	1.32	38	586	6	33	0.73	258
32 158	80	95	1185	5	40	1.51	48	511	10	35	0.33	240
32 160	80	95	1187	5	40	1.21	48	589	6	33	0.96	257
32 161	80	95	1186	15	40	1.16	50	593	8	33	0.89	255
32 162	80	95	1186	15	40	0.96	50	635	9	30	1.27	284
32 163	80	95	1186	0	40	1.27	50	529	-5	29	1.94	286
32 164	80	95	1187	5	40	1.18	50	563	1	31	1.64	269
32 165	80	95	1186	15	40	1.15	50	591	6	33	1.17	256

Table A.4
Optimized map Test points with EGR 0-15%

RPM	800	1000	1200	1400
Test ID	32 60	32 75	32 85	32 94
	32 113	32 23	32 89	32 97
	32 56	32 19	32 31	32 39
	32 141	32 14	32 90	32 98
	32 135	32 76	32 156	32 103
	32 119	32 149	32 32	32 104
	32 131	32 146	32 158	32 42
	32 136	32 152	32 36	32 105
	32 142	32 20	32 160	32 106
	32 132	32 147	32 161	
	32 138	32 153	32 37	
	32 137	32 123	32 162	
	32 44	32 128		
	32 120	32 151		
	32 110	32 148		
	32 144	32 154		
	32 139	32 126		
	32 111	32 129		
	32 121	32 130		
	32 112			

Table A.5
Optimized map Test points EGR 0%

RPM	800	1000	1200	1400
Test ID	32 109	32 13	32 156	32 94
	32 131	32 14	32 82	32 39
	32 43	32 146	32 30	32 96
	32 132	32 67	32 157	32 40
	32 44	32 15		
	32 110	32 147		
	32 133	32 123		
	32 111	32 16		
	32 112	32 148		
	32 124			

Appendix B

FPGA Model

B.1 Angle Counter

Angle has been counted by using A and Z pulses coming from Encoder. A pulse is generated every CAD where as Z pulse is generated every 360 degrees. In engine application we need to count from 0 to 720 degrees that is one complete cycle or 2 rotations. So A pulse was used for counting where as Z pulse was used to reset that counter. Since we need a reset after 720 degrees one more counter was used which counted to two for every Z pulse and then finally reset the A pulse counter. This way we were able to count 720 Degrees. Simulink mode is shown in Figure B.1

```

% A Pulse Counter

function z = xlmax1(x, y, a, b)

if y == a && x == b;

z = 1;

else

z = 0;

end

% Z Pulse Counter

function z = xlmax2(x, y, a, b)

if x == b && y == a;

z = 1;

else

z = 0;

end

```

B.2 Pressure Calculation

Pressure calculation algorithm was divided into four parts namely scaling of input voltage as per transducer calibration, angle synchronous sampling , digital filtering, Pegging. Details about voltage scaling, sampling and pegging can be seen in Figure B.2(a) where as details about filter can be seen in Figure B.2(b). Xilinx Simulink Generator(XSG) doesn't offer blocks for implementing IIR filter directly. Therefore

they were represented in mathematical form. First-In First-Out(FIFO) blocks were used to create angle based delays.

```
% Pegging
function [Press_Peg,T_1] = Pegging(Press,T,ang,Peg)
if (ang == 0)
T_1 = Peg - Press;
else
T_1 = T;
end
Press_Peg = Press+T_1;
end
```

B.3 Volume Calculation

Volume can be derived from Equation (2.3). Similarly dV can be also be calculated by taking differential of V . Instead of calculating these values on-line they were fed to RAM which was accessed every CAD to give angle synchronous V and dV . Layout is shown in Figure B.3

B.4 IMEP, Peak Pressure and Location of peak pressure

IMEP can be calculated using Equation (2.4). This was implemented in the model. Other than this for PP and LPP matlab code was written which compares values between the current and previous CAD and based of that located the maximum values.

```
%Angle Check
function z = Angle_Check(Ang)
if (Ang >= 0 && Ang <= 359)
z = 1;
else
z = 0;
end

% Peak Pressure and it's location
function [LPP,Peak_P] = PP_LPP(Ang,P,Peak_P_PC,LPP_PC)
if(Ang == 719)
Peak_P = 0;
LPP = 0;
elseif(Peak_P_PC < P)
```

```

Peak_P = P;

LPP = Ang;

else

LPP = LPP_PC;

Peak_P = Peak_P_PC;

end

% IMEP, PP and LPP Update

function [I,P,L] = IMEP_Upd (Ang, IMEP, IMEP_PC, LPP, LPP_PC, Peak_P, ←
    Peak_P_PC)

if (Ang == 719)

I = 0;

P = 0;

L = 0;

elseif (Ang > 400)

I = IMEP;

P = Peak_P;

L = LPP;

else

I = IMEP_PC;

P = Peak_P_PC;

L = LPP_PC;

end

```

B.5 Heat Release Calculation

HRR calculation were based on Equation (5.3). This was implemented as is shown in Figure B.5. All the calculations were carried out on CAD basis.

B.6 CA50 Calculation

For CA50 calculation we first need to calculate SOC and EOC. For SOC Equation (2.11) was implemented and is shown in Figure B.6. As for EOC matlab code was written which detected heat release rate values and based of that decide end of combustion. This is shown in Figure B.7. Both these models gave two values as output, Angle and Pressure at that angle. These were the two values needed for calculating CA50.

CA50 was based on Rassweiler-Withrow model. CA50 model calculations were delayed by 120 CAD. This was done so that SOC and EOC calculations are complete, as this model needed values from those two models. Matlab Codes used in the models are given in the section with name of the model as it's commented heading.

```
% SOC  
function [SO, SO_P] = SOC (P1, P2, P3, Ang, SOC_P, P, P_P)
```

```

if(Ang == 0)

SO = 0;

SO_P = 1;

elseif (Ang >= 160 && Ang < 183 && SOC_P == 0)

if(P3 > 200 && P2 > 200 && P1 > 600)

SO = Ang - 3;

SO_P = P;

else

SO = 0;

SO_P = 1;

end

elseif (Ang >= 184 && SOC_P == 0)

if(P3 > 200 && P2 > 200 && P1 > 300)

SO = Ang - 3;

SO_P = P;

else

SO = 0;

SO_P = 1;

end

else

SO = SOC_P;

SO_P = P_P;

end

end

```



```

%EOC

function [EO,P_EO] = EOC(CHRR_D1,CHRR_D2,CHRR_D3,Ang,EO_P,P,P_P,SOC)

if(Ang == 0)

EO = 0;

P_EO = 1;

elseif(Ang > 190 && CHRR_D1 <= 10 && CHRR_D2 <= 10 && CHRR_D3 <= 10 &&↵

    ...

EO_P == 0 && SOC > 10)

EO = Ang - 2;

P_EO = P;

else

EO = EO_P;

P_EO = P_P;

end

end

%CA50

function [CA_50,CP] = CA50(C,Ang,C_P,CA_50_P,SOC,EOC)

if(Ang == 1)

CA_50 = 0;

CP = 10;

elseif(Ang >= SOC && SOC > 1 && Ang <= EOC)

if(C < C_P)

CA_50 = Ang;

```

```
CP = C;  
  
else  
  
CA_50 = CA_50_P;  
  
CP = C_P;  
  
end  
  
else  
  
CA_50 = CA_50_P;  
  
CP = C_P;  
  
end  
  
end
```

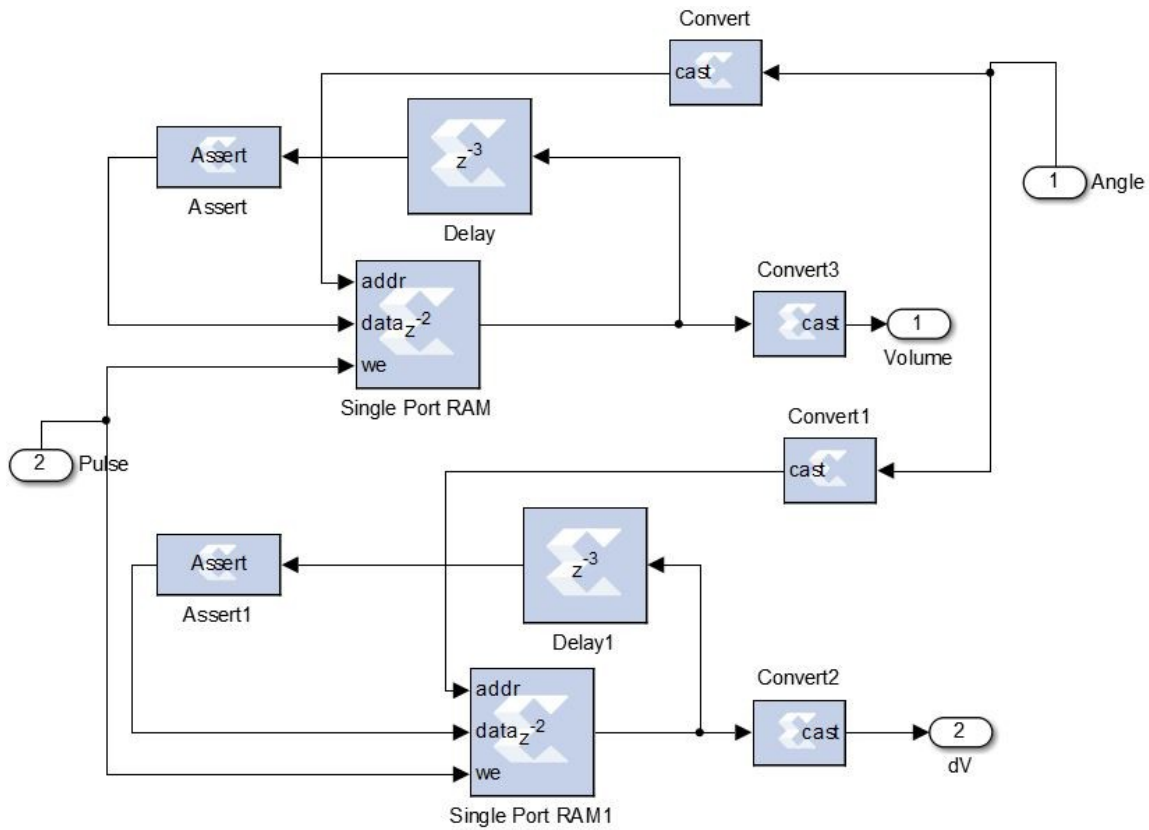



Figure B.3: Volume Calculation

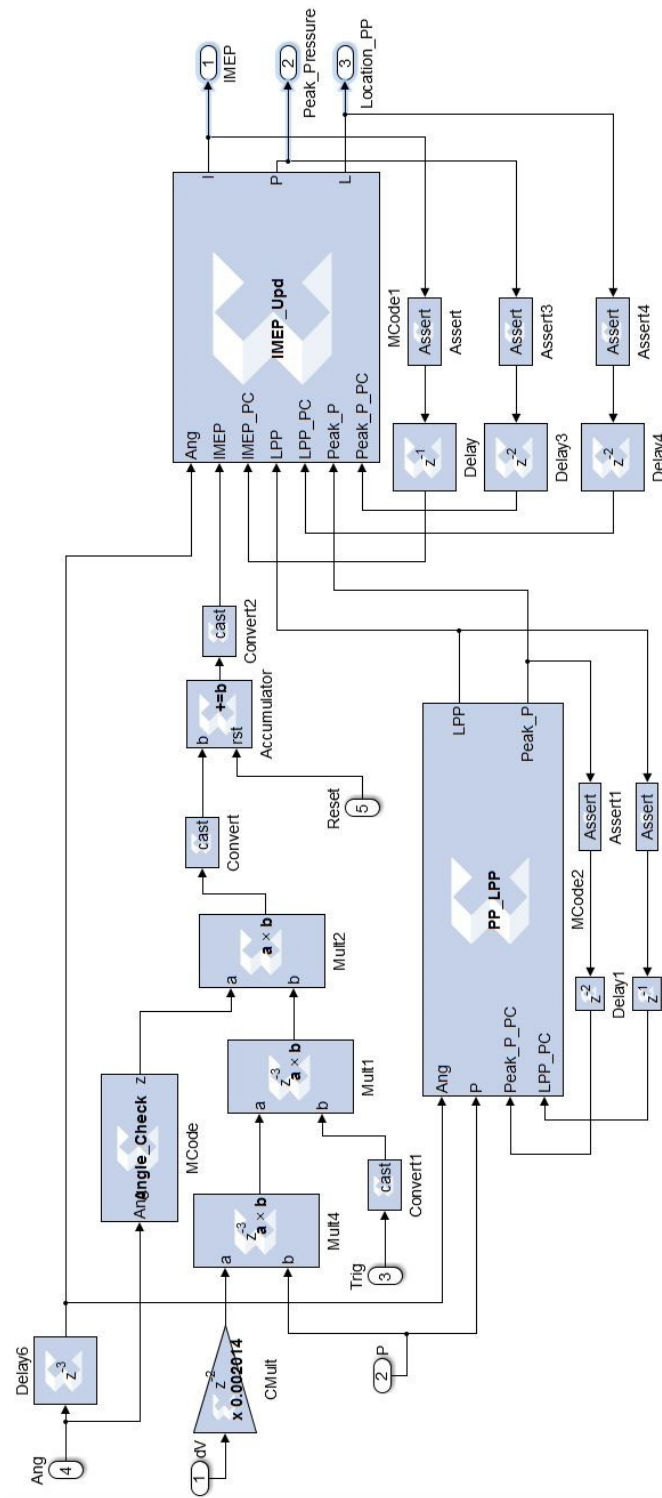


Figure B.4: IMEP, PP and LPP Calculations

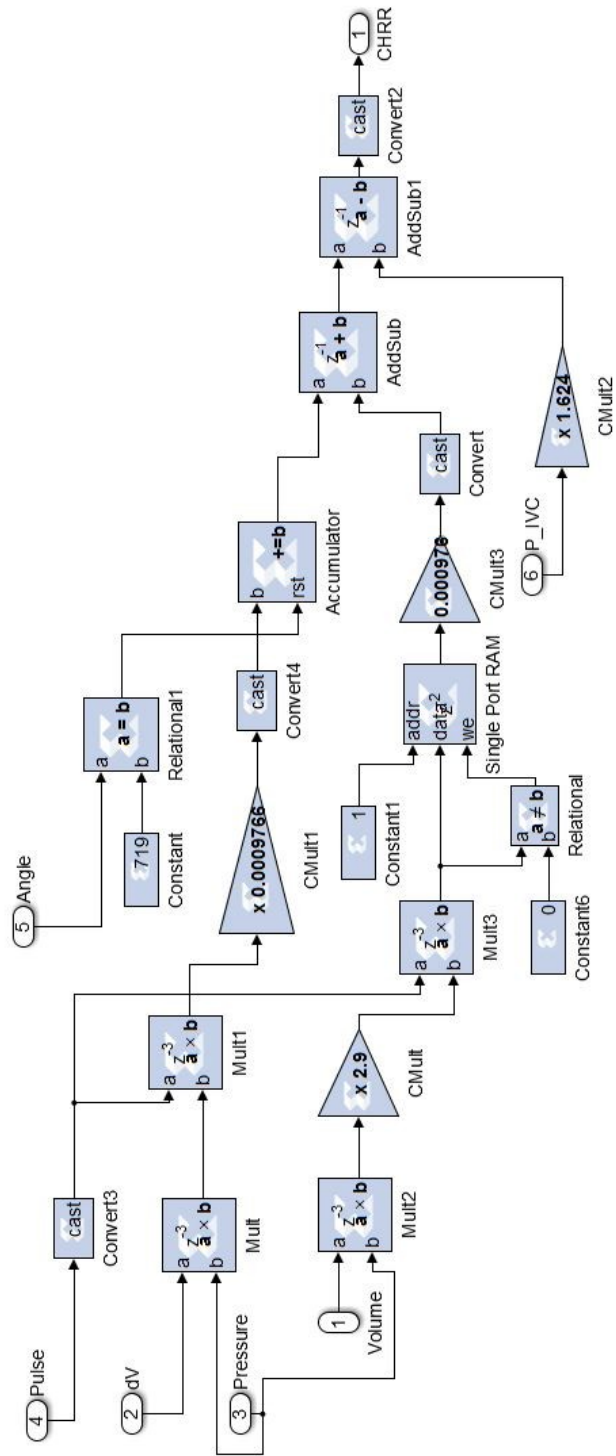


Figure B.5: Heat Release Calculation

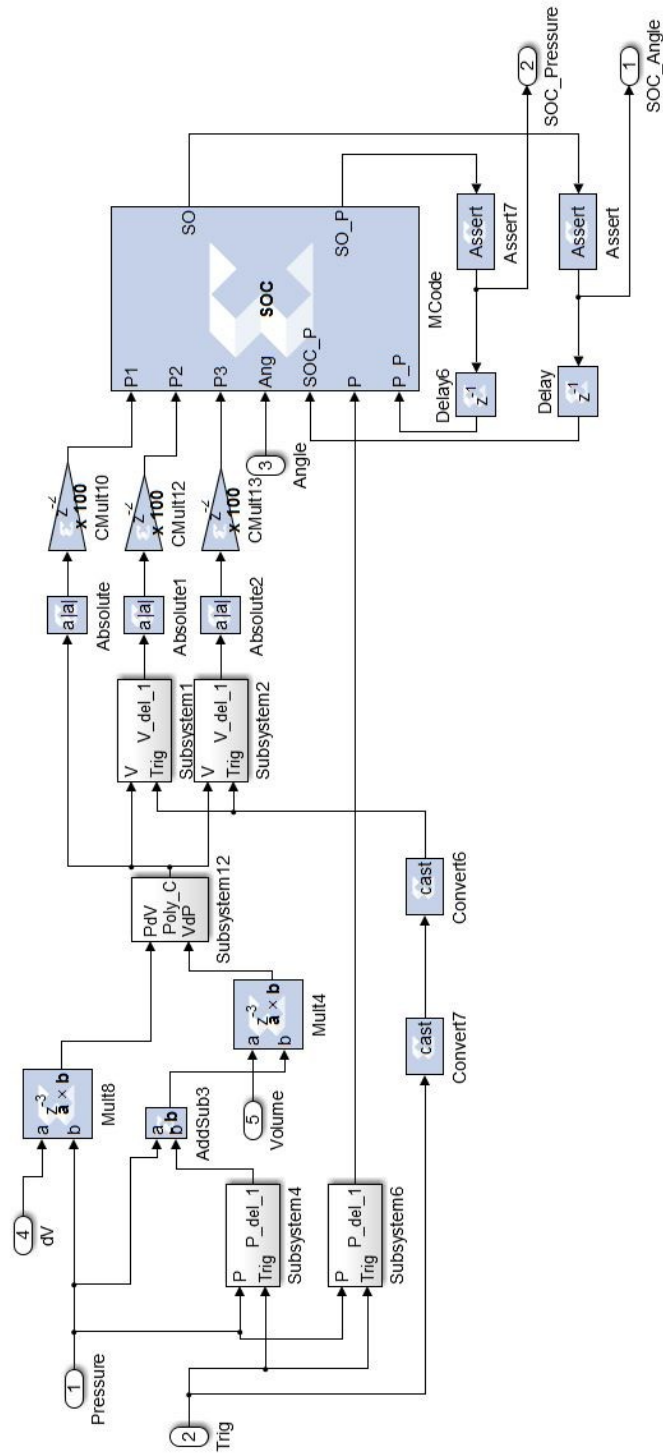


Figure B.6: Start of Combustion

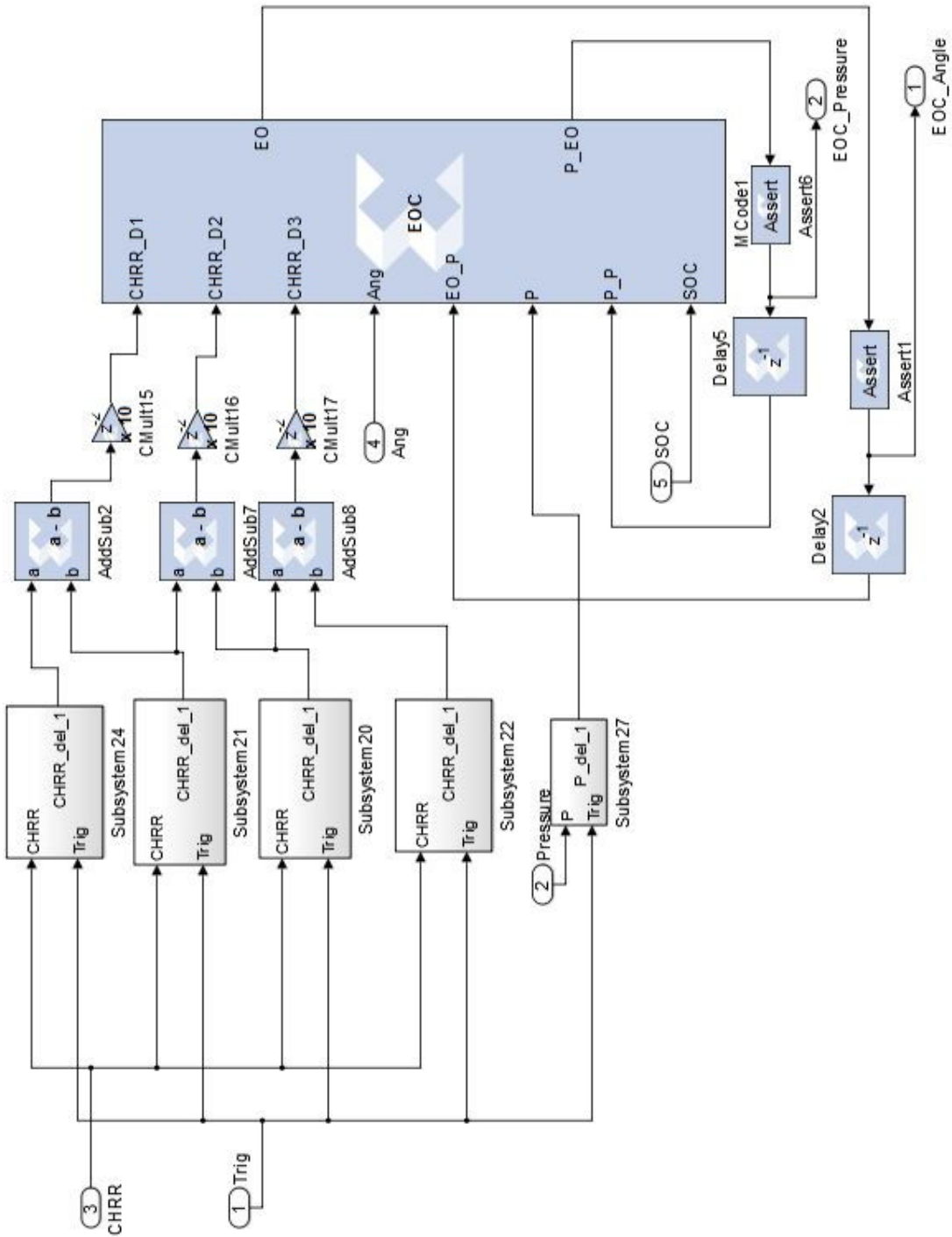


Figure B.7: End of Combustion

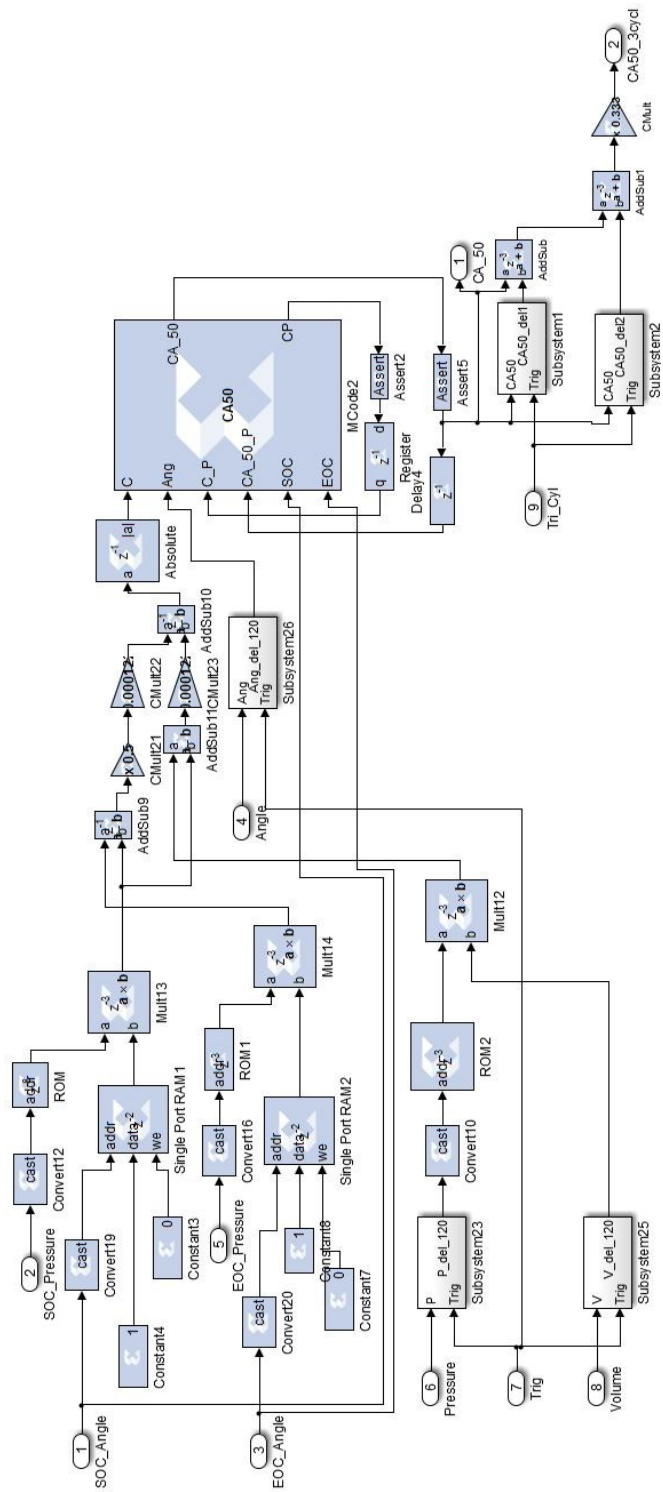


Figure B.8: CA50

Appendix C

Thesis Files

The details about thesis files has been specified in this appendix. All the data, plots, matlab codes and models are stored in the folder \Thesis_Files. Details are given in the following tables.

Table C.1
Test Data Files - Raw and Processed
Folder location: \Thesis_Files

Folder Name	Description
Exp31	Raw as well as processed data files for steady state mapping based of the test matrix 2.3. This composes of steady state base mapping of engine with Diesel/Gasoline
Exp32	Raw as well as processed data files for steady state mapping based of the test matrix 2.4. This composes of steady state mapping of engine with EGR
Exp33	This composes of transient tests - RCCI Domain with diesel/gasoline and RCCI-SI Mode switching with iso-octane/n-heptane.
Exp38	This composes of transient tests - HCCI-SI Mode switching with iso-octane/n-heptane.

Table C.2
Figure Files
Folder location: \Thesis_Files\Figures

File Name	Figure Reference
Matlab_Plots	
Effect_Temp_PR_HRR	Effect of Intake Temperature Fig.3.5 (a)
Effect_Temp_Subplot	Intake Temperature Fig.3.5 (b)
Effect_PR_SameSOI_PR_HRR	Effect of Premixed Ratio Fig.3.6 (a)
Effect_PR_SameSOI_Subplot	Effect of Premixed Ratio Fig.3.6 (b)
Effect_SOI_PR_HRR	Effect of Start of Injection Fig.3.7 (a)
Effect_SOI_Subplot	Effect of Start of Injection Fig.3.7 (b)
Effect_EGR_Same_SOI_PR_HRR	Effect of EGR - SOI same Fig.3.9 (a)
Effect_EGR_Same_SOI_Subplot	Effect of EGR - SOI same Fig.3.9 (b)
Effect_EGR_Same_CA50_PR_HRR	Effect of EGR - CA50 same Fig.3.10 (a)
Effect_EGR_Same_CA50_Subplot	Effect of EGR - CA50 same Fig.3.10 (b)
THrottle_Response_100-15	Throttle Response Fig.4.1 (a)
THrottle_Response_100-15_bad	Throttle Response Fig.4.1 (b)
a_110-130_1000_super	Supercharging Dynamics: Boost response at Constant Speed Fig.4.3 (a)
b_110-130_1600_super	Supercharging Dynamics: Boost response at Constant Speed Fig.4.3 (b)
c_100-120_1600_super	Supercharging Dynamics: Boost response at Constant Speed Fig.4.3 (c)
d_100-130_1600_super	Supercharging Dynamics: Boost response at Constant Speed Fig.4.3 (d)
e_120-100_1600_super	Supercharging Dynamics: Boost response at Constant Speed Fig.4.3 (e)
f_130-100_1600_super	Supercharging Dynamics: Boost response at Constant Speed Fig.4.3 (f)
supercharger_MAP	Supercharger map: Engine speed vs Motor Frequency Fig.4.4
Supercharger_Response_diffspeed	Supercharger Response: Engine Speed Switch Fig.4.5
RCCI_Domain_Switch_pt23	Premixed Ratio Switch Fig.4.6
RCCI_Domain_Switch_pt17	Mass Of Fuel Switch Fig.4.7
RCCI_SI_Pt_30	RCCI - SI - RCCI Switch Fig.4.9
filtervsnon_filter	Comparison of Raw and Filtered Pressure Trace Model Fig.5.2
hrrvsahrr	Comparison of Conventional HRR Model and Reduced HRR Model Fig.5.3
hrrgamma	Effect of γ on Reduced HRR Model Fig.5.4

File Name	Figure Reference
Matlab Plots	
CHRR vs RW	Comparison of Reduced heat Release Model and Rassweiler's Withrow Model Fig.5.5
2_stage_HRR_Pt13_189-218	2 Stage Heat Release Fig.5.6
SOC_Ident	SOC Identification - 2 Stage Heat Release Fig.5.7
CA50_acapvsFPGA	FPGA Validation Fig.5.8 (a)
IMEP_acapvsFPGA	FPGA Validation Fig.5.8 (b)
LPP_acapvsFPGA	FPGA Validation Fig.5.8 (c)
PP_acapvsFPGA	FPGA Validation Fig.5.8 (d)
FPGA_PRSwitch	Premixed Ratio Switch Fig.5.9
FPGA_SOISwitch	SOI Switch Fig.5.10
IMEP_SOI_Controller	IMEP-CA50 Closed loop control Fig.5.12
Visio Plots	
ThesisOrganization	Thesis Organization Fig.1.2
ExperimentalTestSetup_RCCI_NA	Engine Setup Fig.2.1
Drawing1	Data Acquisition and Control Setup Fig.2.3
Setup	Setup and Model Fig.5.1
IMEP_Cntrl	Control Model Fig.5.11
ORIGIN Pro Plots	
RCCI_NA_DG	Engine Map - Intake Temp 40-60-80-100 (deg-C),MAP 95 (kPa), PR 20-40-60 (-) Fig.3.2
RCCI_NA_DG_EGR	Engine Map - Intake Temp 60-80 (deg-C),MAP 95 (kPa), PR 20-40 (-) Fig.3.4
RCCI_NA_DG_Sweep	Effect of Start of Injection Fig.3.8

Table C.3
Data Analysis Scripts
Folder location: \Thesis_Files\Data_Analysis_Code

Folder/File Name	Description
Steady State	Script for steady state data analysis
Transient Script 1	RCCI-SI Combustion Mode switch data analysis
Transient Script 2	RCCI Domain transients data analysis
Data Plot	Plotting for Steady state processed data
Mat2Excel	Read from .mat files and write to excel

Table C.4
Test Setup Files

Folder location: \Thesis_Files\APRC Test Setup Files

Folder Name	Description
Acap files	Contains script files for ACAP analyzer
Dspace Files	Contains 3 folders. Configuration desk and rapidpro files- Contains configuration desk latest hardware topology and rapidpro pin-out files. FPGA M Files- Conatins M files used in FPGA algorithm. Processor+FPGA Model-Contains the most updated processor and FPGA models.

Appendix D

Permissions

Permission for Figure 1.1

The screenshot shows a web interface for RightsLink. At the top left is the Copyright Clearance Center logo. To its right is the RightsLink logo. Further right are navigation buttons for Home, Create Account, Help, and Live Chat. Below the Copyright Clearance Center logo is the SAGE Publishing logo. To the right of the SAGE logo is a metadata table:

Title:	Progress and recent trends in reactivity-controlled compression ignition engines:
Author:	Amin Paykani, Amir-Hasan Kakaee, Pourya Rahnama, Rolf D Reitz
Publication:	International Journal of Engine Research
Publisher:	SAGE Publications
Date:	06/01/2016

Below the metadata table is a 'LOGIN' box with the text: 'If you're a copyright.com user, you can login to RightsLink using your copyright.com credentials. Already a RightsLink user or want to learn more?' At the bottom left of the page is the heading 'Gratis Reuse' followed by a paragraph of text: 'Permission is granted at no cost for use of content in a Master's Thesis and/or Doctoral Dissertation. If you intend to distribute or sell your Master's Thesis/Doctoral Dissertation to the general public through print or website publication, please return to the previous page and select 'Republish in a Book/Journal' or 'Post on intranet/password-protected website' to complete your request.' At the bottom center are two buttons: 'BACK' and 'CLOSE WINDOW'. At the very bottom is a footer with copyright information and contact details.

Figure D.1: Letter of permission for figure 1.1